

Contrails

WADD TECHNICAL REPORT 60-484

PART II

**TRANSIENT AND NONLINEAR EFFECTS ON
HIGH SPEED, VIBRATORY, THERMOELASTIC
INSTABILITY PHENOMENA**

**PART II
AEROTHERMOELASTIC APPLICATIONS**

EUGENE J. BRUNELLE JR.

MASSACHUSETTS INSTITUTE OF TECHNOLOGY

DECEMBER 1960

FLIGHT DYNAMICS LABORATORY
CONTRACT No. AF 33(616)-6185
PROJECT No. 1370
TASK No. 13478

WADD
**WRIGHT AIR DEVELOPMENT DIVISION
AIR RESEARCH AND DEVELOPMENT COMMAND
UNITED STATES AIR FORCE
WRIGHT-PATTERSON AIR FORCE BASE, OHIO**

McGregor & Werner, Inc., Dayton, O.
300 - October 1961 - 6-183

Approved for Public Release

FOREWORD

This report was prepared for the Flight Dynamics Laboratory, Wright Air Development Division, Wright-Patterson Air Force Base, Ohio, by the Aeroelastic and Structures Research Laboratory at the Massachusetts Institute of Technology, Cambridge, Massachusetts. The research and development work was accomplished under Air Force Contract No. AF 33(616)-6185, Project No. 1370, "Dynamic Problems in Flight Vehicles", Task No. 13478, "Prediction Methods for Dynamic Instabilities and Related Gasdynamic Phenomena". Donald J. Ketter, 1st Lt., USAF of the Dynamics Branch, Flight Dynamics Laboratory was the project engineer on this contract. Professor Holt Ashley was the project supervisor and Mr. Eugene J. Brunelle, Jr. was project engineer for the contractor and author. The research covered by this report was started on 15 January 1959 and completed in May 1960. This is Part II of a report which has been published in two separate parts. Part I covered theoretical considerations and Part II covers analytical and computer studies concentrating on aerothermoelastic applications.

The author wishes to thank Mr. Doyle McClure and Mr. Garabed Zartarian for their independent efforts that resulted in sub-section 1.4 of this report entitled "Exact Two-Dimensional Linearized Aerodynamic Theory for an Accelerating Unsteady Supersonic Airfoil". Mrs. Evelyn Mack is gratefully acknowledged for programming and supervising the IBM 704 calculations. The careful typing of this manuscript was performed by Miss Maxine Weiner. The calculations were done in part at the MIT Computation Center, Cambridge, Massachusetts.

ABSTRACT

This report investigates the equations representing the dynamic, torsion-bending motion of a wing which is one major component of an ultra-high performance manned vehicle. Preliminary work required for this investigation is included as an integral part of the report. This preliminary work includes (1) the derivation of an exact two-dimensional linearized aerodynamic theory for an accelerating unsteady supersonic airfoil, (2) the re-derivation of "piston theory" aerodynamics for arbitrary motion, and (3) a derivation for the torsional stiffness loss of an aircraft wing that includes the effects of a specified time-dependent wall temperature due to the given flight mission and that includes the effects of mid-plane stretching.

The computer studies consider a "super X-15" type wing performing two specified flight missions and provide answers in the form of pitch and plunge impulse response time histories. The "exact" solutions are compared with two approximate solutions. The results of the comparisons indicate that a quasi-steady aero-thermoelastic analysis is adequate for all manned vehicles of the foreseeable future. This statement does not apply to the dynamic stability analysis (rigid-body)

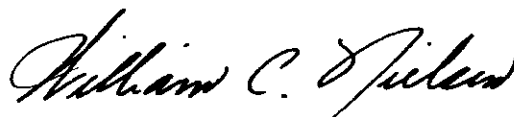
Contrails

of these vehicles since their lower rigid-body frequencies permit a moderate to strong coupling between the governing equations and their time-varying coefficients.

PUBLICATION REVIEW

This report has been reviewed and is approved.

FOR THE COMMANDER:



WILLIAM C. NIELSEN
Colonel, USAF
Chief, Flight Dynamics Laboratory

TABLE OF CONTENTS

<u>Section</u>		<u>Page</u>
I	PRESENTATION OF THE REQUIRED AERODYNAMIC AND AEROTHERMOELASTIC THEORIES	1
	1.1 Introduction	1
	1.2 Loss of Torsional Stiffness Due to Aerodynamic Heating Including the Effects of Mid-Plane Stretching, Finite Acceleration and Varying State Parameters	2
	1.3 Arbitrary Motion Piston Theory	8
	1.4 Exact Two-Dimensional Linearized Aerodynamic Theory for an Accelerating Unsteady Supersonic Airfoil	12
II	THE PURPOSE, DEFINITION AND DESCRIPTION OF THE COMPUTATIONAL EFFORT	25
III	PRESENTATION AND DISCUSSION OF THE SOLUTIONS	44
	REFERENCES	48

LIST OF APPENDICES

<u>Appendix No.</u>		<u>Page</u>
I	COMMENTS ON VARIABLE ALTITUDE FLIGHT	50
II	OUTLINE OF THE PROCEDURES FOR OBTAINING THE UPWASH IMPULSE RESPONSES	52
III	APPROXIMATE RUN TIMES ON THE IBM 704 FOR VARIOUS PROGRAMS	65

LIST OF ILLUSTRATIONS

<u>Figure</u>		<u>Page</u>
1	Wing Planform and Cross Section	66
2	Segment of Twisted Wing	66
3	Non-Zero-Thickness Typical Section	67
4	Two-Dimensional Accelerating Airfoil	68
5	Three-Dimensional Steady State Airfoil	68
6	Lift Due to Impulsive Plunging Motion for Constant F's	69
7	Lift Due to Impulsive Pitch Rate About the Airfoil Leading Edge for Constant F's	70
8	Pitching Moment Due to Impulsive Plunging Motion for Constant F's	71
9	Pitching Moment Due to Impulsive Pitch Rate About the Airfoil Leading Edge for Constant F's	72
10	Flight Path Diagram	73
11	Pulse Representation	74
12	Moment Pulse and Doublet Representation	74
13	Typical Pulse Strength and Pulse Centroid Plots	74
14	Altitude versus Time for the Chosen Flight Missions	75
15	Mach Number versus Time for the Chosen Flight Missions	75
16	Ambient Density versus Time for the Chosen Flight Missions	76

LIST OF ILLUSTRATIONS (Continued)

<u>Figure</u>		<u>Page</u>
17	Wall Temperature versus Time for the Chosen Flight Missions	76
18	Dynamic Pressure versus Altitude for the 9g Accelerated Flight Mission	77
19	Wing Geometry of the Vehicle Performing the Flight Missions	78
20	External Wing Cross-Section Geometry of the Vehicle Performing the Flight Missions	78
21	Effective Torsional Wing Stiffness versus Time for the Chosen Flight Missions and Several Values of the Parameter k .	79
22	Supersonic Three-Dimensional Analogy Planform with a Finite Band of Upwash on the Airfoil between $ost \leq \epsilon$	80
23	Supersonic Three-Dimensional Analogy Planform with an Impulsive Upwash Along the Leading Edge	80
24	Wing Geometry and Forward Mach Cone Representations	81
25	Equations Representing the Various Planform Curves and the Mach Lines	82
26	Integration Region for $ost \leq \epsilon$	83
27	Integration Region for $\epsilon st \leq t_0$	83
28	\bar{h} Time History due to Case 1 Initial Conditions Applied at $t_0 = 0$ and 10 Seconds Compared with Itself Approximately .45 Seconds Later; $ng = 9g$	84

LIST OF ILLUSTRATIONS (Continued)

<u>Figure</u>		<u>Page</u>
29	\bar{h} Time History Due to Case 1 Initial Conditions Applied at $t_0 = 20$ and 30 Seconds; $ng = 9g$	85
30	\bar{h} Time History Due to Case 2 Initial Conditions Applied at $t_0 = 0$ and 10 Seconds Compared with Itself Approximately .45 ^o Seconds Later; $ng = 9g$	86
31	\bar{h} Time History Due to Case 2 Initial Conditions Applied at $t_0 = 20$ and 30 Seconds; $ng = 9g$	87
32	α Time History Due to Case 1 Initial Conditions Applied at $t_0 = 0$ and 10 Seconds Compared with Itself Approximately .45 ^o Seconds Later; $ng = 9g$	88
33	α Time History Due to Case 1 Initial Conditions Applied at $t_0 = 20$ and 30 Seconds; $ng = 9g$	89
34	α Time History Due to Case 2 Initial Conditions Applied at $t_0 = 0$ and 10 Seconds Compared with Itself Approximately .45 ^o Seconds Later; $ng = 9g$	90
35	α Time History Due to Case 2 Initial Conditions Applied at $t_0 = 20$ and 30 Seconds; $ng = 9g$	91
36	\bar{h} Time History Due to Case 1 Initial Conditions Applied at $t_0 = 0$ and 10 Seconds Compared with Itself Approximately .45 ^o Seconds Later; $ng = 270 (1-\cos.2513t)$	92
37	\bar{h} Time History Due to Case 1 Initial Conditions Applied at $t_0 = 20$ and 30 Seconds; $ng = 270 (1-\cos.2513t)$	93
38	\bar{h} Time History Due to Case 2 Initial Conditions Applied at $t_0 = 0$ and 10 Seconds Compared with Itself Approximately .45 ^o Seconds Later; $ng = 270 (1-\cos.2513t)$	94
39	\bar{h} Time History Due to Case 2 Initial Conditions Applied at $t_0 = 20$ and 30 Seconds; $ng = 270 (1-\cos.2513t)$	95

Contrails

LIST OF ILLUSTRATIONS (Continued)

<u>Figure</u>		<u>Page</u>
40	α Time History Due to Case 1 Initial Conditions Applied at $t_0 = 0$ and 10 Seconds Compared with Itself Approximately .45 ^o Seconds Later; $ng = 270 (1-\cos.2513t)$	96
41	α Time History Due to Case 1 Initial Conditions Applied at $t_0 = 20$ and 30 Seconds; $ng = 270 (1-\cos.2513t)$	97
42	α Time History Due to Case 2 Initial Conditions Applied at $t_0 = 0$ and 10 Seconds Compared with Itself Approximately .45 ^o Seconds Later; $ng = 270 (1-\cos.2513t)$	98
43	α Time History Due to Case 2 Initial Conditions Applied at $t_0 = 20$ and 30 Seconds; $ng = 270 (1-\cos.2513t)$	99
44	\bar{h} and α Time Histories Observed First at $t = 0$ Seconds Due to Case 1 Initial Conditions Applied at $t_0 = 0$ Seconds; $ng = 270 (1-\cos.2513t)$	100
45	\bar{h} and α Time Histories Observed First at $t = 0$ Seconds Due to Case 2 Initial Conditions Applied at $t_0 = 0$ Seconds; $ng = 270 (1-\cos.2513t)$	101
46	\bar{h} and α Time Histories Observed First at $t = .4$ Seconds Due to Case 1 Initial Conditions Applied at $t_0 = 0$ Seconds; $ng = 270 (1-\cos.2513t)$	102
47	\bar{h} and α Time Histories Observed First at $t = .4$ Seconds Due to Case 2 Initial Conditions Applied at $t_0 = 0$ Seconds; $ng = 270 (1-\cos.2513t)$	103
48	\bar{h} and α Time Histories Observed First at $t = 2.0$ Seconds Due to Case 1 Initial Conditions Applied at $t_0 = 2.0$ Seconds; $ng = 270 (1-\cos.2513t)$	104
49	\bar{h} and α Time Histories Observed First at $t = 2.0$ Seconds Due to Case 2 Initial Conditions Applied at $t_0 = 2.0$ Seconds; $ng = 270 (1-\cos.2513t)$	105

LIST OF ILLUSTRATIONS (Continued)

<u>Figure</u>		<u>Page</u>
50	\bar{h} and α Time Histories Observed First at $t = 2.4$ Seconds Due to Case 1 Initial Conditions Applied at $t_0 = 2.0$ Seconds; $ng = 270 (1 - \cos.2513t)$	106
51	\bar{h} and α Time Histories Observed First at $t = 2.4$ Seconds Due to Case 2 Initial Conditions Applied at $t_0 = 2.0$ Seconds; $ng = 270 (1 - \cos.2513t)$	107
52	\bar{h} and α Time Histories Observed First at $t = 4.0$ Seconds Due to Case 1 Initial Conditions Applied at $t_0 = 4.0$ Seconds; $ng = 270 (1 - \cos.2513t)$	108
53	\bar{h} and α Time Histories Observed First at $t = 4.0$ Seconds Due to Case 2 Initial Conditions Applied at $t_0 = 4.0$ Seconds; $ng = 270 (1 - \cos.2513t)$	109
54	\bar{h} and α Time Histories Observed First at $t = 6.0$ Seconds Due to Case 1 Initial Conditions Applied at $t_0 = 6.0$ Seconds; $ng = 270 (1 - \cos.2513t)$	110
55	\bar{h} and α Time Histories Observed First at $t = 6.0$ Seconds Due to Case 2 Initial Conditions Applied at $t_0 = 6.0$ Seconds; $ng = 270 (1 - \cos.2513t)$	111

Contrails

LIST OF TABLES

<u>Table</u>		<u>Page</u>
1	Comparison of System Frequencies (cycles/second) Obtained by Various Methods of Analysis due to Case 1 Inputs for the Time Interval $0 \leq t_0 \leq 8$ Seconds; $ng = 270 (1 - \cos .2513t)$	112
2	Comparison of System Frequencies (cycles/second) Obtained by Various Methods of Analysis due to Case 1 Inputs for the Time Interval $10 \leq t_0 \leq 30$ Seconds; $ng = 270 (1 - \cos .2513t)$	113
3	Comparison of System Frequencies (cycles/second) Obtained by Various Methods of Analysis due to Case 2 Inputs for the Time Interval $0 \leq t_0 \leq 8$ Seconds; $ng = 270 (1 - \cos .2513t)$	114
4	Comparison of System Frequencies (cycles/second) Obtained by Various Methods of Analysis due to Case 2 Inputs for the Time Interval $10 \leq t_0 \leq 30$ Seconds; $ng = 270 (1 - \cos .2513t)$	115
5	Comparison of System Frequencies (cycles/second) Obtained by Various Methods of Analysis due to both Case 1 and Case 2 Inputs for the Time Interval $0 \leq t_0 \leq 30$ Seconds; $ng = 9g$	116

LIST OF PRINCIPAL SYMBOLS

a_{∞}	free stream speed of sound
b	airfoil semi-chord
c_m	specific heat of the wing material
$h(t)$	flight mission altitude
$\bar{h}(t)$	vertical displacement of airfoil (plunging motion)
$h(y)$	wing thickness
h^*	heat transfer coefficient
P_{\pm}	upper (lower) wing surface pressure
$P^n = \frac{d^n}{dt^n}$	n^{th} order differential operator
t	time; streamwise space variable for three-dimensional wing
$w_a(x,t)$	upwash on the airfoil surface
w_o	transverse displacement of wing midplane
x_o	dimensionless distance from leading edge to elastic axis
x_1	dimensionless distance from leading edge to aileron hinge line
x, y, z	space variables
A	value of constant forward acceleration
$F = \frac{bA}{a_{\infty}^2}$	Froude number (Acceleration Parameter)
GJ	isothermal torsional stiffness
GJ_{EFF}	effective torsional stiffness
I_{α}	wing cross section moment of inertia about the elastic axis

LIST OF PRINCIPAL SYMBOLS (Continued)

L	wing lift
$L_c(\tau, t-\tau)$	lift due to impulsive plunging motion
$L_\rho(\tau, t-\tau)$	lift due to impulsive pitch rate about the airfoil leading edge
M	Mach number
\bar{M}	wing cross section mass
$M^*(t)$	thermal moment resultant acting on wing cross section
$M_c(\tau, t-\tau)$	moment due to impulsive plunging motion
$M_\rho(\tau, t-\tau)$	moment due to impulsive pitch rate about the airfoil leading edge
M_{x_0}	wing moment about the elastic axis
M_{x_1}	wing moment about the aileron hinge line
S_α	wing cross section static unbalance about the elastic axis
$T(\gamma, \xi, t)$	wing temperature at a point γ, ξ at time t
$T_w(\gamma, \xi, t)$	wing equilibrium wall temperature
$T^*(t)$	thermal force resultant acting on a wing cross section
τ	torque due to thermal gradients and pre-twist
τ_t	total torque (Saint-Venant plus thermally induced torque)
U	airspeed
$\alpha(t)$	airfoil angle of attack
$\beta(t)$	aileron angle of attack relative to $\alpha(t)$

LIST OF PRINCIPAL SYMBOLS (Continued)

γ	specific heat
$\delta(t-\tau)$	unit impulse function (Dirac delta function)
ϵ	width of upwash band on three-dimensional wing
ϵ_x	total strain in X direction, including thermal effects
ξ, η, τ	dummy integration variables
ρ_m	wing mass density
ρ_∞	free stream density
σ_x	total stress in X direction including thermal effects
$\phi(x)$	wing twist distribution
$\phi(x, z, t)$	velocity potential
ω_h	wing plunging oscillation frequency
ω_α	wing pitching oscillation frequency
ω_β	aileron pitching oscillation frequency
$\Theta(t, y)$	non-dimensional wing temperature

Contrails

SECTION I

PRESENTATION OF THE REQUIRED AERODYNAMIC
AND
AEROTHERMOELASTIC THEORIES1.1 Introduction

The object of Part II of this report is to formulate and investigate the equations representing the dynamic, torsion-bending motion of a wing which is one major component of an ultra-high performance manned vehicle that is performing some specified flight mission(s). A necessary step in obtaining this object is the derivation of the terms required to compute the time-varying coefficients of the governing equations. The derivation of these terms is necessary for the following reasons. Firstly, it is noted that a highly accelerated flight mission performed at supersonic speeds may introduce conditions that invalidate the well-known solution (Ref. 1) for the torsional stiffness loss of an aircraft wing that includes the effects of a specified time-dependent wall temperature due to the given flight mission and that includes the effects of large wing deformations due to the large magnitude transient thermal stresses produced by the given flight mission. Secondly, it is noted that although "piston theory" aerodynamics is widely in use throughout the aeronautical industry, its use as a mathematical representation for arbitrary motion may be unfamiliar. Thus it is felt that a brief re-derivation of this topic may be useful to the reader.

Manuscript released by the author December 1960 for publication as a WADD Technical Report.

Contrails

Thirdly, in order to provide an aerodynamic theory that does not yield the simplified quasi-steady results of piston theory and additionally accounts for the direct effects of acceleration, it is necessary to consider the exact two-dimensional linearized aerodynamic theory for an accelerating unsteady supersonic airfoil. Isolated accounts of this theory have appeared during the last decade but none of these works possess the details necessary for the purposes of this report.

Thus the following three sub-sections present the derivations necessary to determine the time-varying coefficients that will be used in the latter sections of this report.

1.2 Loss of Torsional Stiffness due to Aerodynamic Heating Including the Effects of Mid-Plane Stretching, Finite Acceleration and Varying State Values

In recent years several articles (Ref. 1,2,3,) have appeared concerning the loss of wing torsional stiffness due to aerodynamic (kinetic) heating. The solution most widely known to the members of the aeronautical profession however, adopts a mathematical model that considers an infinite acceleration to attain some final Mach number. Thus a constant wall temperature exists during the time that the wing is undergoing a torsional stiffness loss. Additionally, this model is based on the small deflection theory of elasticity. Since this model may be inadequate for the supersonic velocity, finite acceleration flight missions envisioned, the important features of Reference 3 are incorporated into the model presented in this sub-section as well as a means for including the effects of arbitrary finite acceleration and varying state (density, etc.) values.

Contrails

To this end, consider a plate-like wing as shown in Figure 1, which is assumed to have an x-direction uniaxial stress and strain distribution. Utilizing the finite bending theory of thin plates, the total strain in the x-direction is given by

$$\epsilon_x = \epsilon_{ox} - \zeta \frac{\partial^2 w_o}{\partial x^2} + \frac{1}{2} \left(\frac{\partial w_o}{\partial x} \right)^2 \quad (1.1)$$

where

$$\begin{aligned} \epsilon_{ox} &= \text{mid-plane strain at } \zeta = 0 \\ \zeta \frac{\partial^2 w_o}{\partial x^2} &= \text{strain due to bending} \\ \frac{1}{2} \left(\frac{\partial w_o}{\partial x} \right)^2 &= \text{strain due to finite transverse displacement} \end{aligned}$$

Now assuming that the mid-plane strain is given as $\epsilon_{ox} = \delta + \beta y$, where δ and β are as yet undetermined time-dependent coefficients, and by using Singer's approximation for $w_o = kxy$,* where k is the angle of twist per unit length, the total strain is given as

$$\epsilon_x = \delta + \beta y + \frac{1}{2} k^2 y^2 \quad (1.2)$$

Hence the total stress, including thermal gradients, is given as

$$\sigma_x(y,z,t) = E \left\{ \delta + \beta y + \frac{1}{2} k^2 y^2 - \alpha [T(y,z,t) - T_w(y,z,0)] \right\} \quad (1.3)$$

where

E = Modulus of elasticity

*Reference 3 demonstrates that this extremely simple formula yields at most 5% errors in deflections when compared with exact solutions.

Contrails

$T(y,z,t)$ = actual wing temperature at $(y,z,)$
during time t
 $T_w(y,z,0)$ = a reference temperature, chosen to be
the wing equilibrium temperature at
 $t = 0$

In order to insure zero force and moment resultants at all wing cross-sections it is required that

$$\int_A \sigma_x dA = 0$$
$$\int_A y \sigma_x dA = 0$$
(1.4)

where A is the cross-sectional area.

However, the choice of the w_0 function and the additional assumption of a thermally thin wing dictates that $\frac{\partial \sigma_x}{\partial z} = 0$ throughout the wing, thus Eq. (1.4) is replaced by the following simpler statement.

$$\int_{-b}^b h \sigma_x dy = 0$$
$$\int_{-b}^b h y \sigma_x dy = 0$$
(1.5)

where $h = h(y)$ is the local wing thickness. Now if E is at most $E = E(t)$ * the introduction of Eq. (1.3) into Eq. (1.5) yields the results

$$\begin{bmatrix} A & A^* \\ A^* & I_y \end{bmatrix} \begin{Bmatrix} \delta \\ \beta \end{Bmatrix} = \begin{Bmatrix} \alpha T^* - \frac{k^2}{2} I_y \\ \alpha M^* - \frac{k^2}{2} \psi \end{Bmatrix}$$
(1.6)

* In other words, not a function of y and z . Actually $E = \text{const.}$ is a good approximation for the work that follows and is thus considered as such.

Contrails

where

$$A = \int_{-b}^b h dy = \text{cross sectional area}$$

$$A^* = \int_{-b}^b h y dy \quad (= 0 \text{ for a symmetrical cross section})$$

$$I_y = \int_{-b}^b h y^2 dy = \text{moment of inertia}$$

$$\Psi = \int_{-b}^b h y^3 dy \quad (= 0 \text{ for a symmetrical cross section})$$

$$T^*(t) = \int_{-b}^b h [T(t, y) - T_w(0)] dy = \text{thermal force}$$

$$M^*(t) = \int_{-b}^b h y [T(t, y) - T_w(0)] dy = \text{thermal moment}$$

Solving Eq. (1.6) yields the following results:

$$\begin{aligned} \delta(t) &= (AI_y - A^{*2})^{-1} \left\{ \alpha [I_y T^*(t) - A^* M^*(t)] + \frac{k^2}{2} [A^* \Psi - I_y^2] \right\} \\ \beta(t) &= (AI_y - A^{*2})^{-1} \left\{ \alpha [A M^*(t) - A^* T^*(t)] + \frac{k^2}{2} [A^* I_y - A \Psi] \right\} \end{aligned} \quad (1.7)$$

At this point, $\sigma_x(y, t)$ is completely determined once k and $T(t, y) - T_w(0)$ have been specified. The next step in the calculation is to relate the stress distribution to the ensuing loss in torsional stiffness. Following the simplified development given in Reference 1, attention is focused on Figure 2 which pictures a longitudinal "fiber"

Contrails

originally in the position A-B of a wing structure located at a distance r from the axis of twist, which has been given an incremental twist of magnitude $\frac{d\phi}{dx} dx$; thus the fiber is now in the position A'-B'. If the stress σ_x is still axially aligned with the fiber, now in the position A'-B', it is seen that a small component of this stress acts in the plane of the wing cross-section. This stress component is given by $\sigma_x r \frac{d\phi}{dx}$. Thus the incremental twisting moment about the axis of twist is given as $d\tau = \sigma_x r^2 \frac{d\phi}{dx} dA$. Integration over the cross-section yields the result

$$\tau = \frac{d\phi}{dx} \int_A \sigma_x r^2 dA \quad (1.8)$$

When Eq. (1.8) is added to the usual Saint-Venant torque, the total torque τ_t becomes

$$\tau_t = \left\{ GJ + \int_A \sigma_x r^2 dA \right\} \frac{d\phi}{dx} \quad (1.9)$$

It is immediately seen that the bracket term is physically just an effective torsional stiffness which will be denoted by GJ_{eff} . Thus,

$$GJ_{\text{eff}} = GJ + \int_A \sigma_x r^2 dA \quad (1.10)$$

Where GJ is now more descriptively termed an iso-thermal torsional stiffness and will be denoted by $GJ_{\text{Iso-thermal}}$. The next reduction is to incorporate GJ_{eff} into an expression for the square of a wing torsional frequency ω_x^2 since this is the term in which the stiffness appears in the equations of motion. This is accomplished by

Contrails

utilizing the Rayleigh method. Thus, for a constant cross-section wing of semi-span L , ω_α^2 is given by

$$\omega_\alpha^2 = \frac{GJ_{EFF}}{I_\alpha} \int_0^L \left(\frac{d\phi}{dx}\right)^2 dx / \int_0^L \phi^2 dx$$

where ϕ is simply chosen as

$$\phi = \sin \frac{\pi x}{2L}$$

Thus, a simple integration yields the result that

$$\omega_\alpha^2(t) = \frac{\pi^2 GJ_{EFF}(t)}{4L^2 I_\alpha} \quad (1.11)$$

The last step in the calculation of $\omega_\alpha^2(t)$ is to determine the temperature distribution time history of the wing.

Proceeding and assuming a solid thermally-thin wing, the heat balance equation governing the temperature at any chordwise distance y is given by

$$\frac{\partial \Theta}{\partial t} + F \Theta = F D \quad (1.12)$$

with the initial condition

$$\Theta(0, y) = 0$$

where

$$\Theta(t, y) = \frac{T(t, y) - T_w(0)}{T_w(t^*) - T_w(0)} \quad \begin{array}{l} h^* = \text{heat-transfer coefficient} \\ \rho_m = \text{mass density of the wing} \\ c_m = \text{specific heat of the wing} \end{array}$$

$$D(t) = \frac{T_w(t) - T_w(0)}{T_w(t^*) - T_w(0)} \quad \begin{array}{l} h(y) = \text{wing thickness} \\ T(t, y) = \text{wing temperature} \\ T_w(t) = \text{wall temperature} \end{array}$$

$$F(t, y) = \frac{2h^*(t, y)}{\rho_m c_m h(y)}$$

Contrails

$T_w(0)$ = equilibrium wall temperature at $t = 0$

$T_w(t^*)$ = final equilibrium wall temperature at $t = t^*$

Fortunately, Eq. (1.12) is a first order linear differential equation in $\Theta(t, y)$ with time-varying coefficients. Furthermore, y only plays the role of a parameter.

Utilizing a standard technique, the left-hand side of Eq. (1.12) is made an exact differential by multiplying the entire equation by an appropriate integrating factor ν . This integrating factor is given by $e^{\int^t F(\xi, y) d\xi}$.

The solution for $\Theta(t, y)$ then becomes,

$$\Theta(t, y) = e^{-\int^t F(\xi, y) d\xi} \left\{ \text{CONST.} + \int^t F(\eta, y) D(\eta) e^{\int^{\eta} F(\xi, y) d\xi} d\eta \right\} \quad (1.13)$$

where the constant term is determined by the condition

$$\Theta(0, y) = 0$$

Thus, once a particular flight mission is specified and the wing properties are given, the required square of the torsional frequency $\omega_x^2(t)$ can be calculated.

1.3 Arbitrary Motion Piston Theory

Although Ashley and Zartarian (Ref. 4) have suggested the use of piston theory in problems involving arbitrary motion, no work of this nature exists to the authors knowledge. Thus, it may be useful to retrace the formulation of the piston theory equations, retaining the arbitrary motion characteristics of the airfoil in question.

Referring to Figure 3 and noting that (1) lift is defined positive downward (2) moment about the elastic axis is defined positive nose up and (3) moment about the

Contrails

aileron hinge line is defined positive trailing edge down, the expressions for the lift and moments are given by

$$\begin{aligned} \frac{L}{2b} &= \int_0^{x_1-\epsilon} [P_u(x) - P_l(x)] dx + \int_{x_1-\epsilon}^1 [P_u(x) - P_l(x)] dx \\ \frac{M_{x_0}}{4b^2} &= \int_0^{x_1-\epsilon} [P_u(x) - P_l(x)] [x - x_0] dx + \int_{x_1-\epsilon}^1 [P_u(x) - P_l(x)] [x - x_0] dx \\ \frac{M_{x_1}}{4b^2} &= \int_{x_1-\epsilon}^1 [P_u(x) - P_l(x)] [x - x_1] dx \end{aligned} \quad (1.14)$$

At this point the "piston" assumption is introduced by using the second order binomial expansion expression for the pressure difference in a tube with a moving piston to represent the pressure(s) on the upper and lower surface of an oscillating wing. The pressure difference $[P_u(x) - P_l(x)]$ of Eq. (1.14) is then given as

$$P_u - P_l = -2\rho_\infty a_\infty U f(x,t) \left[1 + \frac{U(\gamma+1)}{4a_\infty} \frac{d\tau}{dx} \right] \quad (1.15)$$

where

- ρ_∞ = free stream density
- a_∞ = free stream speed of sound
- U = airspeed
- γ = specific heat
- $\tau(x)$ = non-dimensional thickness

and $f(x,t)$, which describes the oscillatory motion of the wing, is given as

$$f(x,t) = \begin{cases} \frac{\dot{h}(t)}{U} + \alpha(t) + \frac{2b}{U} \dot{\alpha}(t) [x - x_0] & ; 0 \leq x \leq x_1 \\ \frac{\dot{h}(t)}{U} + \alpha(t) + \frac{2b}{U} \dot{\alpha}(t) [x - x_0] + \beta(t) + \frac{2b}{U} \dot{\beta}(t) [x - x_1] & ; 1 \geq x \geq x_1 \end{cases} \quad (1.16)$$

where

$$\bar{h}(t) = \text{dimensional plunging motion}$$

Contrails

$\alpha(t)$ = airfoil angle of attack

$\beta(t)$ = aileron angle of attack relative to the angle α

and it has been tacitly assumed that the airfoil has an aerodynamically unbalanced flap so that $\epsilon = 0$.

Using Eqs. (1.15) and (1.16) the lift and moments given in Eq. (1.14) can be written as

$$\begin{aligned} \frac{-L}{2b} = & 2\rho_{\infty} a_{\infty} U \int_0^1 \left[1 + \frac{U(\gamma+1)}{4a_{\infty}} \left(\frac{d\tau}{dx} \right) \right] \left[\frac{\dot{h}}{U} + \alpha + \frac{zb}{U} \dot{\alpha}(x-x_0) \right] dx \\ & + 2\rho_{\infty} a_{\infty} U \int_{x_1}^1 \left[1 + \frac{U(\gamma+1)}{4a_{\infty}} \left(\frac{d\tau}{dx} \right) \right] \left[\beta + \frac{zb}{U} \dot{\beta}(x-x_1) \right] dx \end{aligned} \quad (1.17)$$

$$\begin{aligned} \frac{-M_{x_0}}{4b^2} = & 2\rho_{\infty} a_{\infty} U \int_0^1 \left[1 + \frac{U(\gamma+1)}{4a_{\infty}} \left(\frac{d\tau}{dx} \right) \right] \left[\frac{\dot{h}}{U} + \alpha + \frac{zb}{U} \dot{\alpha}(x-x_0) \right] [x-x_0] dx \\ & + 2\rho_{\infty} a_{\infty} U \int_{x_1}^1 \left[1 + \frac{U(\gamma+1)}{4a_{\infty}} \left(\frac{d\tau}{dx} \right) \right] \left[\beta + \frac{zb}{U} \dot{\beta}(x-x_1) \right] [x-x_0] dx \end{aligned} \quad (1.18)$$

$$\begin{aligned} \frac{-M_{x_1}}{4b^2} = & 2\rho_{\infty} a_{\infty} U \int_{x_1}^1 \left[1 + \frac{U(\gamma+1)}{4a_{\infty}} \left(\frac{d\tau}{dx} \right) \right] \left[\frac{\dot{h}}{U} + \alpha + \frac{zb}{U} \dot{\alpha}(x-x_0) + \beta + \frac{zb}{U} \dot{\beta}(x-x_1) \right] [x-x_1] dx \end{aligned} \quad (1.19)$$

Since the above equations will be utilized, for the purposes of this report, only in their zero-thickness ($\gamma=0$) form, the $\frac{d\tau}{dx}$ term appearing in Eqs. (1.17), (1.18), and (1.19) will be set equal to zero when performing the integrations. However, if the reader wishes to retain the thickness terms, the following summary of integrals that involve thickness terms in the above formulas may be of interest.

Contrails

$$\int_0^1 \frac{d\tau}{dx} dx = \tau(1) - \tau(0)$$

$$\int_{x_1}^1 \frac{d\tau}{dx} dx = \tau(1) - \tau(x_1)$$

$$\int_0^1 x \frac{d\tau}{dx} dx = \tau(1) - \frac{A_w}{(2b)^2}$$

$$\int_{x_1}^1 x \frac{d\tau}{dx} dx = \tau(1) - x_1 \tau(x_1) - \frac{A_F}{(2b)^2}$$

$$\int_0^1 x^2 \frac{d\tau}{dx} dx = \tau(1) - \frac{2M_w}{(2b)^3}$$

$$\int_{x_1}^1 x^2 \frac{d\tau}{dx} dx = \tau(1) - x_1^2 \tau(x_1) - \frac{2M_F}{(2b)^3}$$

where

A_w = total wing cross-section area

A_F = flap cross-section area

M_w = first area-moment of total wing cross-section about the leading edge

M_F = first area-moment of flap cross-section about the leading edge.

Proceeding, the integrated values of L , M_{x_0} , and M_{x_1} (for zero-thickness) become

$$\begin{aligned} -L = 4b\rho_\infty a_\infty \dot{h} + 4b\rho_\infty a_\infty U \alpha + 4b^2\rho_\infty a_\infty (1-2x_0) \dot{\alpha} + 4b\rho_\infty a_\infty U (1-x_1) \beta \\ + 4b^2\rho_\infty a_\infty (1-x_1)^2 \dot{\beta} \end{aligned} \quad (1.20)$$

$$\begin{aligned} M_{x_1} = 4b^2\rho_\infty a_\infty (x_1[2+x_1]-1) \dot{h} + 4b^2\rho_\infty a_\infty U (x_1[2+x_1]-1) \alpha \\ + \frac{8}{3} b^3\rho_\infty a_\infty (3x_0[1-x_1]^2 - x_1[x_1^2-3]-2) \dot{\alpha} - 4b^2\rho_\infty a_\infty U (1-x_1)^2 \beta \\ - \frac{16}{3} b^3\rho_\infty a_\infty ([1-x_1^3] - 3x_1[1-x_1]) \dot{\beta} \end{aligned} \quad (1.21)$$

$$\begin{aligned}
 M_{x_0} = & 4b^2 \rho_\infty a_\infty (2x_0 - 1) \dot{h} + 4b^2 \rho_\infty a_\infty U (2x_0 - 1) \alpha + 4b^3 \rho_\infty a_\infty \left[4x_0(1-x_0) - \frac{4}{3} \right] \dot{\alpha} \\
 & + 4b^2 \rho_\infty a_\infty U (1-x_1)(2x_0 - 1 - x_1) \beta + \frac{8}{3} b^3 \rho_\infty a_\infty (3x_0[1-x_1]^2 - x_1[x_1^2 - 3] - 2) \dot{\beta}
 \end{aligned} \quad (1.22)$$

1.4 Exact Two-Dimensional Linearized Aerodynamic Theory for an Accelerating Unsteady Supersonic Airfoil

The preceding sub-section has dealt with a theory that utilizes an instantaneous point function relationship between the vertical component of the airfoil velocity and the pressure at any point on a two-dimensional wing. This relationship has been found to be quite satisfactory for constant flow velocity problems in which the flow velocity is within a rather wide range of supersonic speeds. At the lower supersonic speeds however, the piston theory concept yields less accurate results since the time history of the airfoil downwash contributes appreciably to the pressure expressions. Additionally, the piston theory concept is unable to show the direct effects of airfoil forward acceleration in any velocity regime.

In order to overcome these possible deficiencies, this sub-section presents the exact two-dimensional linearized aerodynamic theory for an accelerating unsteady supersonic airfoil. This presentation will then permit a comparison of this more exact theory with the linearized version of piston theory. Since it is not possible, in general, to obtain exact solutions for the theory given in this sub-section, it was decided to solve the relatively easy problem that leads to the determination of the various impulse responses of the airfoil.

Contrails

As will be seen, these impulse responses provide a clear indication of the effects of both the time history of the airfoil motion and the forward acceleration as well as providing the kernel functions necessary for an integral formulation of the lift and moment expressions for arbitrary motion. This work will be facilitated by utilizing a remarkable analogy that exists between a two-dimensional accelerating unsteady airfoil problem and a three-dimensional steady flow airfoil problem in which the main stream Mach number is fixed at $M = \sqrt{2}$. It is perhaps easiest to understand this analogy by first considering the two-dimensional accelerating unsteady airfoil problem and the three-dimensional steady flow problem separately, and then note the conditions under which they are identical. A necessary part of this identification process will include the matching of the boundary conditions of each problem. To this end the statements of both problems are now given, and then compared. The analogy will then be apparent.

Two-Dimensional Accelerating Unsteady Airfoil Problem

Fixing a planar x, z , axis system in space and permitting a two-dimensional airfoil to translate along the negative x -axis with a supersonic velocity $U(t)$, the unsteady equation of motion of this airfoil in terms of its velocity potential ϕ is given (see Fig. 4) by

$$\phi_{xx} + \phi_{zz} = \frac{1}{a_\infty^2} \phi_{t^*t^*} \quad (1.23)$$

with the moving boundary conditions

$$\left. \phi_z \right|_{z=0^+} = W_a(x, t^*) \quad \text{on the airfoil} \quad (1.24)$$

Contrails

$$\varphi_{t^*} = 0 \quad \text{off the airfoil} \quad (1.25)$$

At any given time t^* the position of the airfoil along the x-axis is given by

$$-\int_0^{t^*} U(\xi) d\xi \leq x \leq zb - \int_0^{t^*} U(\xi) d\xi \quad (1.26)$$

and the pressure difference across the airfoil is given as

$$P_L - P_U = 2\rho_\infty \varphi_{t^*} \quad (1.27)$$

A new variable $t = a_\infty t^*$, which has the dimensions of a length, is now introduced so that Eqs. (1.23) through (1.27) become

$$\varphi_{tt} - \varphi_{xx} - \varphi_{zz} = 0 \quad (1.28)$$

$$\left. \varphi_z \right|_{z=0^{\pm}} = w_a(x, t) \quad \text{on the airfoil} \quad (1.29)$$

$$\varphi_t = 0 \quad \text{off the airfoil} \quad (1.30)$$

$$-\frac{1}{a_\infty} \int_0^t U(\xi) d\xi \leq x \leq zb - \frac{1}{a_\infty} \int_0^t U(\xi) d\xi \quad (1.31)$$

$$P_L - P_U = 2\rho_\infty a_\infty \varphi_t \quad (1.32)$$

To reiterate, Eqs. (1.28) through (1.32) represent the unsteady motion problem of a two-dimensional airfoil moving through a fluid with a supersonic velocity $U(t)$. Since the axis system is fixed in the fluid, the airfoil moves with respect to this axis. Thus the boundary conditions, imposed by the presence of the airfoil in the

fluid, must be applied along a moving line segment of length $2b$ in the fluid. Various details of this problem may be obtained in References 5, 6, and 7.

Three Dimensional, Steady Flow Problem

Fixing a spatial t, x, z , axis system on a three-dimensional wing and letting a supersonic airstream flow past this wing with a constant Mach number $M > 1$, the steady flow equation of motion of this wing in terms of its velocity potential ϕ is given (see Fig. 5) by

$$(M^2 - 1)\phi_{tt} - \phi_{xx} - \phi_{zz} = 0 \quad (1.33)$$

with the fixed boundary conditions

$$\left. \phi_z \right|_{z=0^\pm} = W_a(t, x) \quad \text{on the airfoil} \quad (1.34)$$

$$\phi_t = 0 \quad \text{off the airfoil} \quad (1.35)$$

Additionally, the pressure difference is given by

$$P_l - P_u = 2\rho_\infty U \phi_t \quad (1.36)$$

where U is given by the relation $U = Ma_\infty$.

Now that the formulations of both problems have been presented, it is an easy task to determine under what conditions Eq. (1.28) through (1.32) are equivalent to Eqs. (1.33) through (1.36). The first observation is that the boundary conditions (1.29) and (1.30) are identical to (1.34) and (1.35), while the pressure difference formulas (1.32) and (1.36) differ only by a factor of (U/a_∞) .

Contrails

Additionally, if M^2 is given the value $M^2=2$, Eq. (1.33) is identical to Eq. (1.28). The final matching condition is concerned with Eq. (1.31) which gives the position of the two-dimensional airfoil along the x-axis as a function of t^* . This information could have been presented in a slightly different form by explicitly writing down the x coordinates of the airfoil leading edge $x_{L.E.}$ and the airfoil trailing edge $x_{T.E.}$ as a function of t^* . Thus (1.31) would have yielded the information that

$$x_{L.E.} = f_1(t) \quad (1.37)$$

$$x_{T.E.} = f_2(t) \quad (1.38)$$

where

$$f_1(t) = -\frac{1}{a_\infty} \int_0^t U(\tau) d\tau \quad (1.39)$$

$$f_2(t) = z b - \frac{1}{a_\infty} \int_0^t U(\tau) d\tau \quad (1.40)$$

Thus if the three-dimensional wing planform is now defined by the relations $x_{L.E.} - f_1(t) = 0$ and $x_{T.E.} - f_2(t) = 0$, the analogy between the two-dimensional unsteady, accelerating airfoil problem and the three-dimensional steady flow problem is completely established.

Utilizing this analogy it is possible to treat the entire forward speed range, subsonic and supersonic, of the two-dimensional airfoil flying at a constant altitude. However, since a subsonic forward speed

Contrails

requires that the three-dimensional "analogy" wing possess subsonic leading and trailing edges, the computational labor (for example see references 8 and 9) becomes prohibitive. For this reason, the present investigation was limited to speeds of sonic and supersonic magnitudes.

Rigorously speaking, the theory presented above is valid only for constant altitude flight. However the results and discussion contained in Appendix I show that except at $M \leq 1$ the variable altitude cases may be very satisfactorily treated by simply considering the state variables as given functions of time.

At this point all the necessary mathematical tools are available to calculate the time-varying pressure distribution on the two-dimensional supersonic airfoil by first obtaining the pressure distribution on the steady flow, three-dimensional analogy wing and then transforming the result according to Eqs. (1.32) and (1.36). As previously explained the pressure distributions, and eventually the integrated lifts and moments, will be obtained that correspond to the various upwash impulse responses of the two-dimensional airfoil. For the rigid chord airfoil, two upwash impulse responses, corresponding to impulsive plunging motion and to impulsive pitch rate motion (i.e. constant and linear chordwise variation in instantaneous upwash), are required to represent motion dependent forces. The determination of these upwash impulse responses requires careful integration techniques since the already singular integrals inherent in the formulation are further complicated by the required singular upwash distributions. Thus a finite band of upwash will be used in formulating the expressions for the upwash responses and then a limiting process will be used to

Contrails

rigorously determine the true impulse responses. When this limiting process is applied, many integration regions on the three-dimensional analogy wing (these regions being defined by intersections of various Mach lines) vanish, thus these vanishing regions must be examined to make sure that they leave no residual contributions to the pressure distribution. This work, as well as the rest of the details required to obtain the various upwash impulse responses, is quite lengthy. Since an outline of the procedure for obtaining the upwash impulse responses is given in Appendix II, just the final results of this procedure are now presented for a rigid chord* airfoil with a constant forward acceleration.

Lift and Moment Due to Upwash Caused by Impulsive Plunging.

$$L_c(\tau, x') = \begin{cases} -4b\rho_\infty a_\infty \delta(x') & \text{Region I} \\ -\frac{4}{\pi} b\rho_\infty a_\infty \sqrt{1 - \left(\frac{1 - F(\tau, x')}{x'}\right)^2} & \text{Region II} \\ 0 & \text{Region III} \end{cases} \quad (1.41)$$

$$M_c(\tau, x') = \begin{cases} -4b^2\rho_\infty a_\infty [d(x') - x'] & \text{Region I} \\ -\frac{8}{\pi} b^2\rho_\infty a_\infty \left[\frac{x'}{2} \cos^{-1}\left(\frac{-1 + F(\tau, x')}{x'}\right) - \frac{1 + F(\tau, x')}{2} \sqrt{1 - \left(\frac{1 - F(\tau, x')}{x'}\right)^2} \right] & \text{Region II} \\ 0 & \text{Region III} \end{cases} \quad (1.42)$$

*As will be seen in Appendix II, upwash distributions of higher power in the chordwise variable present no difficulties, thus flexible chord airfoils may also be treated by this technique.

Contrails

Lift and Moment Due to Upwash Caused by an Impulsive Pitch Rate about the Leading Edge

$$L_p(\tau, x') = \begin{cases} -4b\rho_\infty a_\infty [\delta(x')/2 + x'/2] & \text{Region I} \\ -\frac{4}{\pi} b\rho_\infty a_\infty \left[\frac{x'}{2} \cos^{-1} \left(\frac{-1+F(\tau, x')}{x'} \right) + \left(\frac{1-F(\tau, x')}{2} \right) \sqrt{1 - \left(\frac{1-F(\tau, x')}{x'} \right)^2} \right] & \text{Region II} \\ 0 & \text{Region III} \end{cases} \quad (1.43)$$

$$M_p(\tau, x') = \begin{cases} 8b^2\rho_\infty a_\infty \left\{ \frac{\delta(x')}{3} + \frac{x'}{2} F(\tau, x') \right\} & \text{Region I} \\ -\frac{8}{\pi} b^2\rho_\infty a_\infty \left\{ \frac{(x')^2}{3} \left[1 - \left(\frac{1-F(\tau, x')}{x'} \right)^2 \right]^{3/2} - F(\tau, x') \left[\frac{1-F(\tau, x')}{2} \sqrt{1 - \left(\frac{1-F(\tau, x')}{x'} \right)^2} + \frac{x'}{2} \cos^{-1} \left(\frac{-1+F(\tau, x')}{x'} \right) \right] \right\} & \text{Region II} \\ 0 & \text{Region III} \end{cases} \quad (1.44)$$

where

$$x' = t - \tau$$

$$F(\tau, x') = [M_0(\tau)] [t - \tau] + \mathcal{F} [t - \tau]^2$$

$$\mathcal{F} = bA/a_\infty^2 = \text{Froude number}$$

A = Value of the constant forward acceleration

$\delta(x')$ = Unit impulse function (Dirac delta function)

- ()_c Refers to constant upwash condition due to impulsive plunging
- ()_l Refers to linearly varying upwash condition due to impulsive pitch rate about the leading edge.

Region I is given by

$$\tau \leq t \leq \tau - \frac{M_0 + 1}{2\mathcal{F}} + \sqrt{\left(\frac{M_0 + 1}{2\mathcal{F}} \right)^2 + \frac{1}{\mathcal{F}}} \quad (1.45)$$

Contrails

Region II is given by

$$\tau - \frac{M_0 + 1}{2\beta} + \sqrt{\left(\frac{M_0 + 1}{2\beta}\right)^2 + \frac{1}{\beta}} \leq t \leq \tau - \frac{M_0 - 1}{2\beta} + \sqrt{\left(\frac{M_0 - 1}{2\beta}\right)^2 + \frac{1}{\beta}} \quad (1.45)$$

Region III is given by

$$t \geq \tau - \frac{M_0 - 1}{2\beta} + \sqrt{\left(\frac{M_0 - 1}{2\beta}\right)^2 + \frac{1}{\beta}}$$

If a non-constant forward acceleration is to be considered, it is only necessary to re-define the $F(\tau, t-\tau)$ term and the integration regions. Thus for non-constant acceleration beginning at $t=\tau=0$, the only changes in the above equations are given as

$$F(\tau, t-\tau) = -\frac{1}{a_\infty} \left[\int_0^\tau U(\xi) d\xi - \int_0^t U(\xi) d\xi \right]$$

$$\text{Region I is given by } 0 \leq t \leq t_4 \quad (1.46)$$

$$\text{Region II is given by } t_4 \leq t \leq t_6$$

$$\text{Region III is given by } t \geq t_6$$

where t_4 and t_6 are given by the following implicit relations

$$t_4 - \tau = 1 - F(\tau, t_4 - \tau) \quad (1.47)$$

$$t_6 - \tau = -1 + F(\tau, t_6 - \tau)$$

In order to obtain an indication of the effects of airfoil time history and forward acceleration, Figures 6 through 9 present the lift and moment impulse responses for instantaneous Mach numbers $M_0(\tau)$ equal to 1.0, 1.5, and 2.0. Zero, moderate and very large accelerations are considered in each case by choosing Froude numbers equal to 0, 1×10^{-2} , and 1×10^{-1} . These Froude numbers correspond to accelerations of 0, 300, and 3000g for a 1 foot semi-chord airfoil or to accelerations of 0,

Contrails

30, and 300g for a 10 foot semi-chord airfoil. Additionally, the influence of very large deceleration ($\ddot{\gamma} = -1 \times 10^{-1}$) is shown for Mach number $M_o(\tau) = 2$. Figures 6 through 9 reveal the following features about the lift and moment impulse responses:

- A. The portions of the lift and moment impulse responses containing the delta functions are independent of Mach number and acceleration. In fact they are equal to the impulse responses calculated by piston theory aerodynamics.
- B. The influence of increasing the Mach number $M_o(\tau)$ and/or the acceleration ($\sim \ddot{\gamma}$) is to cause the lift and moment impulse responses to attenuate more rapidly.
- C. Except at Mach number $M_o(\tau) \cong 1$ the influence of acceleration is microscopic compared to the influence of the Mach number $M_o(\tau)$.
- D. Increasing the Mach number $M_o(\tau)$ brings the present theory rapidly into close agreement with the simpler piston theory results.

Additionally, Figures 6 through 9 imply that it is advantageous to distinguish between the influence of the quasi-steady variation of Mach number (which is the time history effect) and the direct influence of the acceleration (which is embodied in the $\ddot{\gamma}$ terms); since, once it is shown that the quasi-steady variation of Mach number dominates the direct acceleration effects, then the two-dimensional airfoil calculations are somewhat simplified and (perhaps more important for future work) some justification is established for treating the accelerating finite span wing in an approximate quasi-steady manner. In fact, Figures 6 through 9 do show that, except for

Contrails

$M_o(\tau) \cong 1$, even the large acceleration cases ($\mathcal{F} = 1 \times 10^1$) are approximated very well by assuming $\mathcal{F} = 0$ and by just considering the quasi-steady variation of $M_o(\tau)$. Additionally, for a Mach number $M_o(\tau) > 2.5$, even the effect of $M_o(\tau)$ is very small so that piston theory aerodynamics begins to be an accurate representation.

When considering a problem in which arbitrary motion is involved, the lift and moment impulse responses calculated in Eqs. (1.41) through (1.44) are the kernel functions for the integral relations that determine the lift and moment due to a given arbitrary motion. Referring to Figure 10, which illustrates the notation used in describing the airfoils perturbed flight path, the integral relations for the lift and moment about the leading edge due to a given arbitrary motion are given by:

$$L(t) = \int_{-\infty}^{t^+} L_c(\tau, x') [\dot{h}(\tau) + U(\tau) \alpha(\tau)] d\tau + \int_{-\infty}^{t^+} L_l(\tau, x') \dot{\Theta}(\tau) d\tau \quad (1.48)$$

$$M(t) = \int_{-\infty}^{t^+} M_c(\tau, x') [\dot{h}(\tau) + U(\tau) \alpha(\tau)] d\tau + \int_{-\infty}^{t^+} M_l(\tau, x') \dot{\Theta}(\tau) d\tau \quad (1.49)$$

Thus, the presentation of the exact two-dimensional linearized aerodynamic theory for an accelerating unsteady supersonic airfoil is completed.

Finally, as a thought towards further work, it is suggested that a useful approximation of the exact linearized theory may be constructed by considering the lift and moment impulse responses as a collection of weighted pulses. This would reduce the above integrals (Eqs. 1.48 and 1.49) to difference - differential elements. Thus when these relations are substituted into the equations of motion for some system, the system is

Contrails

described by a coupled set of difference - differential equations. The solution of this set of equations, perhaps by Laplace transform methods, may be less time-consuming than solving the original set of integro-differential equations that describe the system's behavior. The success of this method obviously depends on having a large value of the ratio of the characteristic time period of the unsteady motion to the time increment required for the impulse load (lift or moment) response to go to zero: since, if this ratio is large, the effect of an impulse or of a finite load time history on the system will be practically identical. However, if this condition is not met it simply means that more pulses must be used to more accurately describe the load impulse responses. Clearly if the required number of pulses is too large, the original integro-differential equations may still be attractive.

However, referring again to Figures 6 through 9 it is seen that the time increment required for the impulse load responses to go to zero (excepting the $M = 1$ case) is of the order of $2b \times 10^{-3}$ to $2b \times 10^{-2}$ sec., where b is the airfoil semi-chord measured in feet. Thus, at most, two pulses (in addition to the "piston theory pulse") should be adequate for a wide class of problems. Referring to Figures 11 and 12 it is readily seen how the load time history areas are replaced by an "equivalent area" impulse centered at the x' -centroids of the original load time history areas. The distances of the centroids from the $x' = 0$ axis as well as the original areas may be plotted as a function of Mach number $M_o(r)$ with the Froude number \mathcal{F} as a parameter. See Figure 13. However, as mentioned previously, probably only the $\mathcal{F}=0$ plot need be used when $M_o(r) \neq 1$. If successful, this "multi-pulse"

Contrails

piston theory should facilitate response and flutter calculations in the Mach number range from slightly above 1.0 to slightly above 2.5 where the usual piston theory begins to be an accurate representation.

At this point the presentation and discussion of the required aerodynamic and aerothermoelastic theories terminates, the remaining Sections being devoted to an example of high-speed vibratory wing response.

SECTION II

THE PURPOSE, DEFINITION AND DESCRIPTION OF THE COMPUTATIONAL EFFORTS

This section states the purpose of the ensuing computational efforts, briefly defines the problem to be analyzed, describes the equations representing the problem and then discusses the methods of solving the problem. The definition of the problem includes a presentation of the flight missions chosen and a summary of the geometrical and structural properties of the wing associated with the vehicle chosen to perform the flight missions. The calculations necessary for expressing the time-varying coefficients of the above-mentioned equations are also displayed graphically. Finally, the equations of motion are presented and the methods utilized in the computational routines are explained. A short summary of IBM 704 calculation times is presented in Appendix III to give the reader some idea of the "run-time" magnitudes required to perform a study of this general type.

The purpose of the ensuing computational effort is to answer, as completely as possible, the following questions.

- (A) When are time-varying coefficients of importance in aeroelastic applications?
- (B) Do these instances of importance (if any) correspond to aircraft performing flight missions of practical importance?

Contrails

- (C) Given a specific type of flight mission and aircraft, what is the least complicated theory that may be confidently used for analysis purposes?
- (D) Will in fact the answer to (C) be that a quasi-steady linear analysis is adequate for a large variety of flight missions and aircraft?

Emphasis has been placed on the possibility of an affirmative answer for question (D) since this fact would permit the aeroelastician to utilize, with confidence, the standard analysis techniques for a large class of aircraft, performing their various flight missions.

Although it is desired to answer questions (A) through (D) for all types of aeronautical vehicles, the enormous amount of computational effort required to calculate even one exact* reference solution for a problem involving time-varying coefficients necessitates that the different types of aircraft considered and their numerous possible flight missions must be severely limited so that the computational work can be completed using reasonable amounts of time and funds. Accordingly, it was decided to concentrate on manned vehicles operating within the atmosphere. Furthermore, in order to make the computations as useful as possible, two flight missions will be chosen that could conceivably represent the upper bound performance of manned vehicles of the foreseeable future. This choice of flight missions should insure

*The term "exact" here implies the use of the most accurate system developed in Section I.

Contrails

clear indications of how approximately the time-varying system coefficients may be treated and still yield the correct system behavior.

Flight within the atmosphere yields definite bounds on the flight missions possible due to temperature induced material limitations and the specification of a human occupant yields an upper bound on the g loading time history that can be endured by the pilot. For example, Reference 10 presents the maximum Mach number-altitude trajectories permissible (assuming reasonable material properties) due to kinetic heating and high q loadings, while Reference 11 displays the human time-tolerance intervals at different g loadings for various body orientations. Considering the above bounds imposed on the flight missions, a consistent choice of a manned vehicle would be one of a "super X-15" variety or of a boost-glide type which will perform the following two assumed flight missions.

The vehicle starts from a slightly supersonic speed ($M = 1.05$) at 35,000 feet and initiates a vertical climb which culminates in an altitude of about 140,000 feet and a final Mach number $M = 8$; after which time the vehicle remains at a constant altitude and Mach number. The two flight missions are distinguished only by the acceleration time histories used during the vertical climb. The first time history is a constant 9g acceleration while the second time history is an $\alpha / 2(1 - \cos \beta t)$ type acceleration with α and β adjusted so that the time to climb, the final altitude and the final Mach number are approximately equal. The variables summarizing these two flight missions are now presented as functionals of time, and are also given in graphical

Contrails

form in Figures 14 through 17. Additionally, the variation of the dynamic pressure q versus altitude h is shown for the 9g acceleration case in Figure 18.

Flight Trajectory Summary for the 9g

Vertical Acceleration

$$h(t) = \begin{cases} 35000 + 144.9t^2 + 1018t \text{ Ft.}; & 0 \leq t \leq 23.26 \text{ sec.} \\ 137074 \text{ Ft.} & t \geq 23.26 \text{ sec.} \end{cases} \quad (2.1)$$

$$M(t) = \begin{cases} 1.05 + .2985t & ; 0 \leq t \leq 23.26 \text{ sec.} \\ 8.00 & ; t \geq 23.26 \text{ sec.} \end{cases} \quad (2.2)$$

$$\rho(h(t)) = .0034e^{-h(t)/22,000} \text{ slugs/ft.}^3 \quad (2.3)$$

The wall temperature is not an analytical function of time and is therefore expressed in tabular form.

$T_w(t)$ deg. R.	t sec.
471	0
850	5
960	6
1305	10
1450	13
1500	15
1540	20
1530	23
1525	25

(2.4)

Contrails

Flight Trajectory Summary for the $\alpha/2(1 - \cos \beta t)$ Vertical Acceleration

$$\begin{aligned}\alpha &= 540 \\ \beta &= .2513\end{aligned}\tag{2.5}$$

$$h(t) = \begin{cases} 30723 + 4277 \cos (.2513t) + 1018t + 135 t^2 \text{ Ft.}; & 0 \leq t \leq 25 \text{ sec.} \\ 144825 \text{ Ft.} & t \geq 25 \text{ sec.} \end{cases}\tag{2.6}$$

$$M(t) = \begin{cases} 1.05 - 1.1065 \sin (.2513t) + .2780t; & 0 \leq t \leq 25 \text{ sec.} \\ 8 & t \geq 25 \text{ sec.} \end{cases}\tag{2.7}$$

$$\rho_{\infty}(h(t)) = .0034e^{-h(t)/22,000} \text{ slugs/ft.}^3\tag{2.8}$$

$T_W(t)$ deg. R.	t sec.	
471	0	
530	5	
577	6	
1108	10	
1490	13	(2.9)
1630	15	
1680	20	
1600	23	
1490	25	

Summary of the Geometrical and Structural Properties of the Vehicle Wing

The wing geometry is described in Figure 19. Although the planform is rectangular the wing area, wing weight, etc., are roughly the same as the unclassified estimates (available in periodicals) made for the X-15. Structurally the wing is represented by a 3% unsymmetrical (fore and aft) double wedge stainless steel multi-cell thick skin cross section. The number of cells** is not determined since this then allows the required freedom in choosing the iso-thermal fundamental torsional frequency. This freedom in choosing ω_α isothermal is necessary since a wing must be found that is just slightly stable (but not unstable) when analyzed by quasi-steady techniques over some portion of the flight mission. This slightly stable configuration gives some "sensitivity" to the results calculated using non-quasi-steady analyses. In view of these remarks ω_α^2 is found by using a modified form of equation 1.11 (ω_α^2 isothermal = $\{k^2 \pi^2 / 4L^2 I_\alpha\} \{GJ(0)\}$) * where K^2 is adjusted to give an adequate value

of ω_α^2 isothermal. After some mathematical experimenting it is found the $K^2 \cong 4.00$, which appears to be quite high. However, this value of K^2 corresponds to adding only about 0.015 to the existing airfoil thickness ratio. Hence this artifice produces the required changes well within the error bounds of a design analysis.

* $GJ(0)$ denotes the value of GJ at $t = 0$ when no nonlinear mid-plane stretching effect is included.

** spanwise cells

Contrails

Using the assumed values,

$$\bar{M} = 5.8230 \text{ slugs}$$

$$I = 14.216 \text{ slug ft.}^2$$

$$= -3.6394 \text{ slug ft.}$$

$$\frac{\omega_h^2}{\omega_\alpha^2} = 0.20 \quad @ t = 0$$

$$c = 2b = 6.25 \text{ ft.}$$

$$L = 8 \text{ ft.}$$

it is found that

$$\omega_\alpha^2(t) = 0.01085 \text{ GJ}(t)$$

$$\text{GJ}(0) = 5.932 \times 10^6 \text{ ft.}^2$$

$$\omega_\alpha^2(0) = 6.44 \times 10^4 \text{ rad.}^2/\text{sec.}^2$$

$$\omega_h^2(0) = 1.288 \times 10^4 \text{ rad.}^2/\text{sec.}^2$$

By assuming no degradation of elastic properties at constant elevated temperatures,

$$\omega_h^2(0) \cong \omega_h^2(t).$$

Now by using equation 1.10 the GJ_{EFF} may be calculated with just one modification. Equation 1.10 was derived assuming a solid wing, thus some correction must be made for the fact that the wing to be analyzed has a cellular structure. The desired correction has been

Contrails

made by introducing a thermal stress efficiency factor η into the equation for $GJ(t)$ so that this result is now given, referring to Figure 20, as

$$GJ(t) = GJ(0) + 2 \eta \int_{.55C}^0 \sigma_x y^2 t_1(y) dy \\ + 2 \eta \int_0^{.45C} \sigma_x y^2 t_2(y) dy \quad \text{ft.}^2 *$$

where σ_x is given by equation 1.3.

Again after a limited amount of mathematical experimenting, η was assigned a value of $\eta = 0.5000$.** Additionally when assessing σ_x it is necessary to specify the initial twist rate k that introduces the nonlinearity into the analysis. Figure 21 shows the effect of k on $GJ(t)$ for both flight missions and for three values of k .

As can be seen from Figure 21, large reductions in torsional stiffness do not take place. This is primarily due to the fact that, at the altitudes considered, the heat transfer coefficient h^* is quite small since it is directly proportional to the $4/5^{\text{th}}$ power of the atmospheric density.

SUMMARY OF CALCULATION PROCEDURES AND METHODS OF SOLVING THE PROBLEM

The calculations described in this sub-section were designed to numerically solve the system of equations 2.10 and 2.11 with an accuracy of four or five significant figures. Since the solution of these equations depends on what aerodynamic theory is used to describe the lift and moment, what flight mission is chosen, and how exactly (or how approximately) the effects of the time-varying coefficients are treated, it is obvious that

* This expression for $GJ(t)$ assumes that $x \ll y$ so that the r^2 term appearing in equation 1.10 is given by $r^2 \cong y^2$.

** This choice of an "integrated average over the cross-section" value of $\eta = 0.5000$ empirically makes the $GJ(t)$ curve of the correct magnitude and shape.

Contrails

several solutions of varying "exactness" will ensue and that, possibly, each solution may be best obtained by a different calculation procedure. Furthermore, since it is not known a priori how markedly the solutions utilizing the time-varying coefficients and/or the various aerodynamic theories will differ from the damped sinusoidal sums that are characteristic of the quasi-steady solutions, the more exact solutions must be the responses to some suitable set of inputs such that these solutions reveal a significant amount of information about the effects of the time-varying coefficients and the various aerodynamic theories. Clearly, several choices must now be made as to what inputs are to be used, at what times during the flight mission should these inputs be initiated, how long after these input initiations should the response be recorded, how many different approximate solutions are to be attempted, and as to what techniques should be used to obtain the various approximate solutions. These choices are described in the following paragraphs.

Suitable inputs are obtained by using perturbation impulsive loadings (\dot{h} or $\dot{\alpha}$) at some time τ . One advantage of impulsive inputs is their correspondence to velocity initial conditions for a given system. Hence it is possible to obtain the homogeneous response of the system at time t due to specified velocity initial conditions at time τ . The above reference to perturbation is underlined since it is to be understood that the system response is comprised of two parts. The first part being that response due to intentional control and throttle movements throughout the flight mission; the second part being the response to the chosen aerodynamic perturbation inputs

Contrails

occurring at time(s) τ . This further implies that the response of interest in this report, the perturbation response, is zero until $t = \tau$. Thus given a flight mission, and a perturbation input at time τ_i (the i denotes that there may be several values of τ at which one would like to investigate the effects of the input), one will obtain i traces of \bar{h} and α perturbation motions, each trace being zero until $t = \tau_i$ * These \bar{h} and α motions are combinations of the damped normal aeroelastic modes (if they exist) of the system, thus unless one mode predominates in the description of either \bar{h} or α it may be difficult to draw quantitative conclusions about the effective damping ratios of the system, although qualitative conclusions are easily obtained. In the special case of the quasi-steady analysis utilizing piston theory aerodynamics, it is much easier to calculate the frequencies and damping ratios directly with no consideration given to the total \bar{h} and α motion. Had time permitted, the quasi-steady response to \bar{h} and α impulsive inputs would have provided a more direct correlation with the other calculations.

The larger amounts of time required, on even such an efficient high-speed machine as the IBM 704 computer, to calculate the response time histories made it imperative to sparingly choose the times of input initiations and the duration of the recorded response. Thus the cases involving piston theory aerodynamics were studied for inputs at 0, 2, 4,, 28, 30 seconds, with each time history having a one second duration and the cases involving the exact unsteady accelerating aerodynamics were studied for inputs at 0, 2, 4, 6, and 8 seconds, with each time history having a one-half second duration.

* This time is more simply denoted as t_0 in Section III of this report. The use of τ and τ_i in this section is in accord with current engineering symbolism.

Contrails

The solutions involving piston theory aerodynamics were found by first treating the time-varying coefficients exactly and then by using a quasi-steady analysis for the times $t = 0, 2, 4, \dots, 28, 30$ seconds.

When considering the solutions involving the exact unsteady accelerating aerodynamics the results of a preliminary calculation involving the determination of lift and moment responses to impulsive pitch and plunge inputs indicated, for the accelerations involved in the given flight missions and for the stated Mach number range $1.05 \leq M \leq 3$, that the direct effect of the Froude number \mathcal{F} was negligible. Hence the $\mathcal{F} = 0$ approximation is used with excellent justification for all the exact unsteady accelerating aerodynamics relations. Furthermore, it was decided to first compare the results of the more critical flight mission (more critical in the sense of simultaneous high q and high \mathcal{F} occurring) with the simpler piston theory solutions and then to determine if the less critical flight mission should be considered. This decision and its aftermath is discussed in Section III. The calculation procedures for these exact solutions and the approximate procedures are now described in some detail.

The equations treated, referring to Figure 3, are

$$\ddot{h}(t) + \frac{S_0}{\bar{M}} \ddot{\alpha}(t) + \omega_h^2 h(t) = -L(t)/\bar{M} \quad (2.10)$$

$$S/I_0 \ddot{h}(t) + \ddot{\alpha}(t) + \omega_\alpha^2 \alpha(t) = M_a(t)/I_0 \quad (2.11)$$

where

$$\bar{M} = \text{mass} = 5.8230 \text{ slugs}$$

Contrails

$$I_o \equiv I_\alpha = 14.216 \text{ slug ft.}^2$$

$$S_o \equiv S_\alpha = -3.6394 \text{ slug ft.}$$

Now for an unsteady supersonic aerodynamic solution $L(t)$ and $M_a(t)$ are given by

$$L(t) = \int_0^{t^+} L_c(\tau, t-\tau) U(\tau) \left[\frac{\dot{h}(\tau)}{U(\tau)} + \alpha(\tau) \right] d\tau + \int_0^{t^+} L_\rho(\tau, t-\tau) \dot{\alpha}(\tau) d\tau \quad (2.12)$$

$$M_a(t) = \int_0^{t^+} M_c(\tau, t-\tau) U(\tau) \left[\frac{\dot{h}(\tau)}{U(\tau)} + \alpha(\tau) \right] d\tau + \int_0^{t^+} M_\rho(\tau, t-\tau) \dot{\alpha}(\tau) d\tau \quad (2.13)$$

while for a piston theory solution:

$$L(t) = \frac{\rho_\infty(t)}{2} U^2(t) S \left[\frac{4}{M(t)} \left(\frac{\dot{h}(t)}{U(t)} + \alpha(t) \right) + \left(\frac{4}{M(t)} \left(\frac{1}{2} - a \right) - (\gamma+1) \frac{A_w}{c^2} \right) \frac{c \dot{\alpha}(t)}{U(t)} \right] \quad (2.14)$$

$$M_a(t) = \frac{\rho_\infty(t)}{2} U^2(t) S_c \left[\left(\frac{4}{M(t)} \left(a - \frac{1}{2} \right) + (\gamma+1) \frac{A_w}{c^2} \right) \left(\frac{\dot{h}(t)}{U(t)} + \alpha(t) \right) + \left(\frac{4}{M(t)} \left\{ a(1-a) - \frac{1}{3} \right\} - (\gamma+1) \left\{ \frac{2aA_w}{c^2} - \frac{2M_w}{c^3} \right\} \right) \frac{c \dot{\alpha}(t)}{U(t)} \right] \quad (2.15)$$

Contrails

where

A_w = total wing cross-section area

M_w = first area-moment of total wing
cross-section about the leading edge

The piston theory solution of the problem was found first, as the differential equations could be solved numerically with an accuracy of five significant figures and could be compared with a difference equation solution of the same set. This comparison is important, since it gives the basis for a statement of accuracy concerning the difference equations used to solve the unsteady aerodynamics set of equations. A preliminary study was done to determine whether operational calculus methods could be employed to reduce the exact solution of the unsteady aerodynamics set to a feasible IBM 704 problem. Results of this study showed that an estimated minimum of 100 hours of machine time would be necessary for this solution due to the presence of changing functions of $(t - \tau, \tau)$ under the integral sign. Therefore, the decision to use difference equation approximations was made since the comparison of the exact solution with the difference equation solution of the piston theory formulation showed that 4 to 5 significant figure accuracy could be obtained by using a Δt of 0.001 sec. and by approximating the true value of $\bar{h}(t)$ and $\alpha(t)$ at the end of the first 0.001 second interval by the piston theory exact solution values.

The entire study as described was done for an acceleration of $ng = 270 (1 - \cos 0.2513t)$ letting $\varphi = 0$ and the complete piston theory and quasi-steady study was done for an acceleration of $ng = 9g$. Each of these

Contrails

accelerations was broken up into two cases. Case 1 is a time history following a unit impulse on $\dot{h}(t)$ at time t_0 where $\dot{\alpha}(t_0) = 0$; Case 2 assumes $\dot{h}(t_0) = 0$ and $\dot{\alpha}(t_0) = 1.0$.

Before the main body of calculations could be started, a suitable k had to be found (as mentioned previously). By finding $GJ(t)$ in a separate preliminary calculation, it was determined that $k = 0.006$ was a reasonable choice. Then $GJ(t)$ was approximated by a series of cubic equations yielding five significant figures for use in solving equations 2.10 and 2.11.

Substituting the given values into equations 2.10 and 2.11 the piston theory system for both ng's becomes:

$$\begin{aligned} \ddot{h}(t) - .625\ddot{\alpha}(t) &= -2084.4\rho_{\infty}(t)\left\{\dot{h}(t) - .3125\dot{\alpha}(t)\right\} \\ &\quad - 1.288 \times 10^4 \bar{h}(t) - 20844\rho_{\infty}(t)U(t)\alpha(t) \end{aligned} \quad (2.16)$$

$$\begin{aligned} -.256\ddot{h}(t) + \ddot{\alpha}(t) &= 853.77\rho_{\infty}(t)\left\{.3125\dot{h}(t) - 3.3529\dot{\alpha}(t)\right\} \\ &\quad + \left\{266.80\rho_{\infty}(t)U(t) - \omega_{\alpha}^2(t)\right\}\alpha(t) \end{aligned} \quad (2.17)$$

As stated previously, these equations were first solved numerically and then the finite difference forms of these equations were solved for several time histories in order that the aforementioned comparison could be made. Additionally, this set of equations was solved in a quasi-steady manner, for times $t = 0, 2, 4, \dots, .28, 30$ seconds. This quasi-steady calculation was

Contrails

performed in the classical manner by letting $p^n = \frac{d^n}{dt^n}$ in the equations 2.16 and 2.17 and then solving for the roots of the resultant quartic in p . One thus obtains four sets of roots in the form $a \pm ib$ and $c \pm id$, where a and c are proportional to the instantaneous (quasi-steady) damping ratio ξ of the system and b and d are the instantaneous frequencies of the system.

To treat the unsteady supersonic aerodynamics solution, equations 2.10 and 2.11 were written in operational form:

$$\begin{aligned} \ddot{x}_i(t) - L_{ii}^*(t)\{x_i(t)\} - L_{ij}^*\{x_j(t)\} &= f_i^*(t) \\ + q_i^*(t) \int_0^t & \left[\tilde{K}_{ii}^*(\tau, t-\tau)x_i(\tau) + \tilde{K}_{ij}^*(\tau, t-\tau)x_j(\tau) \right. \\ & \left. + \bar{K}_{ii}^*(\tau, t-\tau)\dot{x}_i(\tau) - \bar{K}_{ij}^*(\tau, t-\tau)\dot{x}_j(\tau) \right] d\tau \end{aligned} \quad \begin{array}{l} i, j = 1, 2 \\ i \neq j \\ (2.18) \end{array}$$

where 1 denotes the \bar{h} motion and 2 denotes the α motion and

$$L_{ii}^*(t) = a_{ii}^*(t) \frac{d}{dt} + b_{ii}^*(t)$$

$$L_{ij}^*(t) = d_{ij}^*(t) \frac{d^2}{dt^2} + a_{ij}^*(t) \frac{d}{dt} + b_{ij}^*(t)$$

Contrails

It is most convenient to remove the dirac portion of the expression from under the integral sign yielding equation 2.19, where \tilde{C}_{kl}^* and \bar{C}_{kl} are the coefficients of the dirac portion of the kernel multiplying x_l and \dot{x}_l respectively, and \tilde{K}_{kl} and \bar{K}_{kl} are the kernels with the dirac portion removed.

$$\begin{aligned} \ddot{x}_i(t) = & L_{ii}^*(t) \{x_i(t)\} + L_{ij}^*(t) \{x_j(t)\} + g_i^*(t) \{ \tilde{C}_{ii} x_i(t) + \tilde{C}_{ij} x_j(t) \\ & + \bar{C}_{ii} \dot{x}_i(t) + \bar{C}_{ij} \dot{x}_j(t) \} + f_i^*(t) + g_i^*(t) \int_0^t \{ \tilde{K}_{ii} x_i(\tau) \\ & + \tilde{K}_{ij} x_j(\tau) + \bar{K}_{ii} \dot{x}_i(\tau) + \bar{K}_{ij} \dot{x}_j(\tau) \} d\tau \end{aligned} \quad (2.19)$$

where

$$\begin{aligned} f_i^*(t) &= 0 & a_{ii}^* &= a_{ij}^* = 0 \\ d_{12}^* &= -S_0/M & d_{21}^* &= -S_0/I_0 \\ b_{11}^* &= -\omega_h^2 & b_{22}^* &= -\omega_a^2 & b_{ij} &= 0 \\ g_1^* &= -S/cM & g_2^* &= S/cI_0 \\ \tilde{C}_{11} &= \tilde{C}_{21} = 0 & \tilde{C}_{12} &= 2\rho_\infty a_\infty cV & \tilde{C}_{22} &= 2\rho_\infty a_\infty c^2 U(a - \frac{1}{2}) \\ \bar{C}_{11} &= 2\rho_\infty a_\infty c & \bar{C}_{12} &= 2\rho_\infty a_\infty c^2 (\frac{1}{2} - a) & \bar{K}_{11} &= \bar{K}_{21} = 0 \\ \bar{C}_{21} &= 2\rho_\infty a_\infty c^2 (a - \frac{1}{2}) & \bar{C}_{22} &= -2\rho_\infty a_\infty c^3 (\frac{1}{3} - a(1-a)) \\ x' &= \frac{a_\infty}{c}(t-\tau) \\ f &= f(x', \tau) = M(\tau)x' \\ x_2' &= [1 + M(\tau)]^{-1} \end{aligned}$$

* The subscripts k and l denoting any particular value of the free indices i and j respectively.

Contrails

$$\tilde{K}_{12} = \begin{cases} 0 & 0 \leq x'_1 \leq x'_2 \\ \frac{2}{\pi} \rho_{\infty} a_{\infty}^2 U \sqrt{1 - \left(\frac{1-f}{x'_1}\right)^2} & x'_2 < x'_1; f \leq 1+x' \\ 0 & f \geq 1+x' \end{cases}$$

$$\tilde{K}_{22} = \begin{cases} \rho_{\infty} a_{\infty}^2 c U x' \\ \frac{2}{\pi} \rho_{\infty} a_{\infty}^2 c U \left[\frac{x'}{2} \cos^{-1} \left(\frac{f-1}{x'_1} \right) + \left(a - \frac{1+f}{2} \right) \sqrt{1 - \left(\frac{1-f}{x'_1} \right)^2} \right] \\ 0 \end{cases}$$

$$\bar{K}_{11} = \begin{cases} 0 \\ \frac{2}{\pi} \rho_{\infty} a_{\infty}^2 \sqrt{1 - \left(\frac{1-f}{x'_1} \right)^2} \\ 0 \end{cases}$$

$$\bar{K}_{21} = \begin{cases} \rho_{\infty} a_{\infty}^2 c x' \\ \frac{2}{\pi} \rho_{\infty} a_{\infty}^2 c \left\{ \frac{x'}{2} \cos^{-1} \left(\frac{f-1}{x'_1} \right) + \left(a - \frac{1+f}{2} \right) \sqrt{1 - \left(\frac{1-f}{x'_1} \right)^2} \right\} \\ 0 \end{cases}$$

$$\bar{K}_{12} = \begin{cases} \rho_{\infty} a_{\infty}^2 c x' \\ \frac{2}{\pi} \rho_{\infty} a_{\infty}^2 c \left\{ \frac{x'}{2} \cos^{-1} \left(\frac{f-1}{x'_1} \right) + \left(\frac{1-f}{2} - a \right) \sqrt{1 - \left(\frac{1-f}{x'_1} \right)^2} \right\} \\ 0 \end{cases}$$

$$\bar{K}_{22} = \begin{cases} -\rho_{\infty} a_{\infty}^2 c^2 f x' \\ \frac{2}{\pi} \rho_{\infty} a_{\infty}^2 c^2 \left\{ -f \left[\frac{x'}{2} \cos^{-1} \left(\frac{f-1}{x'_1} \right) \right] + \left[\frac{f(f-1)}{2} + a(1-a) \right] \sqrt{1 - \left(\frac{1-f}{x'_1} \right)^2} \right. \\ \left. + \frac{x'^2}{3} \left[1 - \left(\frac{1-f}{x'_1} \right)^2 \right]^{3/2} \right\} \\ 0 \end{cases}$$

Contrails

By using central difference approximations, set

$$\dot{X}_n(t) \cong \frac{X_{n+1}(t) - X_{n-1}(t)}{2(t_{n+1} - t_n)} = \frac{X_{n+1}(t) - X_{n-1}(t)}{2\Delta}$$

$$\ddot{X}_n(t) \cong \frac{X_{n+1}(t) - 2X_n(t) + X_{n-1}(t)}{\Delta^2}$$

and replacing the integral occurring in equation 2.19 by

$$\begin{aligned} I_{ijn} \cong & q_i \sum_{k=0}^{n-1} W_k \left[\tilde{K}_{ii}(t_k, t_n - t_k) X_k^{(i)} + \tilde{K}_{ij}(t_k, t_n - t_k) X_k^{(j)} \right. \\ & + \bar{K}_{ii}(t_k, t_n - t_k) \left(\frac{X_{k+1}^{(i)} - X_{k-1}^{(i)}}{2\Delta} \right) \\ & \left. + \bar{K}_{ij}(t_k, t_n - t_k) \left(\frac{X_{k+1}^{(j)} - X_{k-1}^{(j)}}{2\Delta} \right) \right] \end{aligned}$$

(where W_k is the weighting factor corresponding to the trapezoidal rule of numerical integration) one obtains the difference equations,

$$\begin{aligned} \beta_{iin} X_{n+1}^{(i)} + \beta_{ijn} X_{n+1}^{(j)} = & \Gamma_{iin} X_n^{(i)} + \Gamma_{ijn} X_n^{(j)} + \Delta_{iin} X_n^{(i)} \\ & + \Delta_{ijn} X_{n-1}^{(j)} + I_{ijn} \end{aligned} \quad (2.20)$$

where

$$\begin{aligned} i \neq j \\ \beta_{iin} = & \frac{1}{\Delta^2} - \frac{a_{iin}^*}{2\Delta} - \frac{g_i^* C_{iin}}{2\Delta} \\ \beta_{ijn} = & -\frac{d_{ijn}^*}{\Delta^2} - \frac{a_{ijn}^*}{2\Delta} - \frac{g_i^* C_{ijn}}{2\Delta} \end{aligned}$$

Contrails

$$\Gamma_{iin} = \frac{z}{\Delta^2} + b_{iin}^* + g_i^* \tilde{C}_{iin}$$

$$\Gamma_{ijn} = \frac{-2d_{ijn}}{\Delta^2} + b_{ijn}^* + g_i^* C_{ijn}$$

$$\Delta_{iin} = \frac{1}{\Delta^2} - \frac{a_{iin}^*}{2\Delta} - \frac{g_i^* \tilde{C}_{ii}}{2\Delta}$$

$$\Delta_{ijn} = \frac{d_{ijn}^*}{\Delta^2} - \frac{a_{ijn}^*}{2\Delta} - \frac{g_i^* \tilde{C}_{ij}}{2\Delta}$$

$$\Delta = t_n - t_{n-1}$$

To start the solution of these difference equations, Case 1 and Case 2 initial conditions were used, the values from the piston theory solution at $t_0 + 0.001$ sec. (the piston theory solution = the unsteady aerodynamics solution to five significant figures at $t_0 + 0.001$ sec.), and the exact derivatives at $t = t_0$ rather than the difference approximations. These measures were taken to insure at least 4 figures of accuracy in the results, since it was found that a sizeable error can be introduced by using the stated difference equation between t_0 and $t_0 + 0.001$ sec.

Since the GJ(t) calculation, the piston theory differential equation solution, and the difference equation solution utilizing the exact unsteady accelerating aerodynamic theory were all done by means of an IBM 704, programs written in the Share Assembly language are available for future use by interested people or agencies. Problems similarly formulated with different parameters could be solved by making only minor modifications to the existing programs.

SECTION III

PRESENTATION AND DISCUSSION OF THE SOLUTIONS

Once the calculations described in Section II have been completed the resulting plethora of information must be presented in an organized fashion such that the answers to questions (A) thru (D)^{*}, posed in the first page of Section II of this report, may be obtained. To this end, the impulse response time histories \bar{h} and α were examined over their full time range and then grouped into the following two categories. The first category contained \bar{h} and α time histories, utilizing piston theory aerodynamics, for the two acceleration time histories and both Case 1 and Case 2 inputs. The second category contained \bar{h} and α time histories, utilizing first piston theory aerodynamics and then unsteady accelerating aerodynamics, which were examined over the time interval $0 \leq t \leq 8$ seconds for the $n_g = 270 (1 - \cos .2513t)$ acceleration time history and both Case 1 and Case 2 inputs. Note that the \bar{h} and α time histories grouped in the above two categories are exact solutions of the problem within the framework of the mathematical model chosen for the aerodynamics, et cetera. Thus these time histories yield the most accurate response curves of the aircraft wing. A third category of information was formed by compiling the quasi-steady frequency calculations, as well as the instantaneous frequencies obtained from the exact solutions utilizing first piston theory aerodynamics and then unsteady accelerating aerodynamics, over the entire time range for both acceleration time histories. This bloc of information obviously yields the crudest possible, and most easily obtainable, description of the wing motion^{**}. At this point, the "best" and the

* For the chosen class of "manned vehicles".

** In order to directly compare the quasi-steady portion of the category three information with categories one and two, a quasi-steady analysis of the wing response due to Case 1 and Case 2 inputs should have been made. However, time limitations dictated the approach pursued here.

Contrails

"worst" solutions are available for inspection. Note that if additional solutions intermediate to the "best" and "worst" are required, the theories developed in Part I of this report are then applicable. The need for these additional solutions must be a consequence of a poor correlation between the "worst" and the "best" solution; therefore, the comparison of these latter solutions should be first pursued.

Since categories 1, 2 and 3 contain so much data,^{*} these data were re-examined and then sorted, within each category, into its essential and non-essential elements^{**}, the essential elements of each category being presented in this report. The essential elements of the first, second and third categories are contained in Figures 28 thru 43, Figures 44 thru 55 and Tables 1 thru 5, respectively.

Thus Figures 28 thru 43 present \bar{h} and α time histories utilizing piston theory aerodynamics near the times $t = t_0$ and $t \cong t_0 + .45$ seconds, where $t_0 = 0, 10, 20$ and 30 seconds, for the two acceleration time histories and the Case 1 and Case 2 inputs. This category of information should demonstrate whether the \bar{h} and α impulse responses are similar to the general type of impulse response $W(\tau, t - \tau)$ for a time-varying system or if indeed they are more nearly like the impulse response $W(\tau - \tau)$ for a constant coefficient system. The above-mentioned demonstrations may be carried out by noting the behavior of the delayed trace at $t \cong t_0 + .45$ seconds with respect to the trace observed just after the application of the impulsive input at $t = t_0$.

Figures 44 thru 55 present comparisons between the \bar{h} and α time histories obtained by first using piston theory aerodynamics and then using unsteady accelerating aerodynamics in the exact analysis. The t_0 time range for these comparisons is concentrated in the early portions of the

* Necessarily so, because the only feasible calculational procedure dictated a step by step (time-wise) method as described in Section II of this report.

** Non-essential being used here to indicate a redundant or repetitive type of information.

ng = 270 (1-cos.2513t) flight mission since it is in this time interval that the greatest solution differences should appear due to the two aerodynamic theory representations. This category of information should establish the relative merits of using the "more accurate" (but computationally difficult) unsteady accelerating aerodynamic theory as opposed to using the "less accurate" (but computationally simpler) piston theory aerodynamics.

Tables 1 thru 5 present comparisons between the quasi-steady and the instantaneous frequencies over the entire time range. This category of information should give supporting evidence to the trends established by an analysis of Figures 28 thru 55.

Now that the usefulness and purpose of the above three categories of information has been delineated the conclusions obtained from these categories may be presented.

Figures 28 thru 43 generally demonstrate, in any given time interval, that the \bar{h} and α time histories exhibit the usual characteristics of a constant coefficient system coupled mode response. One of a few exceptions to this general statement is Figure 34 in which the α time history is seen to grow slightly for $t_0 \cong 10.45$ seconds. However this growth may be predicted on a quasi-steady basis since at this particular time GJ and ρ_∞ are beginning to show reasonable decreases. It is thus correct to state that the coupled \bar{h} and α impulse responses are not similar to the general type of impulse response $W(\tau, \tau - \tau)$ but are indeed very nearly like the constant coefficient system impulse responses $W(\tau - \tau)$.

Figures 44 thru 55 demonstrate that there is no justification for employing the unsteady accelerating aerodynamics (linear) theory instead of the second-order piston theory aerodynamics.

Finally, an inspection of Tables 1 thru 5 reveals that in most cases the quasi-steady frequencies and the instantaneous frequencies are almost identical. The worst frequency correlation, which occurs in only a few cases, is of the order of 5%.

Contrails

Thus evidences of the time-varying coefficients are seen but they are small. It is seen that the omission of the $ng = 9g$ calculations suggested in the last page of Section II proved to be the correct procedure since the more critical $ng = 270 (1 - \cos .2513t)$ flight mission produced such unspectacular results.

The answers to questions (A) thru (D) posed at the beginning of Section II may now be answered by the following statements:

- (A) Time-varying coefficients are apparently of little importance in the aeroelastic analysis of manned aircraft.
- (B) It is suggested that time-varying coefficients would be of importance in the aeroelastic analysis of an anti-missile missile, et cetera.
- (C) Quasi-steady analysis appears to be still a remarkably good method of analysis. It is suggested that a more complete quasi-steady analysis should be made, however, to obtain both the frequencies and mode shapes as well as the response to some specified impulsive input. This procedure insures knowledge of the pertinent amplitude growths.

REFERENCES

1. Budiansky, Bernard and Mayers, J., "Influence of Aerodynamic Heating on the Effective Torsional Stiffness of Thin Wings," pp 1081-1093, Vol. 23, No. 12, December 1956, Journal of the Aeronautical Sciences.
2. Bisplinghoff, R. L., and Dugundji, J., "Influence of Aerodynamic Heating on Aeroelastic Phenomena," Monograph reprinted from High Temperature Effects in Aircraft Structures, AGARDograph No. 28, N. J. Hoff editor, Pergamon Press, London, 1959.
3. Singer, Josef, "Thermal Buckling of Solid Wings of Arbitrary Aspect Ratio," pp 573-580, Journal Aero/Space Sciences, Vol. 25, No. 9, September 1958.
4. Ashley, Holt and Zartarian, Garabed, "Piston Theory - A New Aerodynamic Tool for the Aeroelastician," Journal of Aeronautical Sciences, Vol. 23, No. 13, pp 1109-1118, December 1956.
5. Lomax, H., Heaslet, M. A., Fuller, F. B., and Sluder, L., "Two and Three-Dimensional Unsteady Lift Problems in High Speed Flight," NACA Report 1077, 1952.
6. Miles, J. W., "Unsteady Supersonic Flow," Chapter 13, Monograph prepared for the Air Research and Development Command, U.S.A.F., March 1955.
7. Frankl, F. I. and Karpovich, E. A., "Gas Dynamics of Thin Bodies," Chapters 3 and 4, Interscience Publishers, Inc., New York.
8. Evvard, J., "Use of Source Distributions for Evaluating Theoretical Aerodynamics of Thin Finite Wings at Supersonic Speeds," NACA TR 951.
9. Krasil-shchikova, E. A., "Effect of the Tip Edge on the Motion of a Wing at Supersonic Speeds," D.A.N., Vol. LVIII, No. 4, 1947 and "Effect of the Vortex Sheet for Steady Motion of a Wing at Supersonic Speeds," D.A.N., Vol. LVIII, No. 6, 1947.

REFERENCES (Continued)

10. Rogers, Milton, "Aerothermoelasticity," p 35, Fig. 1, Vol. 17, No. 10, October 1958, Aero/Space Engineering.
11. Space Handbook - Astronautics and its Applications by Robert W. Buchhiem and the Staff of The Rand Corporation, Random House, New York, 1959.

APPENDIX I. COMMENTS ON VARIABLE ALTITUDE FLIGHT

Rigorous inclusion of a non-homogenous atmosphere adds considerable difficulty to the aerodynamics problem. It is then of interest to determine an order of magnitude check on the influence of the variation of state parameters with altitude. For supersonic flight, the impulse response functions lend themselves nicely to such a check since the load due to impulsive motion must be identically zero for times after the airfoil trailing edge moves ahead of the foremost leading edge disturbance wave. For vertical flight at constant Mach number, this time is approximately

$$\Delta t \cong \frac{c}{a_{\infty}(M-1)}$$

and the corresponding vertical distance traveled is

$$\Delta h \cong \frac{Mc}{(M-1)}$$

Thus, except for $M \cong 1$, the change in altitude is of the order of the airfoil chord and hence negligible.* Positive acceleration reduces Δh further. Deceleration to subsonic speeds could allow past disturbances to reach the airfoil. Solution to the latter seems out of the realm of practicability at the present, since it involves at least analysis for subsonic unsteady flow and at most inclusion of dissipation due to viscosity which is conceivably of importance here. Thus, since loads due to arbitrary motion can be determined from superposition of the impulse responses, one concludes that it is sufficient to use the impulse response functions developed for the homogenous atmosphere with a quasi-steady representation of the change in state variables. This, of course, holds only for the supersonic case. The subsonic case is

* Even Mach numbers close to $M = 1$ produce moderate altitude changes Δh . For example, when $M = 1.05$, Δh is given by: $\Delta h \cong 20c$

Contrails

more difficult to justify; but due to the complexity of the problem, it is not felt that it is practical to proceed along these lines at present.

As a matter of interest, the difficulty in accounting for the non-homogenous atmosphere is discussed in the following. The isentropic relation is

$$P/P_{\infty} = (\rho/\rho_{\infty})^{\gamma}, \quad \gamma = 1.4$$

whereas the altitude pressure-density relation is

$$P_{\infty}/P_0 = (\rho_{\infty}/\rho_0)^K, \quad K = \begin{cases} 1.23, & 0 \leq h \leq 35,000 \text{ (Ft.)} \\ 1.00, & 35,000 \leq h \leq \infty \text{ (Ft.)} \end{cases}$$

Hence one cannot establish the barotropic relation $P = \rho(P)$ so that the quantity $\int \frac{dp}{\rho(p)}$ encountered in Kelvin's theorem and thus the Bernoulli pressure formula is not a proper integral. Thus one cannot justify the existence of a velocity potential. If one makes the approximation that $K = \gamma$, then the linearized mathematical problem can be formulated as a potential problem, the potential satisfying the wave equation with a variable speed of sound. This would of course be limited to some relatively narrow altitude band for which the above approximation is good. The solution to this latter problem is no trivial matter, particularly for the subsonic case for which its need seems most apparent.

APPENDIX II

Outline of the Procedures for Obtaining the Upwash Impulse Responses

If a finite band of upwash (width ϵ) is present on the three-dimensional wing planform, the planform possessing supersonic leading and trailing edges, Figure 22 depicts the regions in which the velocity potential is of interest and must be computed.

When $\epsilon \rightarrow 0$ and the upwash magnitude w is defined in general as $w = \frac{1}{\epsilon} f(\xi, \tau)$ we have the case in which a spacewise impulse of upwash exists on the three-dimensional airfoil at $\tau = 0$. Referring to Figure 23, it is seen that Regions I, II, and VI collapse onto the $\tau = 0, \xi = 0$ point, Region III collapses onto the $\tau = 0$ line and all other regions collapse onto the Mach lines except IX, VII, and IV. Also points 4 and 5, and 7 and 6 merge, and point 3 coincides with the origin. Thus, if the collapsed regions yield no limiting contribution to the three-dimensional wing pressure distribution, it is observed that one need calculate only the pressure in Regions IV, VII, and IX. However, since one always expects a pressure distribution to occur at the position of the applied upwash, at least Regions I, II and III must contribute some limiting pressure distribution.

The first step in calculating the pressure distributions is to express the velocity potential ϕ at some point (t, x) in terms of the wing planform geometry and the upwash w . As is well known, the velocity potential ϕ is an integral* of all properly weighted upwash elements that occur in the forward Mach-cone emanating from the point (t, x) . For any given point (t, x) ,

* Consult References 5, 6 and 7 for the details of this integral formulation of ϕ .

Contours

this forecone will intersect the wing planform at two positions. Thus, these two positions may be on the leading edge $\tau = 0$, on the side edge $\xi = -M_0\tau - \mathcal{F}\tau^2$ or may be on both portions of the planform. Figure 24 illustrates the possible forecone-planform intersections. The intersection points are labeled 1 and 2, the point having the largest negative value of ξ being denoted as point 2. For convenience the equations of the curves representing the wing geometry and the forward Mach-cones are also shown on Figure 24. Calculating the positions of points 1 and 2 in terms of the vortex coordinates of the forward Mach-cone and whether these points are on the leading edge $\tau = 0$ or the side edge $\xi = -(M_0\tau + \mathcal{F}\tau^2)$ it is seen that,

$$(\tau_1, \xi_1) = \begin{cases} (0, t+x); & \text{if on leading edge } \tau = 0 \\ \left(-\left(\frac{M_0-1}{2\mathcal{F}}\right) + \sqrt{\left(\frac{M_0-1}{2\mathcal{F}}\right)^2 - \frac{t+x}{\mathcal{F}}}, \right. \\ \left. t+x + \sqrt{\frac{M_0-1}{2\mathcal{F}} - \frac{t+x}{\mathcal{F}}} \right) & ; \text{ if on side edge} \\ & \xi = -(M_0\tau + \mathcal{F}\tau^2) \end{cases}$$

$$(\tau_2, \xi_2) = \begin{cases} (0, -t+x); & \text{if on leading edge } \tau = 0 \\ \left(-\left(\frac{M_0+1}{2\mathcal{F}}\right) + \sqrt{\left(\frac{M_0+1}{2\mathcal{F}}\right)^2 + \frac{t-x}{\mathcal{F}}}, \right. \\ \left. -t+x - \left(\frac{M_0+1}{2\mathcal{F}}\right) + \sqrt{\left(\frac{M_0+1}{2\mathcal{F}}\right)^2 + \frac{t-x}{\mathcal{F}}} \right) & ; \text{ if on side} \\ & \text{edge } \xi = \\ & -(M_0\tau + \mathcal{F}\tau^2) \end{cases}$$

The values of $\phi(t, x)$ for all nine regions are now presented in their basic form, before simplification or integration. Notice that these expressions must necessarily differ only in their integration limits providing the upwash $w(\tau, \xi)$ is left in implicit form.

Contrails

Region I

$$\varphi_I(t,x) = -\frac{1}{\pi} \int_{\tau_1}^{\tau_2} \int_{-M_0\tau - \frac{x}{\gamma}}^{x+t-\tau} \frac{W(\tau,\xi) d\xi d\tau}{\sqrt{(t-\tau)^2 - (x-\xi)^2}} - \frac{1}{\pi} \int_{\tau_2}^t \int_{x-t+\tau}^{x+t-\tau} \frac{W(\tau,\xi) d\xi d\tau}{\sqrt{(t-\tau)^2 - (x-\xi)^2}}$$

where $\tau_1 = -\left(\frac{M_0-1}{2\gamma}\right) + \sqrt{\left(\frac{M_0-1}{2\gamma}\right)^2 - \left(\frac{t+x}{\gamma}\right)}$

$$\tau_2 = -\left(\frac{M_0+1}{2\gamma}\right) + \sqrt{\left(\frac{M_0+1}{2\gamma}\right)^2 + \left(\frac{t-x}{\gamma}\right)}$$

Region II

$$\varphi_{II}(t,x) = -\frac{1}{\pi} \int_0^{\tau_2} \int_{-M_0\tau - \frac{x}{\gamma}}^{x+t-\tau} \frac{W(\tau,\xi) d\xi d\tau}{\sqrt{(t-\tau)^2 - (x-\xi)^2}} - \frac{1}{\pi} \int_{\tau_2}^t \int_{x-t+\tau}^{x+t-\tau} \frac{W(\tau,\xi) d\xi d\tau}{\sqrt{(t-\tau)^2 - (x-\xi)^2}}$$

where $\tau_2 = -\left(\frac{M_0+1}{2\gamma}\right) + \sqrt{\left(\frac{M_0+1}{2\gamma}\right)^2 + \frac{t-x}{\gamma}}$

Region III

$$\varphi_{III}(t,x) = -\frac{1}{\pi} \int_0^t \int_{x-t+\tau}^{x+t-\tau} \frac{W(\tau,\xi) d\xi d\tau}{\sqrt{(t-\tau)^2 - (x-\xi)^2}}$$

Region IV

$$\varphi_{IV}(t,x) = -\frac{1}{\pi} \int_0^{\epsilon} \int_{x-t+\tau}^{x+t-\tau} \frac{W(\tau,\xi) d\xi d\tau}{\sqrt{(t-\tau)^2 - (x-\xi)^2}}$$

Contrails

Region V

$$\varphi_{\text{V}}(t,x) = -\frac{1}{\pi} \int_0^{\tau_2} \int_{-M_0\tau - \tau^2}^{x+t-\tau} \frac{W(\tau, \xi) d\xi d\tau}{\sqrt{(t-\tau)^2 - (x-\xi)^2}} - \frac{1}{\pi} \int_{\tau_2}^{\epsilon} \int_{x-t+\tau}^{x+t-\tau} \frac{W(\tau, \xi) d\xi d\tau}{\sqrt{(t-\tau)^2 - (x-\xi)^2}}$$

where $\tau_2 = -\left(\frac{M_0+1}{2\mathcal{G}}\right) + \sqrt{\left(\frac{M_0+1}{2\mathcal{G}}\right)^2 + \frac{t-x}{\mathcal{G}}}$

Region VI

$$\varphi_{\text{VI}}(t,x) = -\frac{1}{\pi} \int_{\tau_1}^{\tau_2} \int_{-M_0\tau - \tau^2}^{x+t-\tau} \frac{W(\tau, \xi) d\xi d\tau}{\sqrt{(t-\tau)^2 - (x-\xi)^2}} - \frac{1}{\pi} \int_{\tau_2}^{\epsilon} \int_{x-t+\tau}^{x+t-\tau} \frac{W(\tau, \xi) d\xi d\tau}{\sqrt{(t-\tau)^2 - (x-\xi)^2}}$$

where

$$\tau_1 = -\left(\frac{M_0-1}{2\mathcal{G}}\right) + \sqrt{\left(\frac{M_0-1}{2\mathcal{G}}\right)^2 - \frac{t+x}{\mathcal{G}}}$$

$$\tau_2 = -\left(\frac{M_0+1}{2\mathcal{G}}\right) + \sqrt{\left(\frac{M_0+1}{2\mathcal{G}}\right)^2 + \frac{t-x}{\mathcal{G}}}$$

Region VII

$$\varphi_{\text{VII}}(t,x) = -\frac{1}{\pi} \int_0^{\epsilon} \int_{-M_0\tau - \tau^2}^{x+t-\tau} \frac{W(\tau, \xi) d\xi d\tau}{\sqrt{(t-\tau)^2 - (x-\xi)^2}}$$

Region VIII

$$\phi_{\text{VIII}}(t, x) = -\frac{1}{\pi} \int_{\tau_2}^t \int_{-M_0\tau - \xi\tau^2}^{x+t-\tau} \frac{w(\tau, \xi) d\xi d\tau}{\sqrt{(t-\tau)^2 - (x-\xi)^2}}$$

where $\tau_2 = -\left(\frac{M_0+1}{2\xi}\right) + \sqrt{\left(\frac{M_0+1}{2\xi}\right)^2 + \frac{t-x}{\xi}}$

Region IX

$$\phi_{\text{IX}}(t, x) \equiv 0$$

The second step in the analysis is to compute $\frac{\partial \phi}{\partial t}$ since the pressure difference across both the two-dimensional accelerating airfoil and the three-dimensional steady flow ($M = \sqrt{2}$) planform is proportional to this quantity. From this point on, the upwash is assumed to originate from a constant impulsive downwash on the two-dimensional accelerating airfoil. Thus the final quantities obtained will be L_c and M_c . Notice that the linearly varying upwash and indeed any upwash proportional to x^n causes no changes in the method of analysis. The validity of the following arguments would still exist, only the actual integrations being more complex. Thus, using the upwash $w(\tau, \xi) = \frac{1}{\epsilon}$, the $\frac{\partial \phi}{\partial t}$ terms are now obtained. The two basic integrations over the dummy variable ξ are,

$$I_1(t, \tau, x) = \int_{x-t+\tau}^{x+t-\tau} \left[(t-\tau)^2 - (x-\xi)^2 \right]^{-\frac{1}{2}} d\xi$$

$$I_2(t, \tau, x) = \int_{-M_0\tau - \xi\tau^2}^{x+t-\tau} \left[(t-\tau)^2 - (x-\xi)^2 \right]^{-\frac{1}{2}} d\xi$$

Contrails

Since the integrands are identical, both I_1 and I_2 may be computed by the same process. To this end, let $\lambda = x - \xi$ and $B = t - \tau$ since $t - \tau$ is a constant as far as this integration is concerned. These substitutions yield the results that,

$$d\xi = -d\lambda$$

$$\text{as } \xi \rightarrow -M_0\tau - \mathcal{J}\tau^2, \lambda \rightarrow x + M_0\tau + \mathcal{J}\tau^2$$

$$\text{as } \xi \rightarrow x + t - \tau, \lambda \rightarrow -t + \tau$$

$$\text{as } \xi \rightarrow x - t + \tau, \lambda \rightarrow t - \tau$$

Hence, I_1 and I_2 reduce to:

$$I_1(B, x) = \int_{-B}^B \frac{d\lambda}{\sqrt{B^2 - \lambda^2}} = \left[\sin^{-1} \frac{\lambda}{B} \right]_{-B}^B$$

$$I_2(B, \tau, x) = \int_{-B}^B \frac{d\lambda}{\sqrt{B^2 - \lambda^2}} = \left[\sin^{-1} \frac{\lambda}{B} \right]_{-B}^{x + M_0\tau + \mathcal{J}\tau^2}$$

Evaluating the limits these integrals become,

$$I_1(B, x) = \frac{\pi}{2} - \left(-\frac{\pi}{2}\right) = \pi$$

$$I_2(B, \tau, x) = \sin^{-1} \left(\frac{x + M_0\tau + \mathcal{J}\tau^2}{B} \right) + \frac{\pi}{2}$$

Contrails

Proceeding, the integrations over the τ dummy variable have the following forms,

$$\begin{array}{lll}
 I_3 = \int_0^t I_i d\tau & I_4 = \int_0^\epsilon I_i d\tau & I_5 = \int_0^{\tau_2} I_i d\tau \\
 I_6 = \int_{\tau_1}^{\tau_2} I_i d\tau & I_7 = \int_{\tau_2}^t I_i d\tau & I_8 = \int_{\tau_2}^\epsilon I_i d\tau
 \end{array}$$

where I_i is either I_1 or I_2 .

When $I_i = I_1$, the integrals may be written down immediately.

$$\begin{array}{lll}
 I_{3(i=1)} = \pi t & I_{4(i=1)} = \pi \epsilon & I_{6(i=1)} = \pi \tau_2 \\
 I_{6(i=1)} = \pi (\tau_2 - \tau_1) & I_{7(i=1)} = \pi (t - \tau_2) & I_{8(i=1)} = \pi (\epsilon - \tau_2)
 \end{array}$$

When $I_i = I_2$ it is most advantageous not to compute I_3 through I_7 , but instead to compute $\partial/\partial t$ (I_3) through $\partial/\partial t$ (I_7) immediately. These relations are now determined using Leibnitz's rule which states,

$$\frac{\partial}{\partial t} \int_{P(t)}^{Q(t)} f(t, \tau) d\tau = \int_{P(t)}^{Q(t)} \frac{\partial f(t, \tau)}{\partial t} d\tau + f(t, Q(t)) \frac{dQ(t)}{dt} - f(t, P(t)) \frac{dP(t)}{dt}$$

Thus, noting that $\partial/\partial t$ (I_3)_(i=2) and $\partial/\partial t$ (I_7)_(i=2) need not be computed, the remaining quantities are given by

Contrails

$$\frac{\partial}{\partial t}(I_4)_{(i=2)} = \int_0^\epsilon \frac{\partial}{\partial t} \left[\sin^{-1} \left(\frac{x + M_0 \tau + \mathcal{F} \tau^2}{t - \tau} \right) \right] d\tau$$

$$\frac{\partial}{\partial t}(I_5)_{(i=2)} = \int_0^{\tau_2} \frac{\partial}{\partial t} \left[\sin^{-1} \left(\frac{x + M_0 \tau + \mathcal{F} \tau^2}{t - \tau} \right) \right] d\tau + \frac{\pi}{2} \frac{\partial \tau_2}{\partial t} + \sin^{-1} \left(\frac{x + M_0 \tau_2 + \mathcal{F} \tau_2^2}{t - \tau_2} \right) \frac{\partial \tau_2}{\partial t}$$

$$\begin{aligned} \frac{\partial}{\partial t}(I_6)_{(i=2)} &= \int_{\tau_1}^{\tau_2} \frac{\partial}{\partial t} \left[\sin^{-1} \left(\frac{x + M_0 \tau + \mathcal{F} \tau^2}{t - \tau} \right) \right] d\tau + \frac{\pi}{2} \left[\frac{\partial \tau_2}{\partial t} - \frac{\partial \tau_1}{\partial t} \right] + \sin^{-1} \left(\frac{x + M_0 \tau_2 + \mathcal{F} \tau_2^2}{t - \tau_2} \right) \frac{\partial \tau_2}{\partial t} \\ &\quad - \sin^{-1} \left(\frac{x + M_0 \tau_1 + \mathcal{F} \tau_1^2}{t - \tau_1} \right) \frac{\partial \tau_1}{\partial t} \end{aligned}$$

$$\frac{\partial}{\partial t}(I_8)_{(i=2)} = \int_{\tau_2}^\epsilon \frac{\partial}{\partial t} \left[\sin^{-1} \left(\frac{x + M_0 \tau + \mathcal{F} \tau^2}{t - \tau} \right) \right] d\tau - \frac{\pi}{2} \frac{\partial \tau_2}{\partial t} - \sin^{-1} \left(\frac{x + M_0 \tau_2 + \mathcal{F} \tau_2^2}{t - \tau_2} \right) \frac{\partial \tau_2}{\partial t}$$

By explicitly denoting τ_1 and τ_2 in terms of M_0 , \mathcal{F} , t and x the $\sin^{-1}(\quad)$ terms reduce to the following values.

$$\sin^{-1} \left(\frac{x + M_0 \tau_2 + \mathcal{F} \tau_2^2}{t - \tau_2} \right) = \frac{\pi}{2}$$

$$\sin^{-1} \left(\frac{x + M_0 \tau_1 + \mathcal{F} \tau_1^2}{t - \tau_1} \right) = \frac{-\pi}{2}$$

Contrails

Using the accumulated information above, the $\frac{\partial \phi}{\partial t}$ terms for all regions may now be presented.

$$\frac{\partial \phi}{\partial t} \text{I} = -\frac{1}{\epsilon} - \frac{1}{\epsilon\pi} \int_{\tau_1}^{\tau_2} \frac{\partial}{\partial t} \left[\sin^{-1} \left(\frac{x + M_0 \tau + \mathcal{F} \tau^2}{t - \tau} \right) \right] d\tau$$

$$\frac{\partial \phi}{\partial t} \text{II} = -\frac{1}{\epsilon} - \frac{1}{\epsilon\pi} \int_0^{\tau_2} \frac{\partial}{\partial t} \left[\sin^{-1} \left(\frac{x + M_0 \tau + \mathcal{F} \tau^2}{t - \tau} \right) \right] d\tau$$

$$\frac{\partial \phi}{\partial t} \text{III} = -\frac{1}{\epsilon}$$

$$\frac{\partial \phi}{\partial t} \text{IV} = 0$$

$$\frac{\partial \phi}{\partial t} \text{V} = -\frac{1}{\epsilon\pi} \int_0^{\tau_2} \frac{\partial}{\partial t} \left[\sin^{-1} \left(\frac{x + M_0 \tau + \mathcal{F} \tau^2}{t - \tau} \right) \right] d\tau$$

$$\frac{\partial \phi}{\partial t} \text{VI} = -\frac{1}{\epsilon\pi} \int_{\tau_1}^{\tau_2} \frac{\partial}{\partial t} \left[\sin^{-1} \left(\frac{x + M_0 \tau + \mathcal{F} \tau^2}{t - \tau} \right) \right] d\tau$$

$$\frac{\partial \phi}{\partial t} \text{VII} = -\frac{1}{\epsilon\pi} \int_0^{\epsilon} \frac{\partial}{\partial t} \left[\sin^{-1} \left(\frac{x + M_0 \tau + \mathcal{F} \tau^2}{t - \tau} \right) \right] d\tau$$

$$\frac{\partial \phi}{\partial t} \text{VIII} = -\frac{1}{\epsilon\pi} \int_{\tau_1}^{\epsilon} \frac{\partial}{\partial t} \left[\sin^{-1} \left(\frac{x + M_0 \tau + \mathcal{F} \tau^2}{t - \tau} \right) \right] d\tau$$

$$\frac{\partial \phi}{\partial t} \text{IX} = 0$$

Since the lift at any station t is proportional to the chordwise integration of the $\frac{\partial \phi}{\partial t}$ terms, the method for determining whether limiting (as $\epsilon \rightarrow 0$) values of lift remain due to the collapsed regions is now

Contrails

obvious. It is required that several carefully chosen chordwise integrations be made and then take the limit as $\epsilon \rightarrow 0$. The collapsed regions may then be inspected for lift contributions. The same procedure is then used to compute a quantity proportional to the moment. Notice that this same technique, when the proper constants of proportionality are supplied, determines the lift and the moment contributions of the non-collapsed regions also. Furthermore, this method can be used when the upwash is any power in the variable X .

In order to facilitate these proposed integrations Figure 25 presents the equations of the various curves of importance and the following tabulation gives the t stations at which various regions begin and end, these t stations being denoted by the t coordinate of points 3 through 7 shown in Figure 25.

$$t_3 = \frac{\epsilon}{2} [M_0 + 1 + \gamma \epsilon]$$

$$t_4 = -\left(\frac{M_0 + 1}{2\gamma}\right) + \sqrt{\left(\frac{M_0 + 1}{2\gamma}\right)^2 + \frac{1}{\gamma}}$$

$$t_5 = -\left(\frac{M_0 + 1}{2\gamma}\right) + \sqrt{\left(\frac{M_0 + 1}{2\gamma}\right)^2 + [\epsilon(M_0 + 1 + \gamma \epsilon) + 1] / \gamma}$$

$$t_6 = -\left(\frac{M_0 - 1}{2\gamma}\right) + \sqrt{\left(\frac{M_0 - 1}{2\gamma}\right)^2 + \frac{1}{\gamma}}$$

$$t_7 = -\left(\frac{M_0 - 1}{2\gamma}\right) + \sqrt{\left(\frac{M_0 - 1}{2\gamma}\right)^2 + [1 + \epsilon(M_0 - 1 + \gamma \epsilon)] / \gamma}$$

The first integration to be carried out will be for the regions $0 \leq t \leq \epsilon$. Thus choosing some t between 0 and ϵ , the lift is proportional to the following expression.

Contrails

$$L_c \sim \int_{-M_0 t - \mathcal{J}t^2}^{-t} \frac{\partial}{\partial t} \phi_I dx + \int_{-t}^t \frac{\partial}{\partial t} \phi_{II} dx + \int_t^{1-M_0 t - \mathcal{J}t^2} \frac{\partial}{\partial t} \phi_{III} dx$$

Since all three integrands contain $-\frac{1}{\epsilon}$, and in fact $\frac{\partial \phi}{\partial t} \phi_{III}$ is identically equal to $-\frac{1}{\epsilon}$, this $-\frac{1}{\epsilon}$ term can be removed and treated as a single integration across the plannform. Utilizing this equivalent expression and writing out the remainder of the integrands explicitly yields the following.

$$L_c \sim -\frac{1}{\epsilon} \int_{-M_0 t - \mathcal{J}t^2}^{1-M_0 t - \mathcal{J}t^2} dx - \frac{1}{\epsilon \pi} \int_{-M_0 t - \mathcal{J}t^2}^{-t} dx \int_{\tau_1}^{\tau_2} \frac{\partial}{\partial t} \sin^{-1} \left(\frac{x + M_0 \tau + \mathcal{J} \tau^2}{t - \tau} \right) d\tau$$

$$-\frac{1}{\epsilon \pi} \int_{-t}^t dx \int_0^{\tau_2} \frac{\partial}{\partial t} \sin^{-1} \left(\frac{x + M_0 \tau + \mathcal{J} \tau^2}{t - \tau} \right) d\tau$$

As presently written, the double integrals are to be evaluated by first holding X constant, integrating over the appropriate τ interval and then integrating over the indicated X interval. This integration is difficult to do by this sequence of operations, thus a change in the order of integration is appropriate. Referring to Figure 26, which illustrates the τ, X region of integration, the expression proportional to L_c is given as,

$$L_c \sim -\frac{1}{\epsilon} - \frac{1}{\epsilon \pi} \int_0^t d\tau \int_{X(\tau_1)}^{X(\tau_2)} \frac{\partial}{\partial t} \sin^{-1} \left(\frac{x + M_0 \tau + \mathcal{J} \tau^2}{t - \tau} \right) dx$$

$$= -\frac{1}{\epsilon} - \frac{1}{\epsilon \pi} \int_0^t d\tau \int_{-M_0 \tau - \mathcal{J} \tau^2 - t + \tau}^{-M_0 \tau - \mathcal{J} \tau^2 + t - \tau} \frac{x + M_0 \tau + \mathcal{J} \tau^2}{\sqrt{(t - \tau)^2 - (x + M_0 \tau + \mathcal{J} \tau^2)^2}} dx$$

Carrying out the integration, $L_c \sim -\frac{1}{\epsilon}$.

Contrails

Noting that the upwash $w = \frac{1}{\epsilon}$ or that $w\epsilon = 1$ even as the $\epsilon \rightarrow 0$ limit is taken, it is seen that L_c is proportional to a unit delta function at $t = 0$. Therefore,

$L_c \sim \delta(t - 0)$ when $t = 0$. This value is in fact proportional to the zero-thickness second-order piston theory value as should be expected.

Observing that the distance between some point X and the planform leading edge, at some time t , is equal to $X + M_0 t + \mathcal{J} t^2$, the expression proportional to the moment for $0 \leq t \leq \epsilon$ is given by

$$M_c \sim \frac{1}{2\epsilon} - \frac{1}{\epsilon\pi} \int_0^t \frac{d\tau}{(t-\tau)} \int_{-(M_0\tau + \mathcal{J}\tau^2) - t + \tau}^{-(M_0\tau + \mathcal{J}\tau^2) + t - \tau} \frac{(x + M_0\tau + \mathcal{J}\tau^2)(x + M_0t + \mathcal{J}t^2)}{\sqrt{(t-\tau)^2 - (x + M_0\tau + \mathcal{J}\tau^2)^2}} dx$$

Using the identity that $x + M_0t + \mathcal{J}t^2 = x + M_0\tau + \mathcal{J}\tau^2 + M_0(t-\tau) + \mathcal{J}(t-\tau)^2 + 2\tau(t-\tau)$ the integration is easily executed and yields the following result.

$$M_c \sim \frac{1}{2\epsilon} - \frac{1}{4\epsilon} t^2$$

As $\epsilon \rightarrow 0$ the product $\frac{t^2}{\epsilon} \rightarrow 0$, since $t \leq \epsilon$. Thus M_c is also impulsive, as should be expected, at $t = 0$.

$$M_c \sim \frac{1}{2} \delta(t-0) ; t=0$$

The second integration to be carried out is for $\epsilon < t \leq t_3$. Making use of Figure 27, the integrals for the lift and moment proportionals become,

$$L_c \sim \frac{1}{\epsilon\pi} \int_0^\epsilon \frac{d\tau}{(t-\tau)} \int_{-(M_0\tau + \mathcal{J}\tau^2) - t + \tau}^{-(M_0\tau + \mathcal{J}\tau^2) + t - \tau} \frac{(x + M_0\tau + \mathcal{J}\tau^2) dx}{[(t-\tau)^2 - (x + M_0\tau + \mathcal{J}\tau^2)^2]^{1/2}} \equiv 0$$

$$M_c \sim \frac{1}{\epsilon\pi} \int_0^\epsilon \frac{\pi(t-\tau)}{2} d\tau = \frac{1}{2} \left(t - \frac{\epsilon}{2}\right)$$

Now as $\epsilon \rightarrow 0, t \rightarrow 0$ if $t \leq t_3$ so that M_c for this τ region goes to zero.

Contrails

In a similar fashion the lifts and moments can be computed for the limiting case of $\epsilon \rightarrow 0$. The results of these calculations have been presented in Section 1.4 of this report, and reflect the results that no singularities occur across the collapsed regions except those regions that contribute to the impulse functions at $t = 0$.

APPENDIX III

Approximate times on the 704 for the following programs

	Time
1. Compute GJ(t) (one k)	9 mins.
$0 \leq t \leq 23.26 \text{ sec.}$ $nq = 9q$	
2. Compute GJ(t) (one k)	3.5 mins.
$23.26 \leq t \leq 1200 \text{ sec.}$ $nq = 9q$	
3. Piston theory differential equations	8 mins.
$nq = 270(1 - \cos .2513t)$ $0 \leq t \leq 1.0 \text{ sec.}, \Delta t = .001 \text{ sec.}$	
4. Unsteady Aerodynamics Difference Equations	
$nq = 270(1 - \cos .2513t)$ $0 \leq t \leq .500 \text{ sec.}, t_0 = 0 \text{ sec.}$	110 mins.
$8 \leq t \leq 8.5 \text{ sec.}, t_0 = 8 \text{ sec.}$	7 mins.

It is to be noted that the computing time factor from computation (3) to (4) is about 20 for the early time calculations $0 \leq t_0 \leq 4 \text{ sec.}$

Contrails

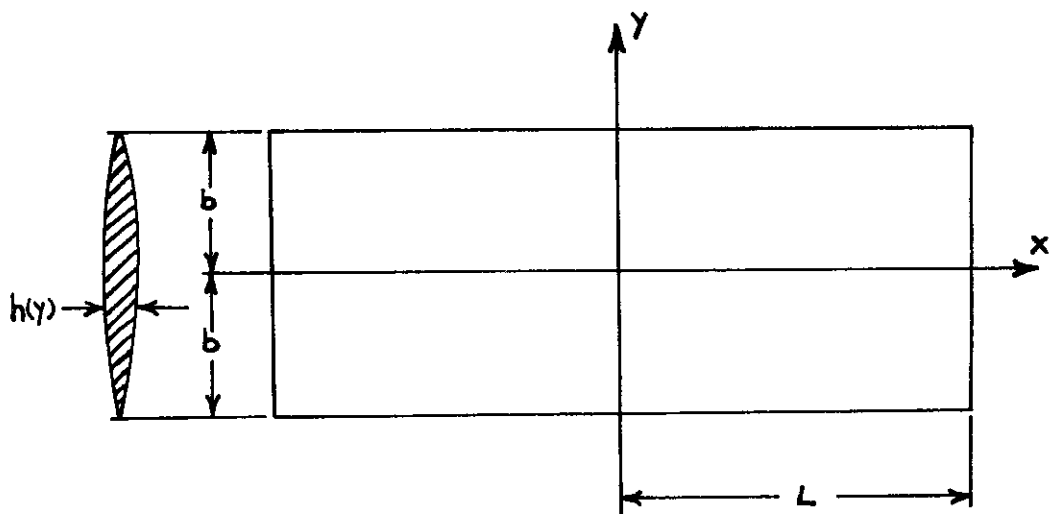
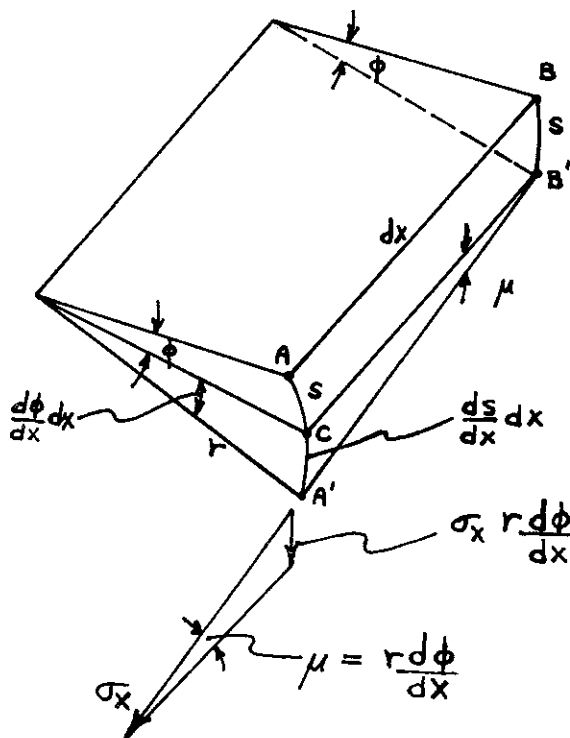


Fig. 1 Wing Planform and Cross Section



For small angles,

$$CA' = \frac{ds}{dx} dx = \mu dx = r \left(\frac{d\phi}{dx} dx \right)$$

Thus:

$$\mu = r \frac{d\phi}{dx}$$

Fig. 2 Segment of Twisted Wing

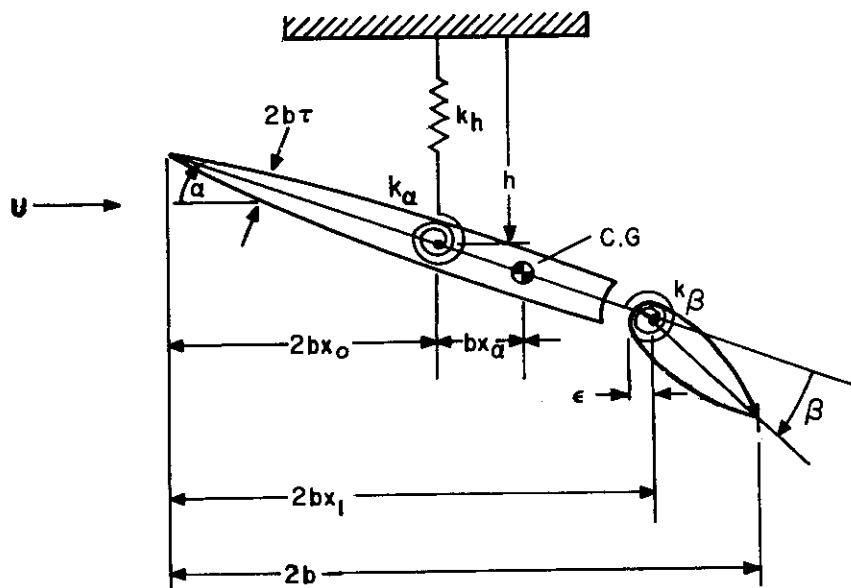


Fig. 3 Non-Zero-Thickness Typical Section

Contrails

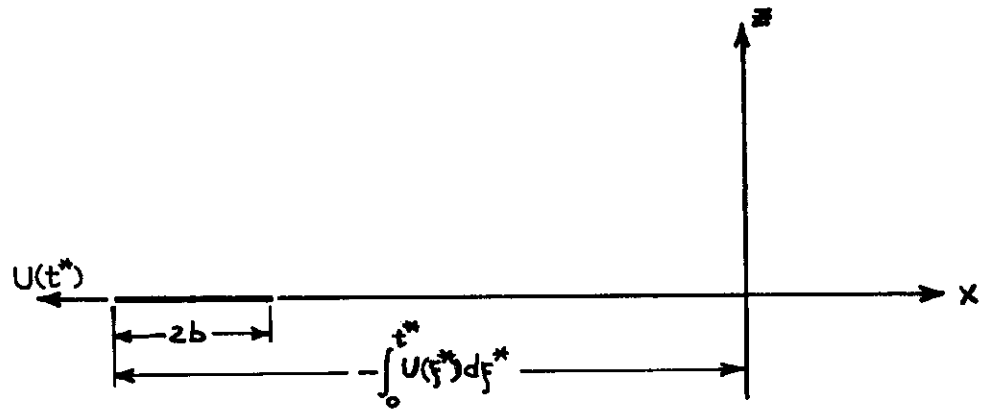


Fig. 4 Two-Dimensional Accelerating Airfoil

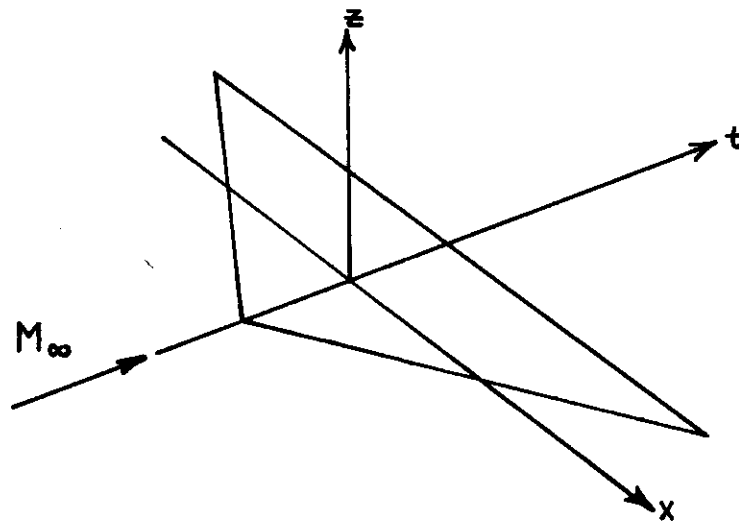


Fig. 5 Three-Dimensional Steady State Airfoil

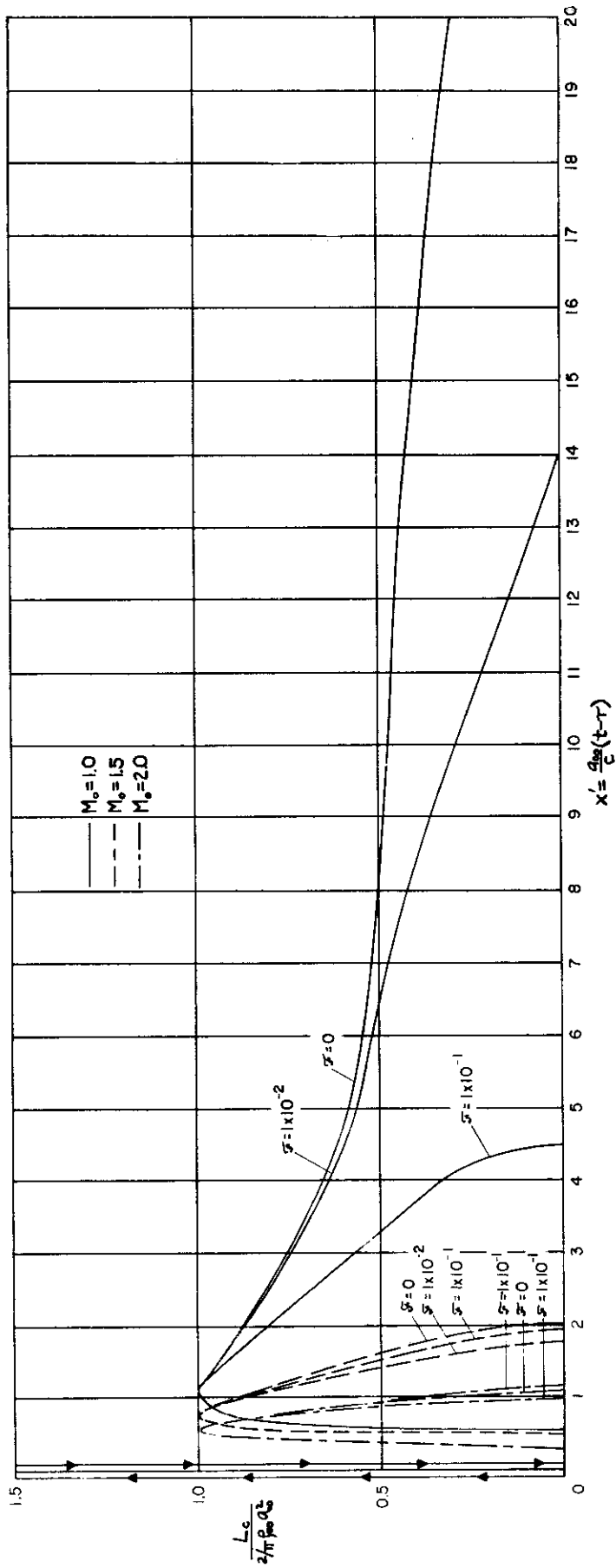


Fig. 6 Lift Due to Impulsive Plunging Motion for Constant \dot{S}

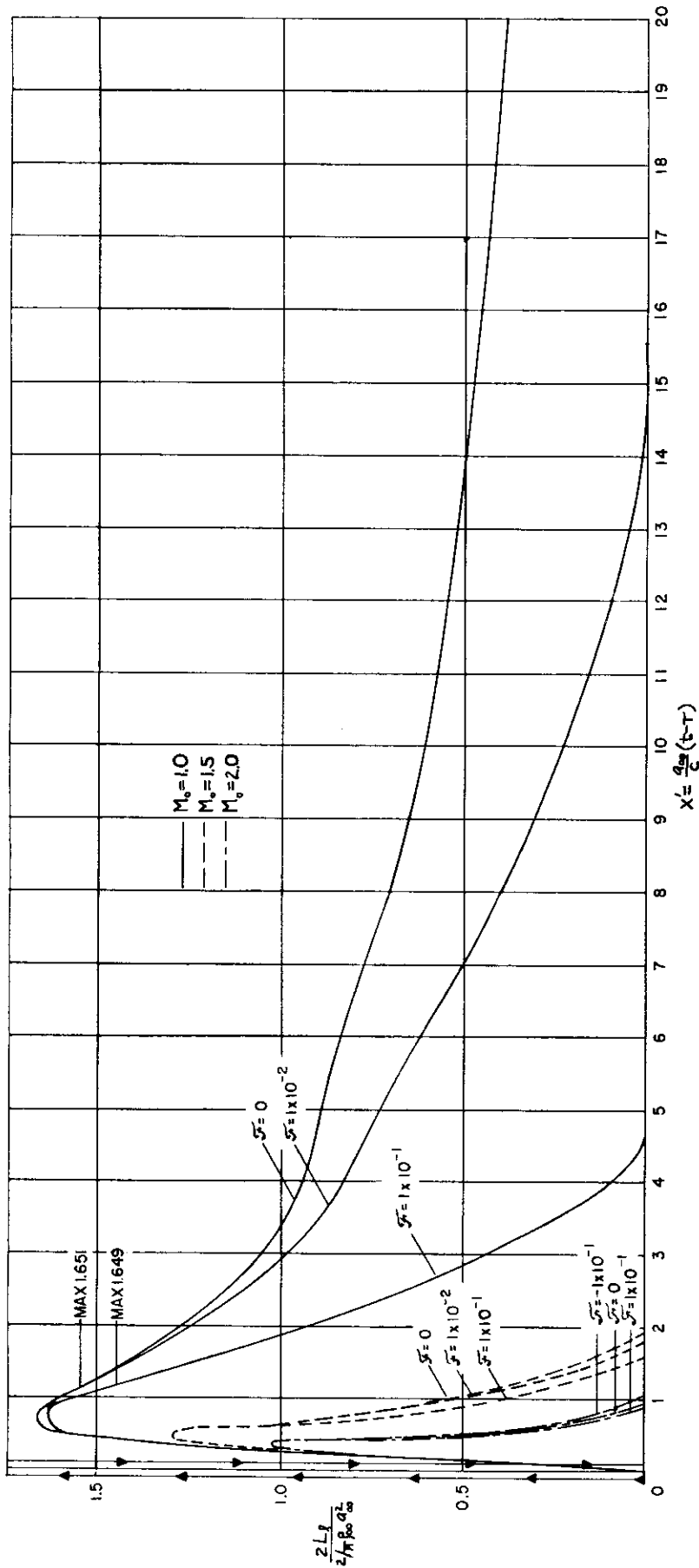


Fig. 7 Lift Due to Impulsive Pitch Rate About the Airfoil Leading Edge for Constant $\dot{\alpha}$

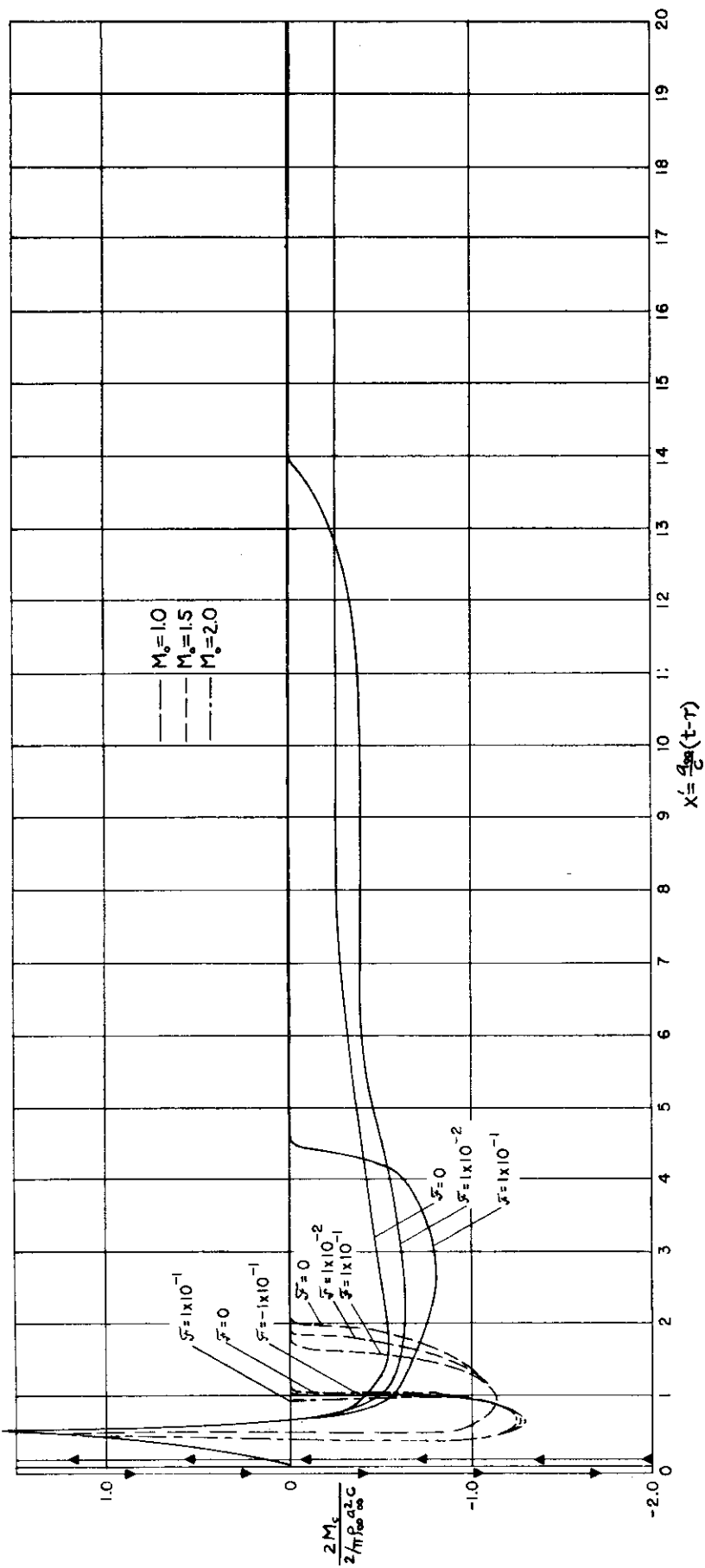


Fig. 8 Pitching Moment Due to Impulsive Plunging Motion for Constant $\mathcal{F}'s$

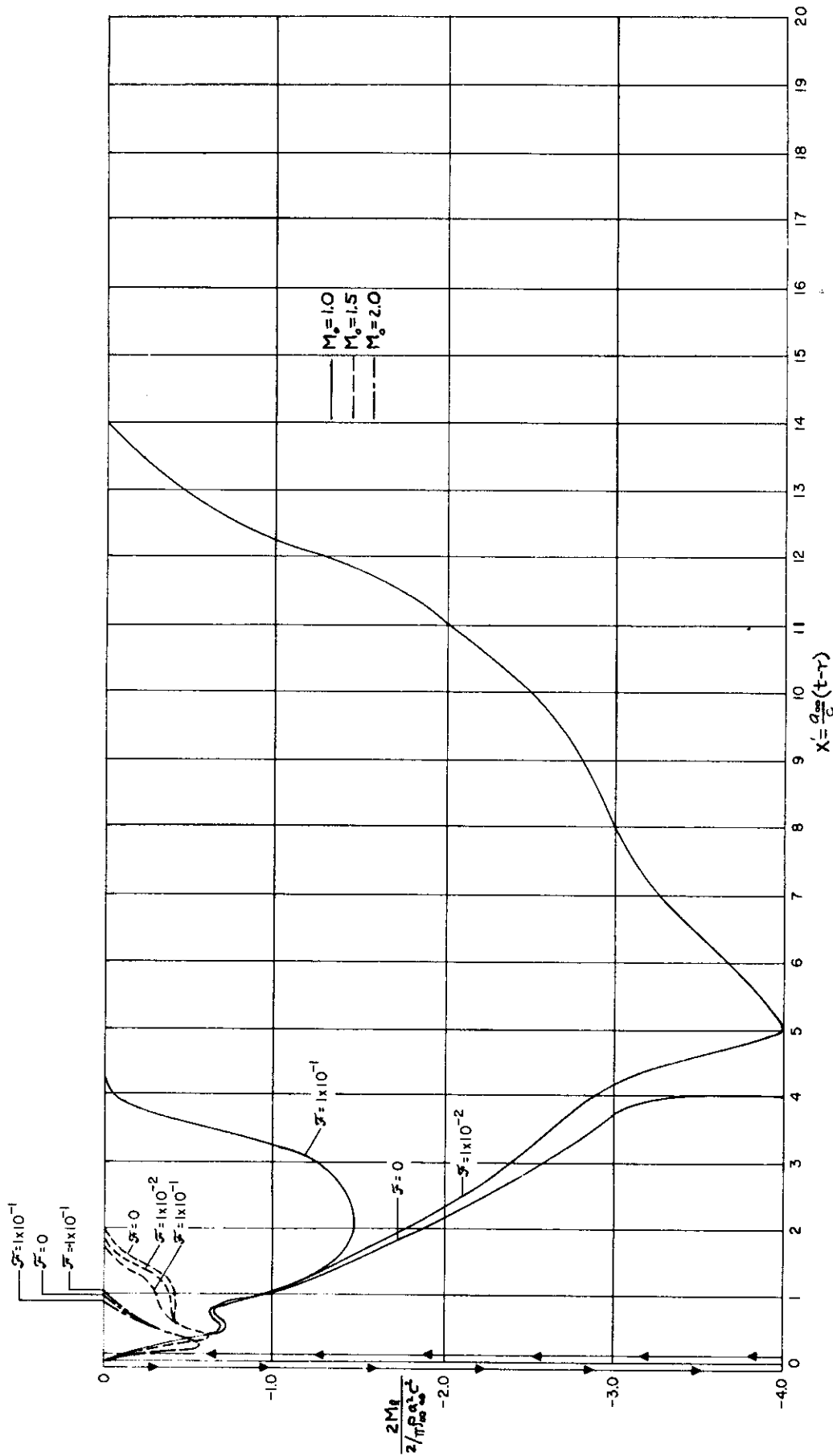


Fig. 9 Pitching Moment Due to Impulsive Pitch Rate About the Airfoil Leading Edge for Constant γ 's

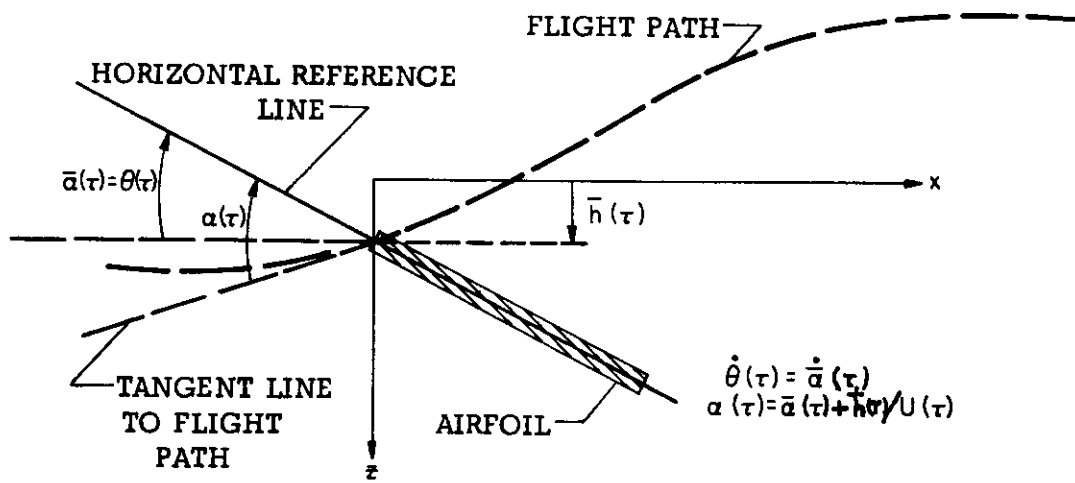


Fig. 10 Flight Path Variables

Contrails

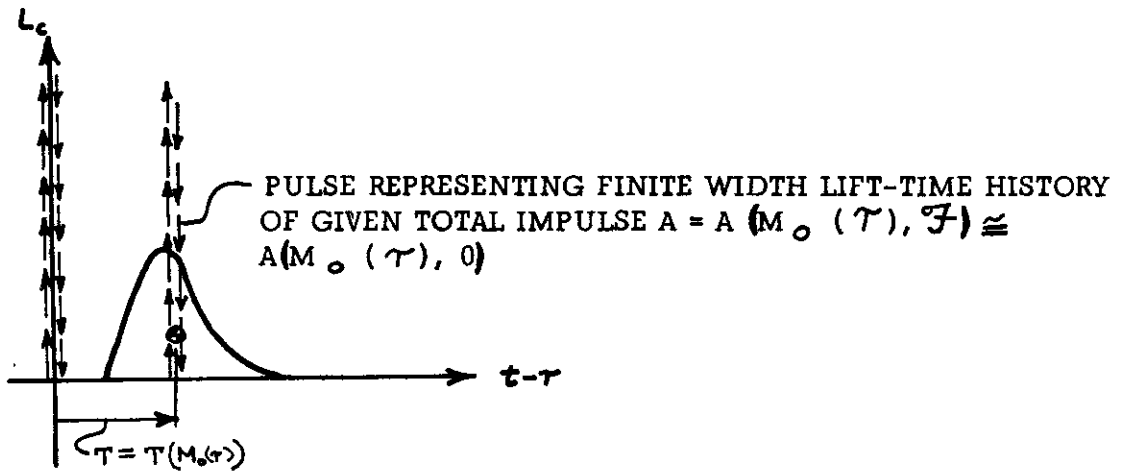


Fig. 11 Pulse Representation

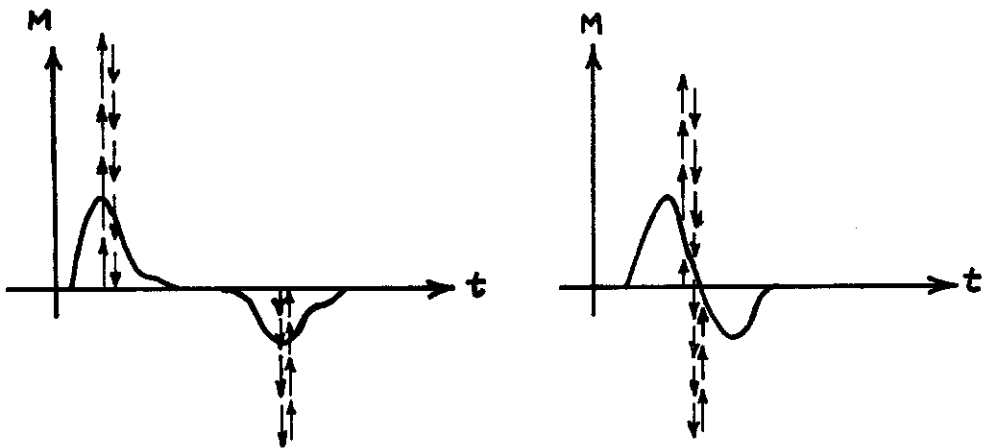


Fig. 12 Moment Pulse and Doublet Representation

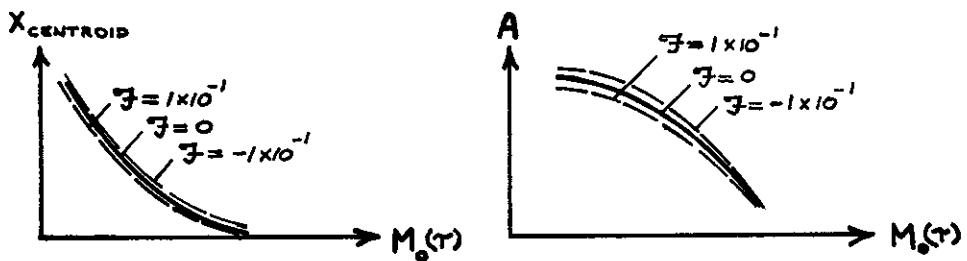


Fig. 13 Typical Pulse Strength and Pulse Centroid Plots

Contrails

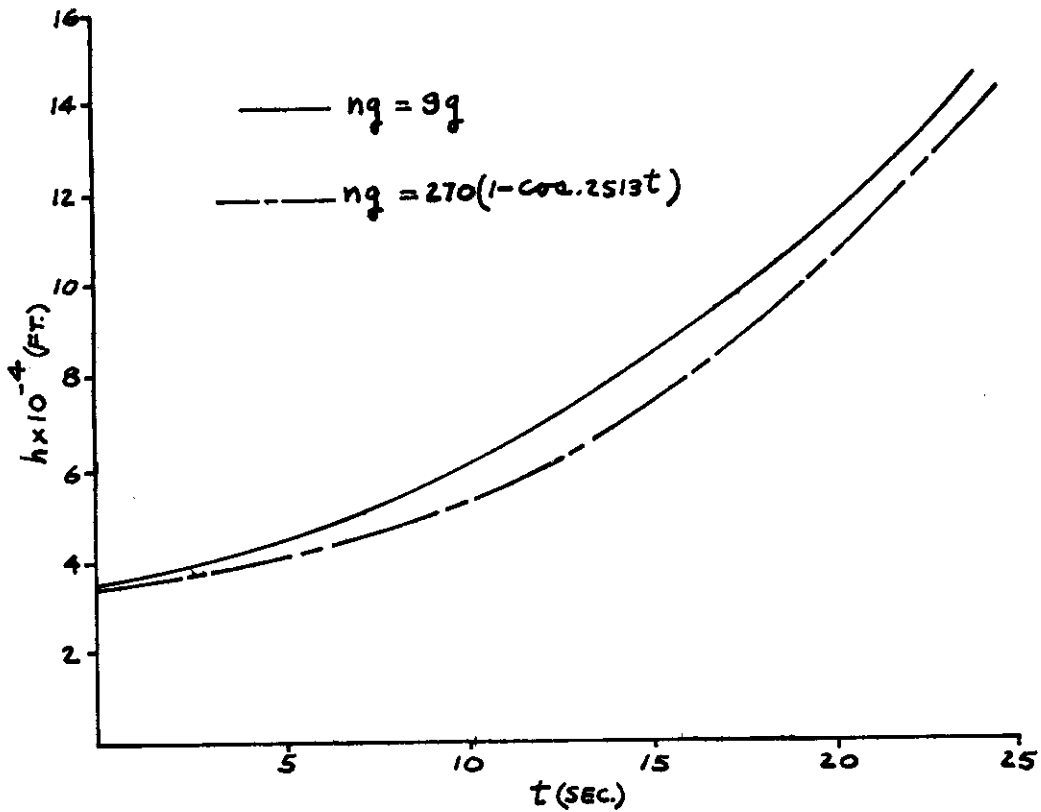


Fig. 14 Altitude versus Time for the Chosen Flight Missions

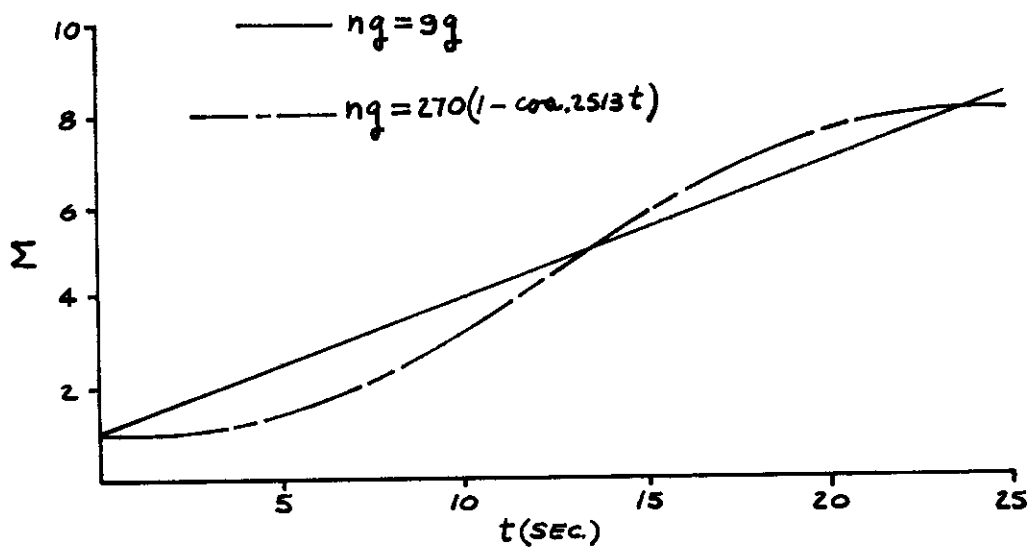


Fig. 15 Mach Number versus Time for the Chosen Flight Missions

Contrails

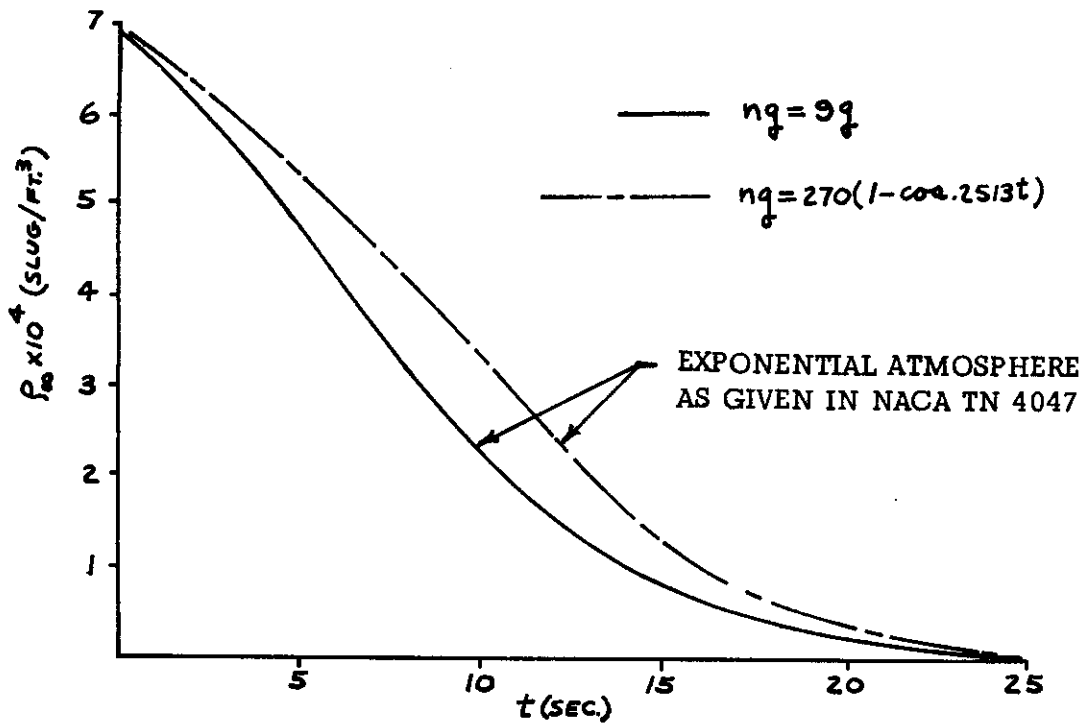


Fig. 16 Ambient Density versus Time for the Chosen Flight Missions

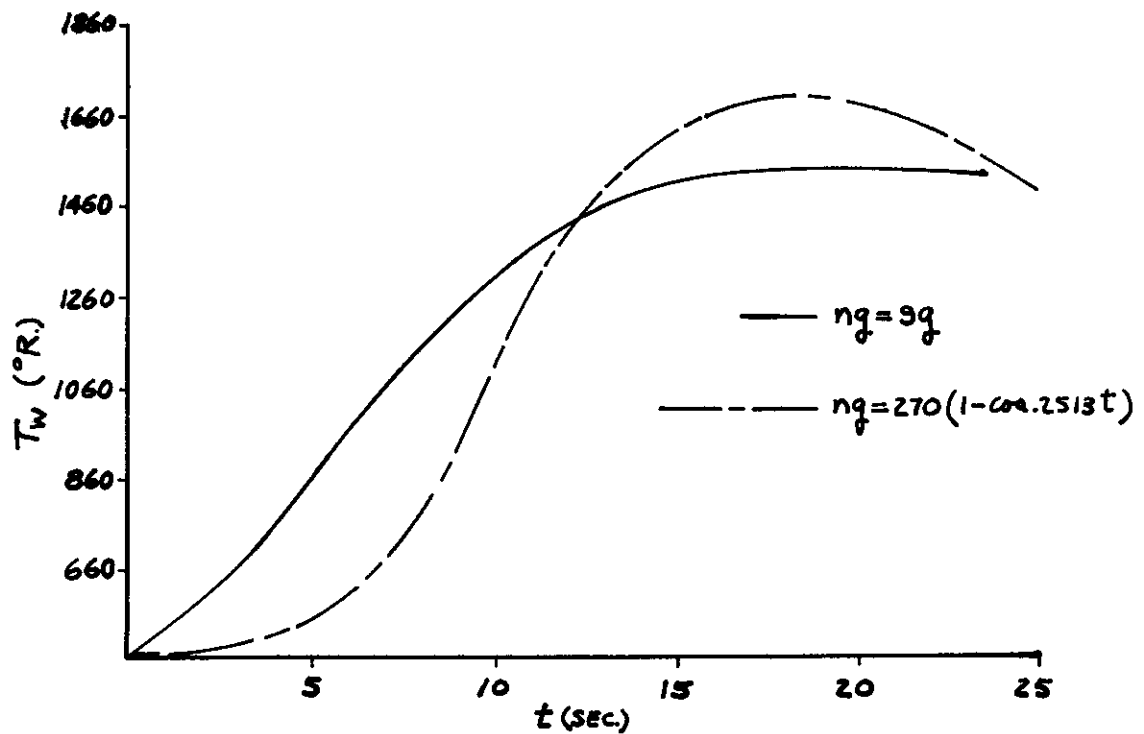


Fig. 17 Wall Temperature versus Time for the Chosen Flight Missions

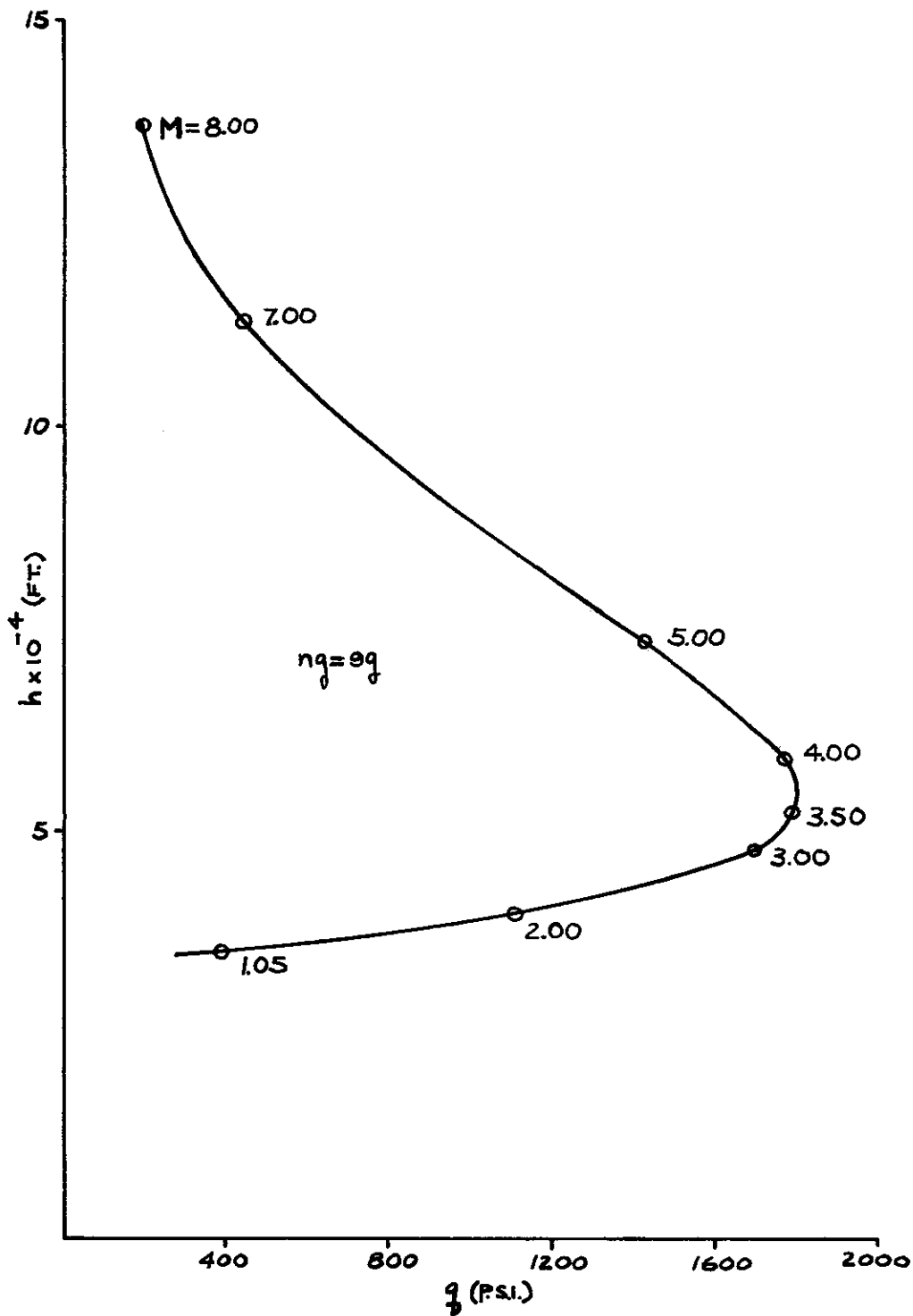


Fig. 18 Dynamic Pressure versus Altitude for the 9g Accelerated Flight Mission

Contrails

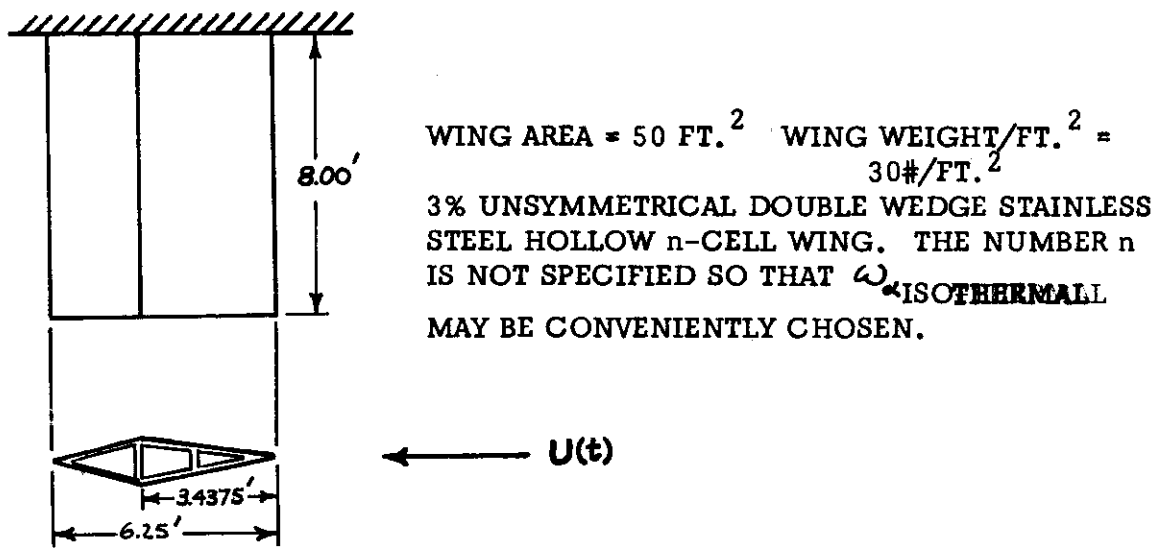


Fig. 19 Wing Geometry of the Vehicle Performing the Flight Missions

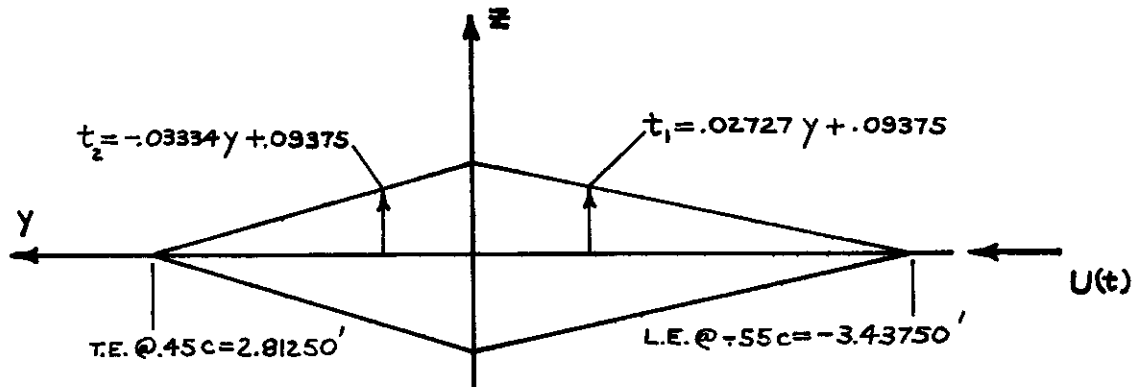


Fig. 20 External Wing Cross-Section Geometry of the Vehicle Performing the Flight Missions

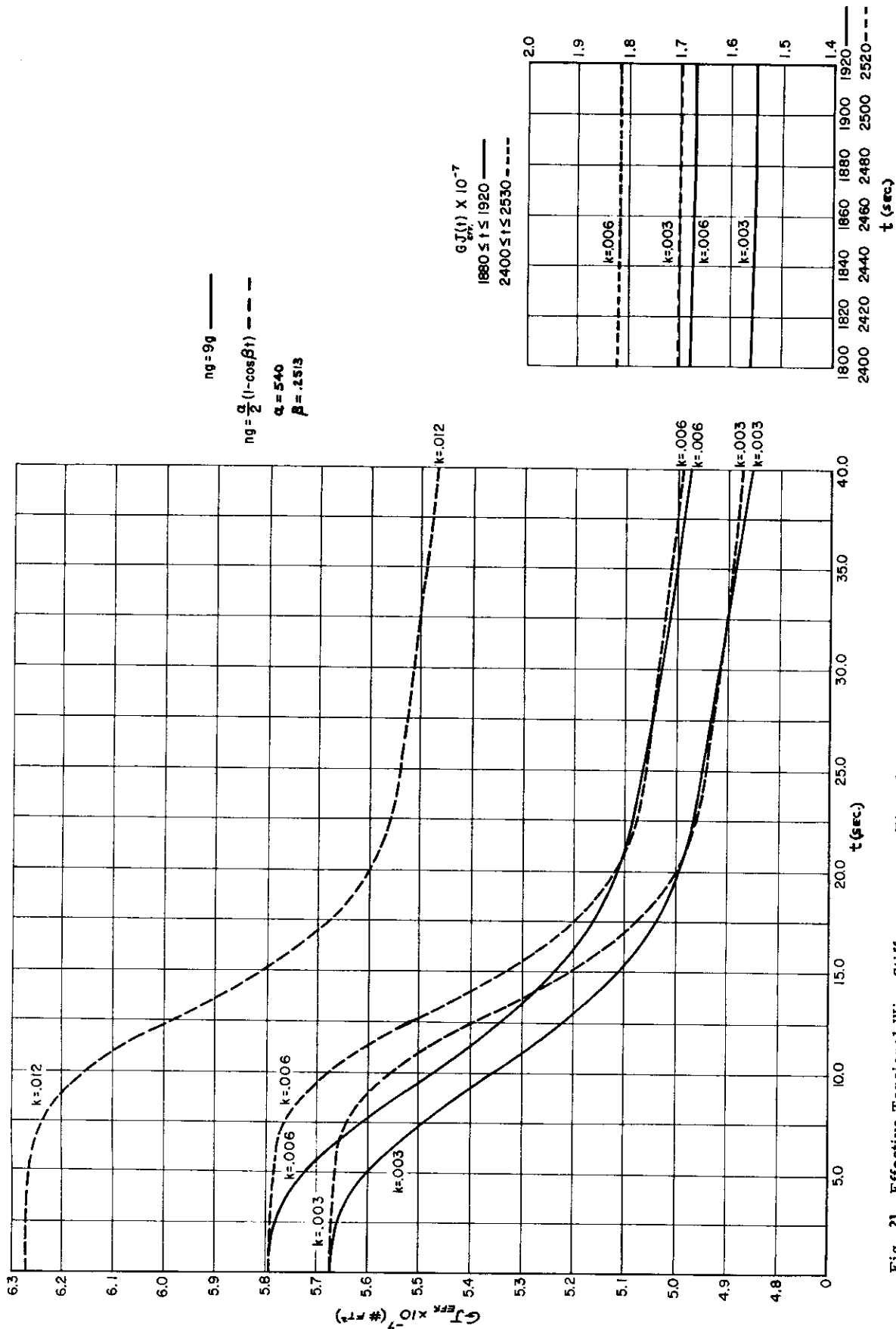


Fig. 21 Effective Torsional Wing Stiffness versus Time for the Chosen Flight Missions and Several Values of the Parameter k

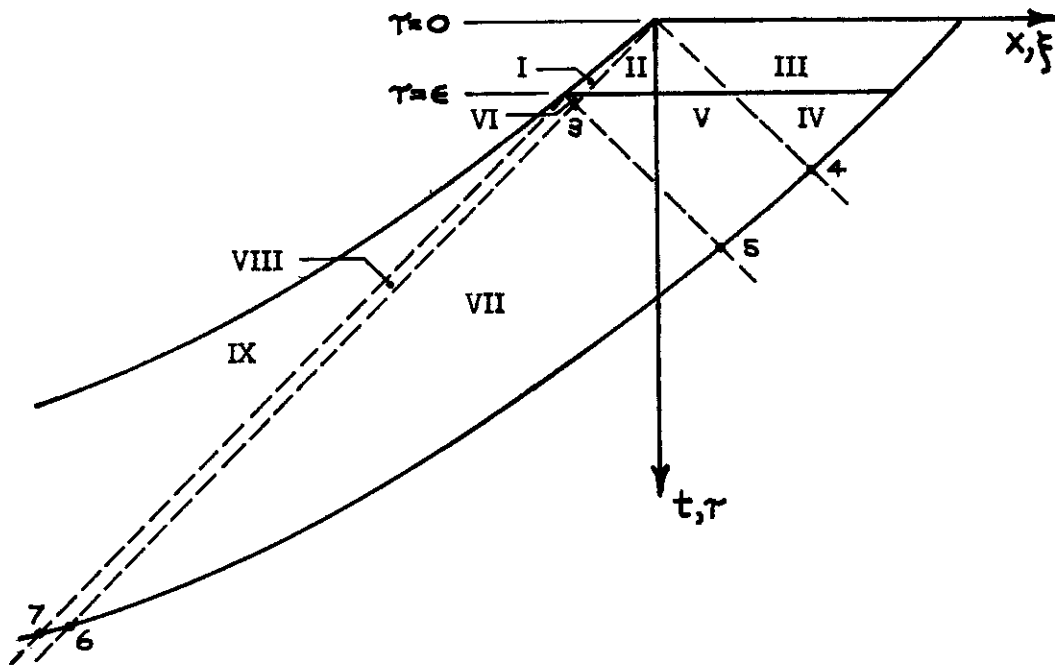


Fig. 22 Supersonic Three-Dimensional Analogy Planform with a Finite Band of Upwash on the Airfoil Between $0 \leq t \leq \epsilon$

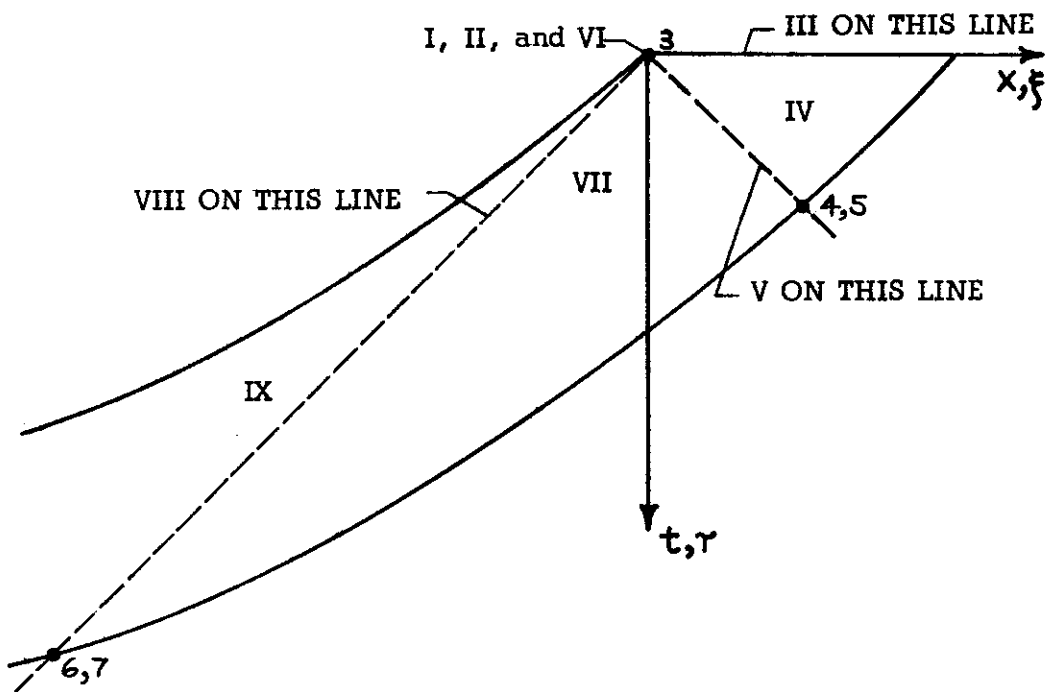


Fig. 23 Supersonic Three-Dimensional Analogy Planform with an Impulsive Upwash Along the Leading Edge

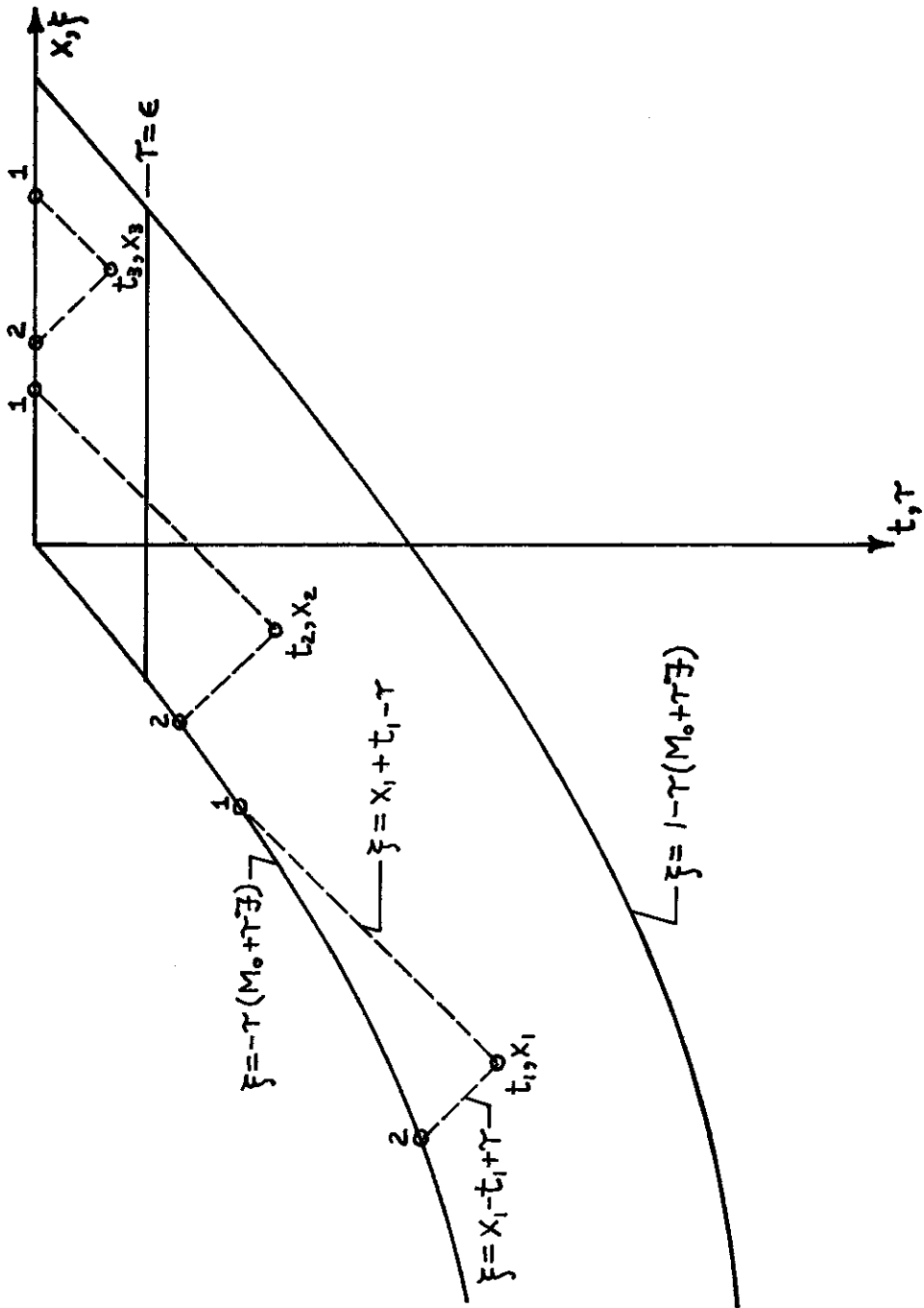


Fig. 24 Wing Geometry and Forward Mach Cone Representations

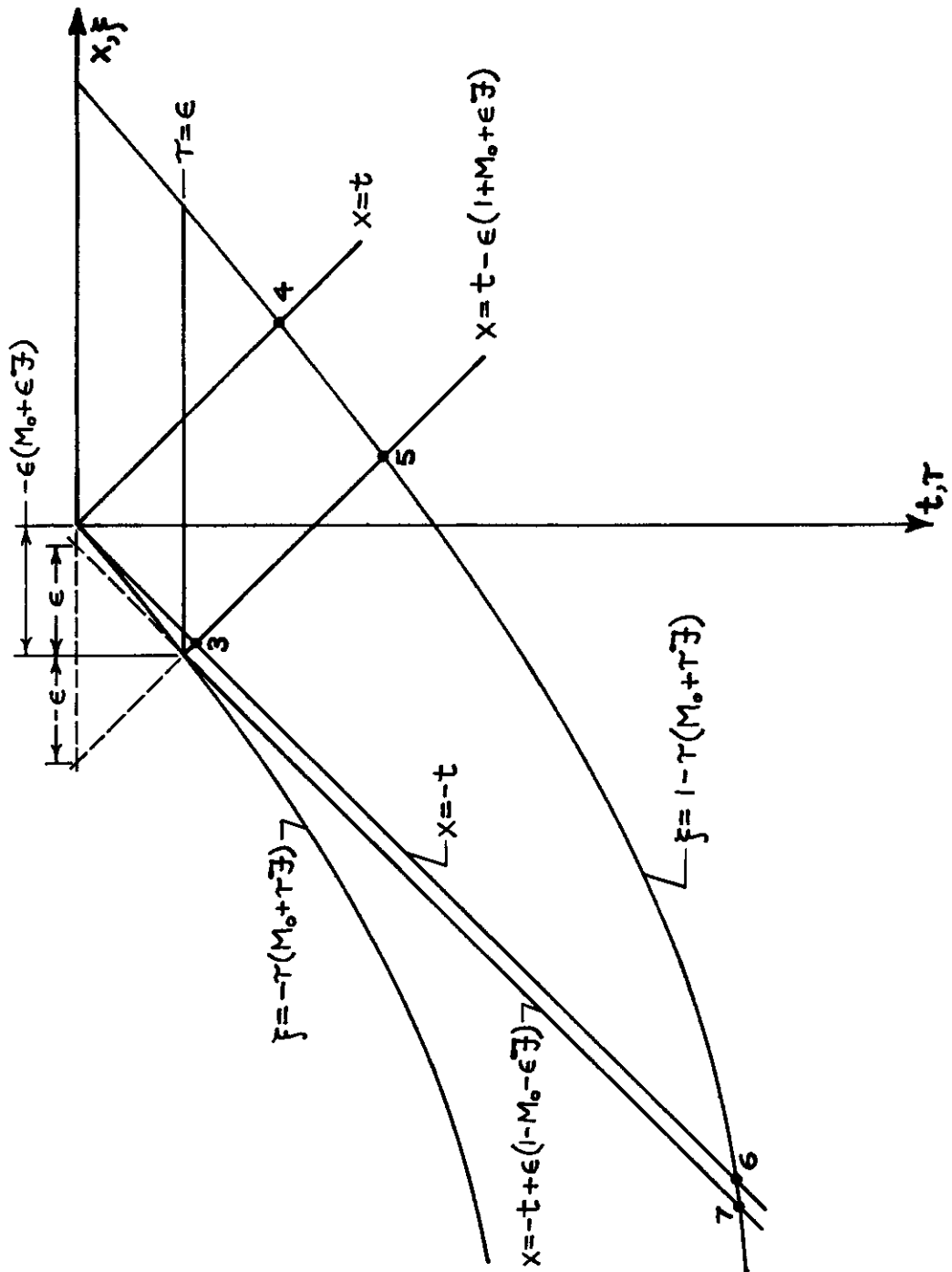


Fig. 25 Equations Representing the Various Planform Curves and the Mach Lines

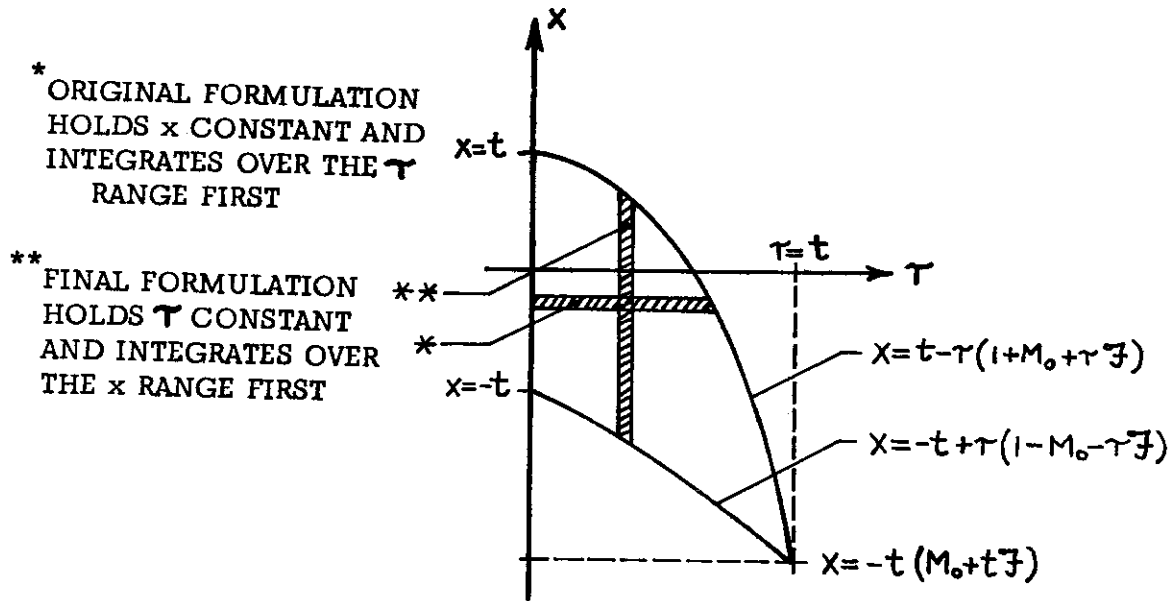


Fig. 26 Integration Region for $0 \leq t \leq \epsilon$

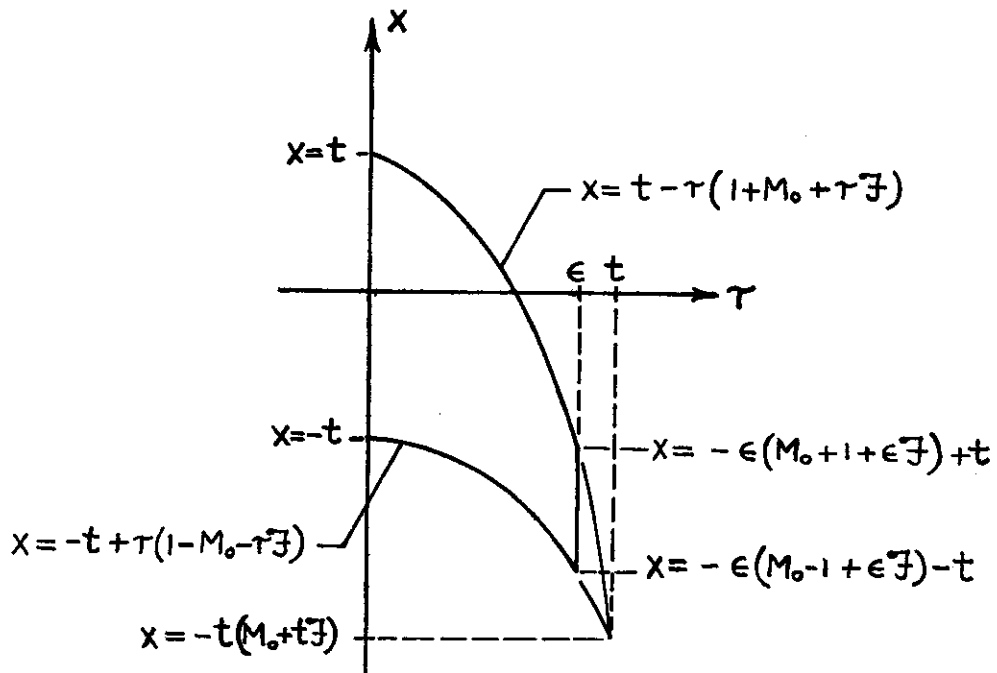


Fig. 27 Integration Region for $\epsilon \leq t \leq t_3$

Contrails

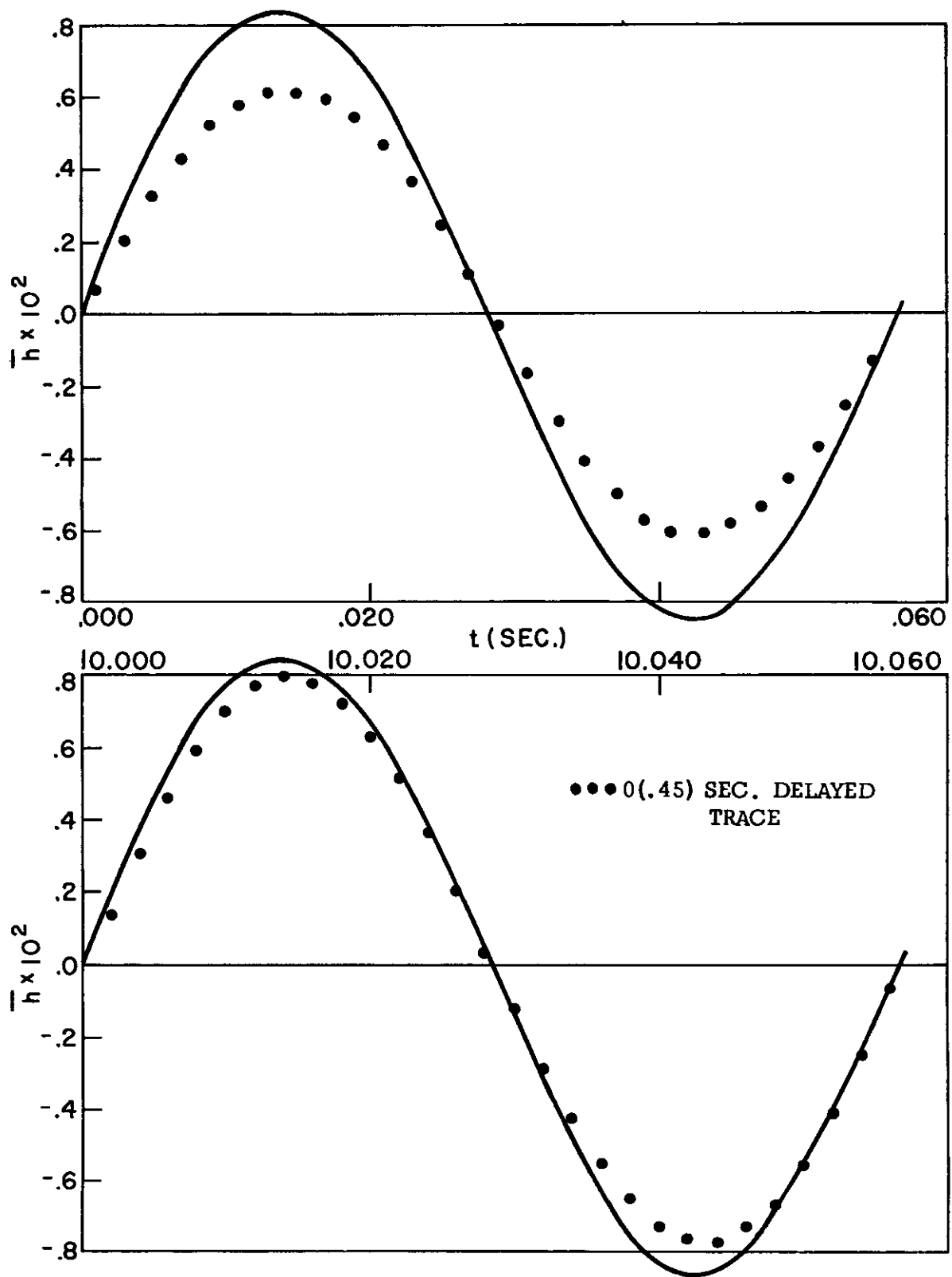


Fig. 28 \bar{h} Time History Due to Case 1 Initial Conditions Applied at $t_0 = 0$ and 10 Seconds Compared with Itself Approximately .45 Seconds Later; $ng = 9g$

Contrails

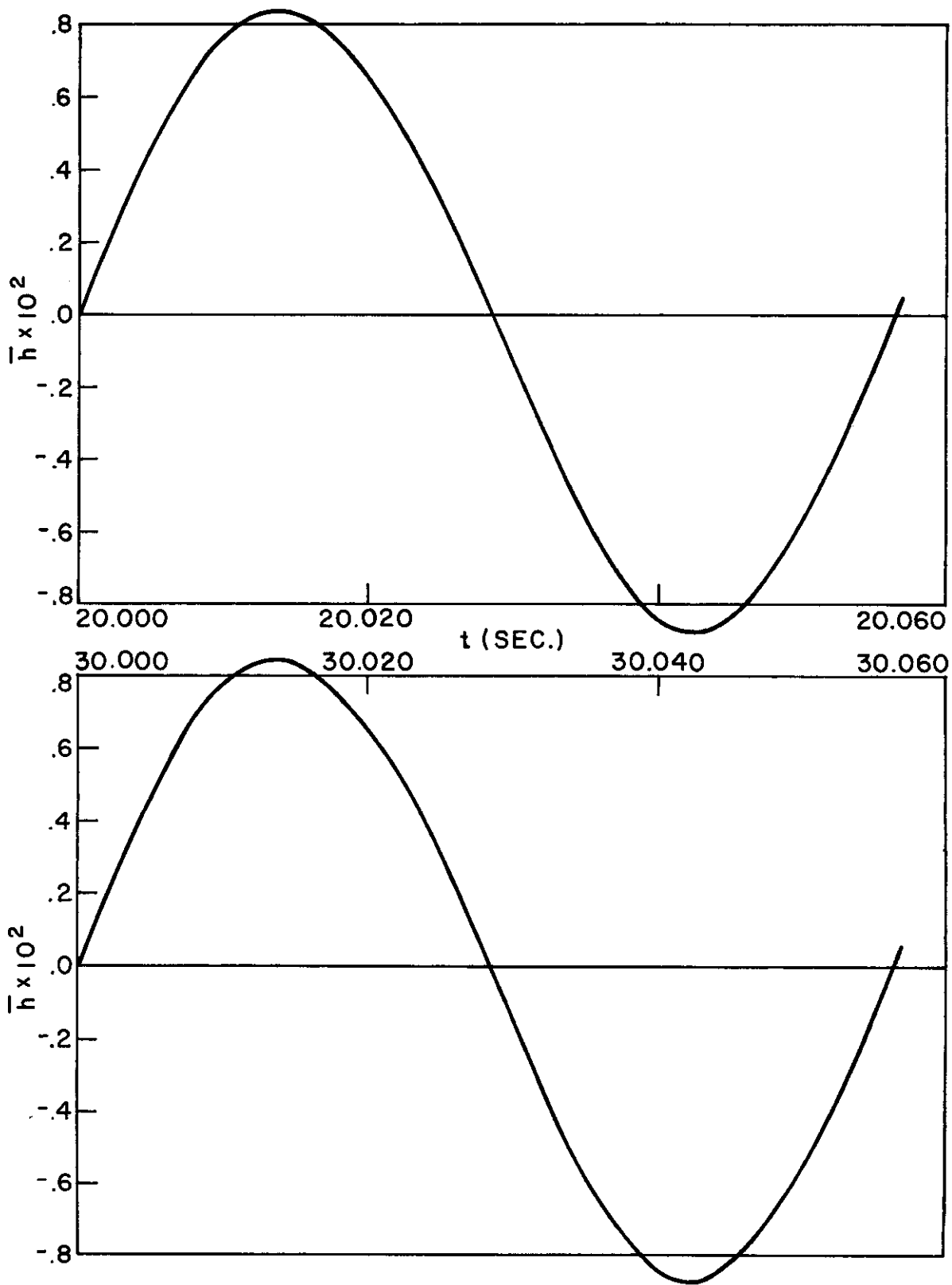


Fig. 29 \bar{h} Time History Due to Case 1 Initial Conditions Applied at $t_0 = 20$ and 30 Seconds; $ng = 9g$

Contrails

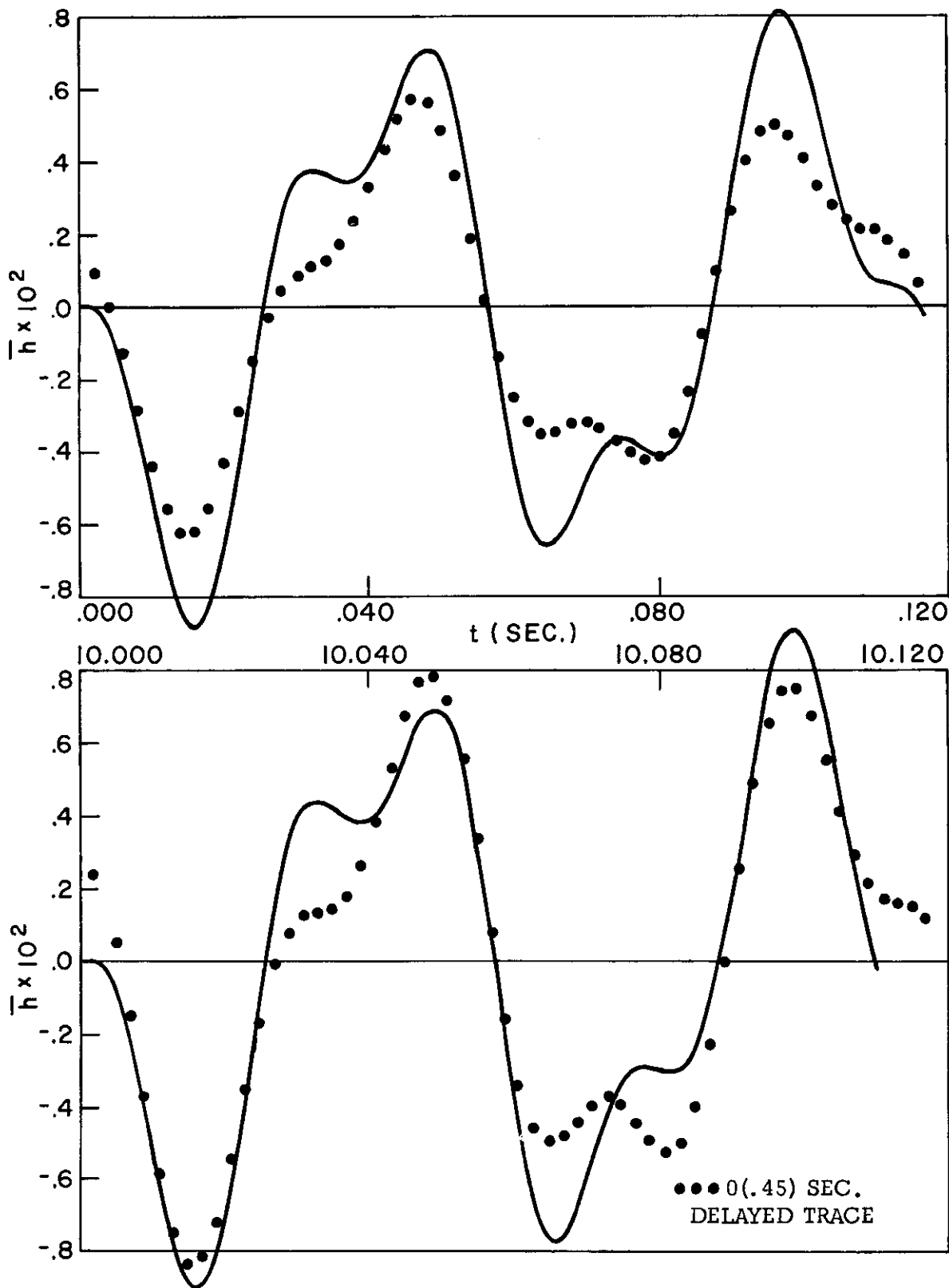


Fig. 30 \bar{h} Time History Due to Case 2 Initial Conditions Applied at $t_0 = 0$ and 10 Seconds Compared with Itself Approximately .45 Seconds Later; $n_g = 9g$

Contrails

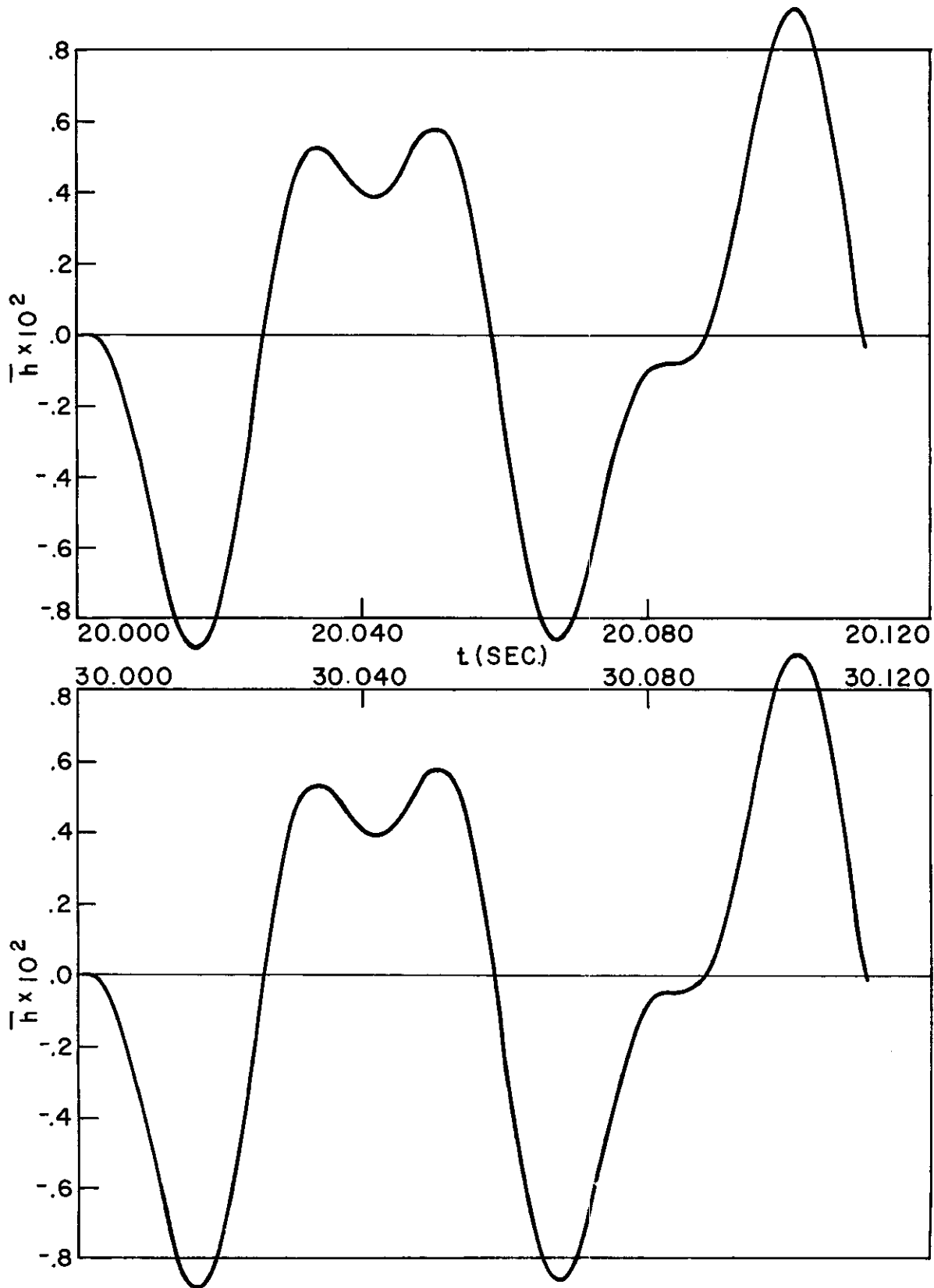


Fig. 31 \bar{h} Time History Due to Case 2 Initial Conditions Applied at $t_0 = 20$ and 30 Seconds; $n_g = 9g$

Contrails

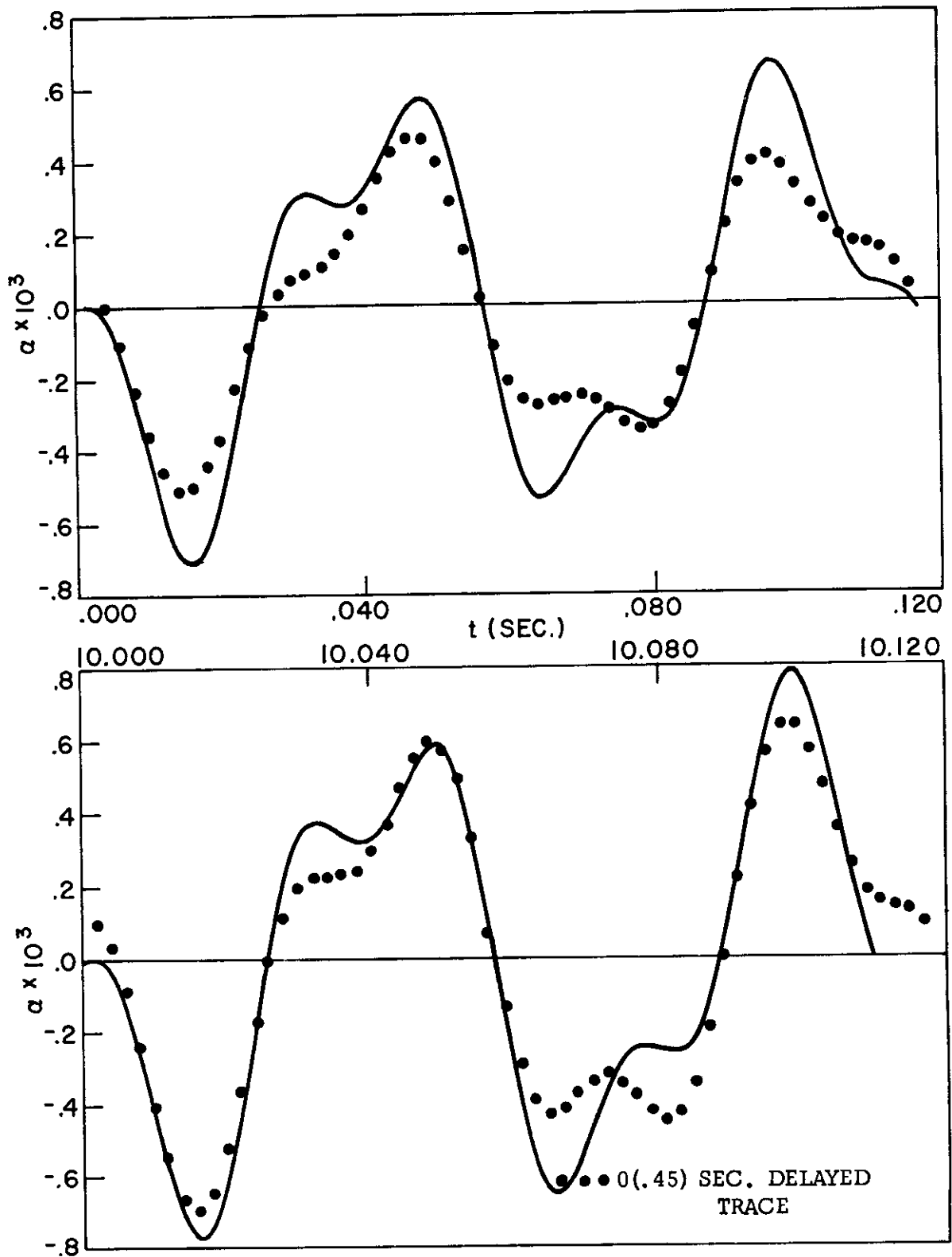


Fig. 32 α Time History Due to Case 1 Initial Conditions Applied at $t_0 = 0$ and 10 Seconds Compared with Itself Approximately .45 Seconds Later; $n_g = 9g$

Contrails

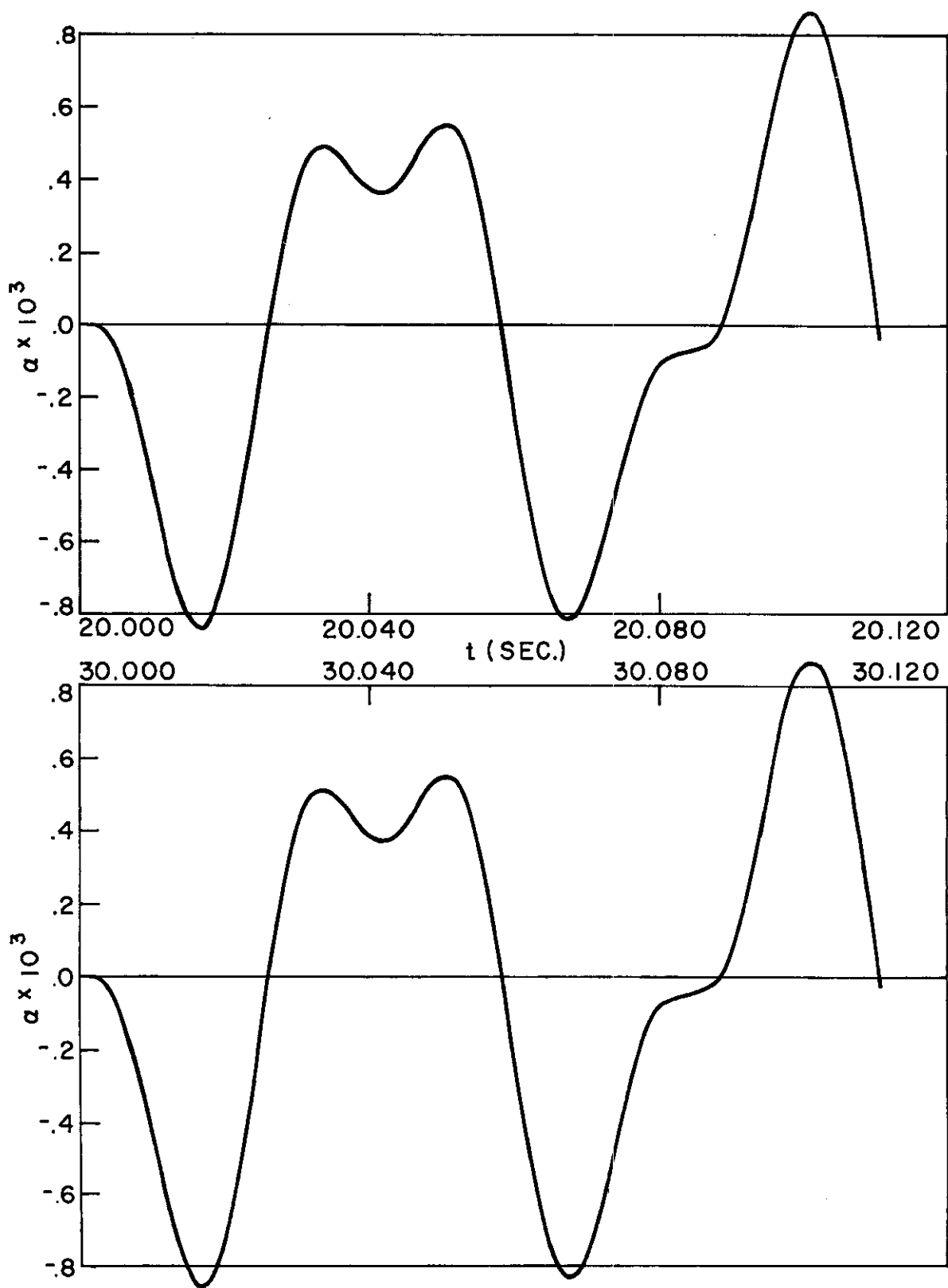


Fig. 33 α Time History Due to Case 1 Initial Conditions Applied at $t_0 = 20$ and 30 Seconds; $n_g = 9g$

Contrails

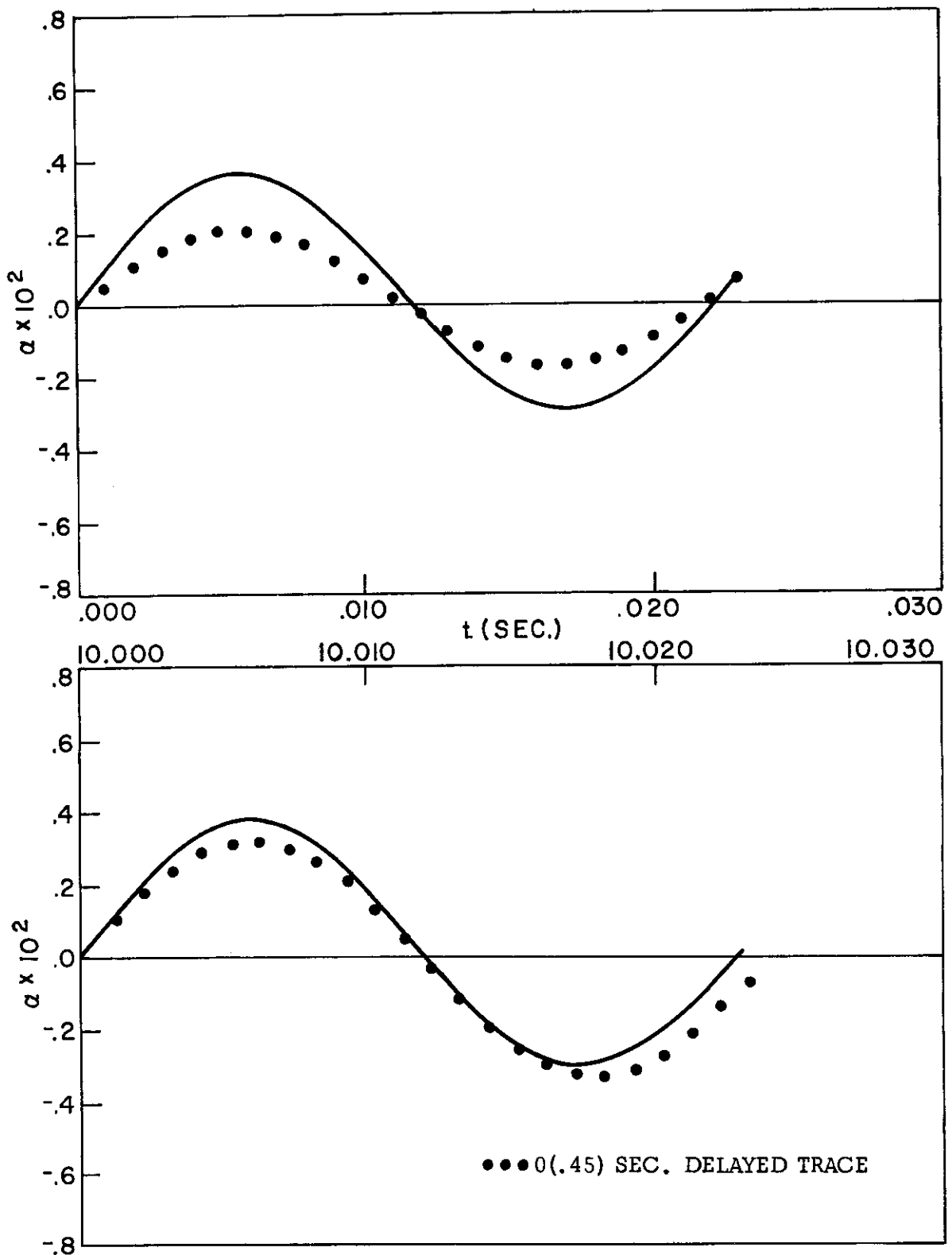


Fig. 34 α Time History Due to Case 2 Initial Conditions Applied at $t_0 = 0$ and 10 Seconds Compared with Itself Approximately .45 Seconds Later; $n_g = 9g$

Contrails

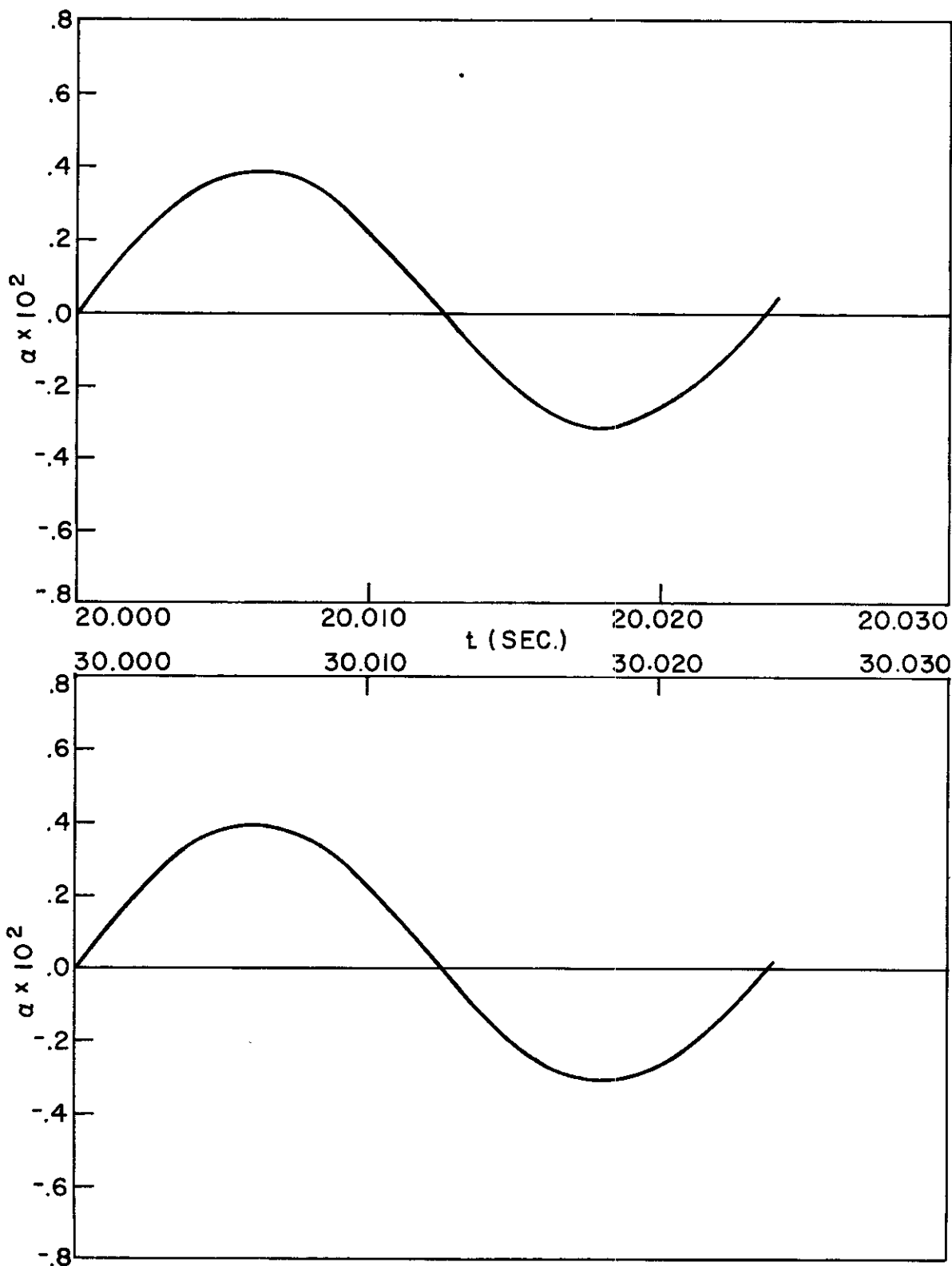


Fig. 35 α Time History Due to Case 2 Initial Conditions Applied at $t_0 = 20$ and 30 Seconds; $n_g = 9g$

Contrails

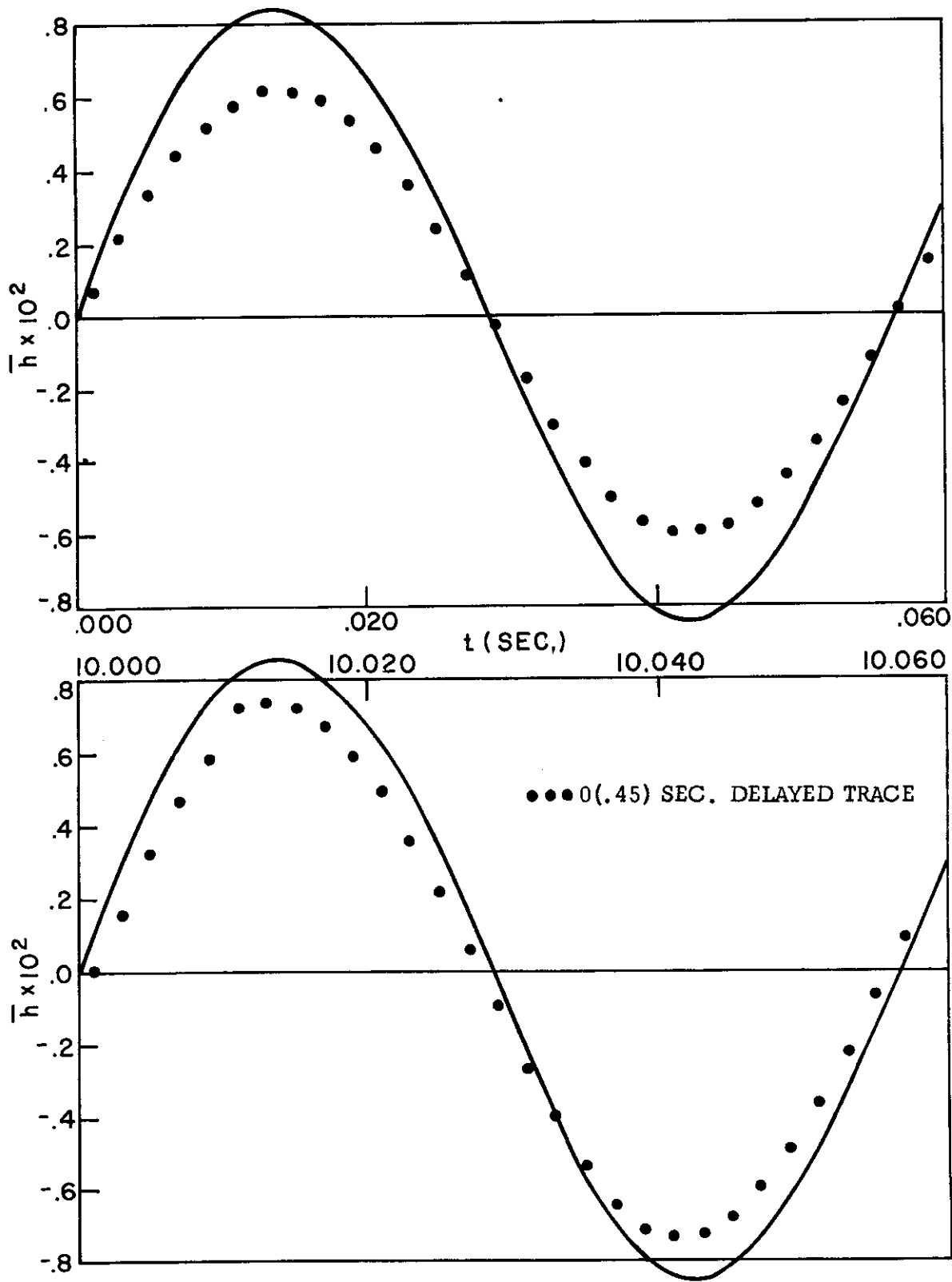


Fig. 36 \bar{h} Time History Due to Case 1 Initial Conditions Applied at $t_0 = 0$ and 10 Seconds Compared with Itself Approximately .45 Seconds Later; $n_g = 270 (1 - \cos .2513t)$

Contrails

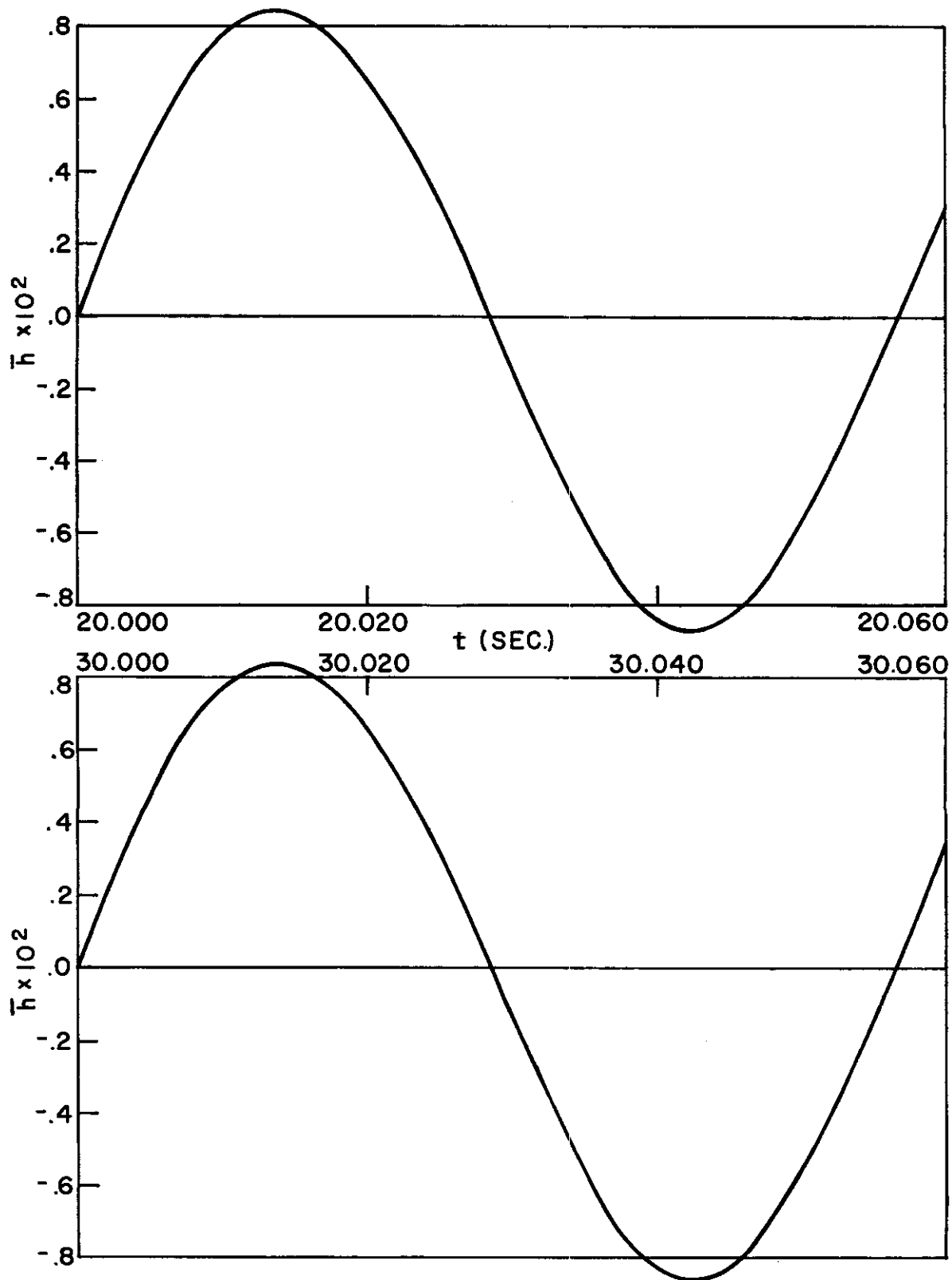


Fig. 37 \bar{h} Time History Due to Case 1 Initial Conditions Applied at $t_0 = 20$ and 30 Seconds; $n_g = 270 (1 - \cos .2513t)$

Contrails

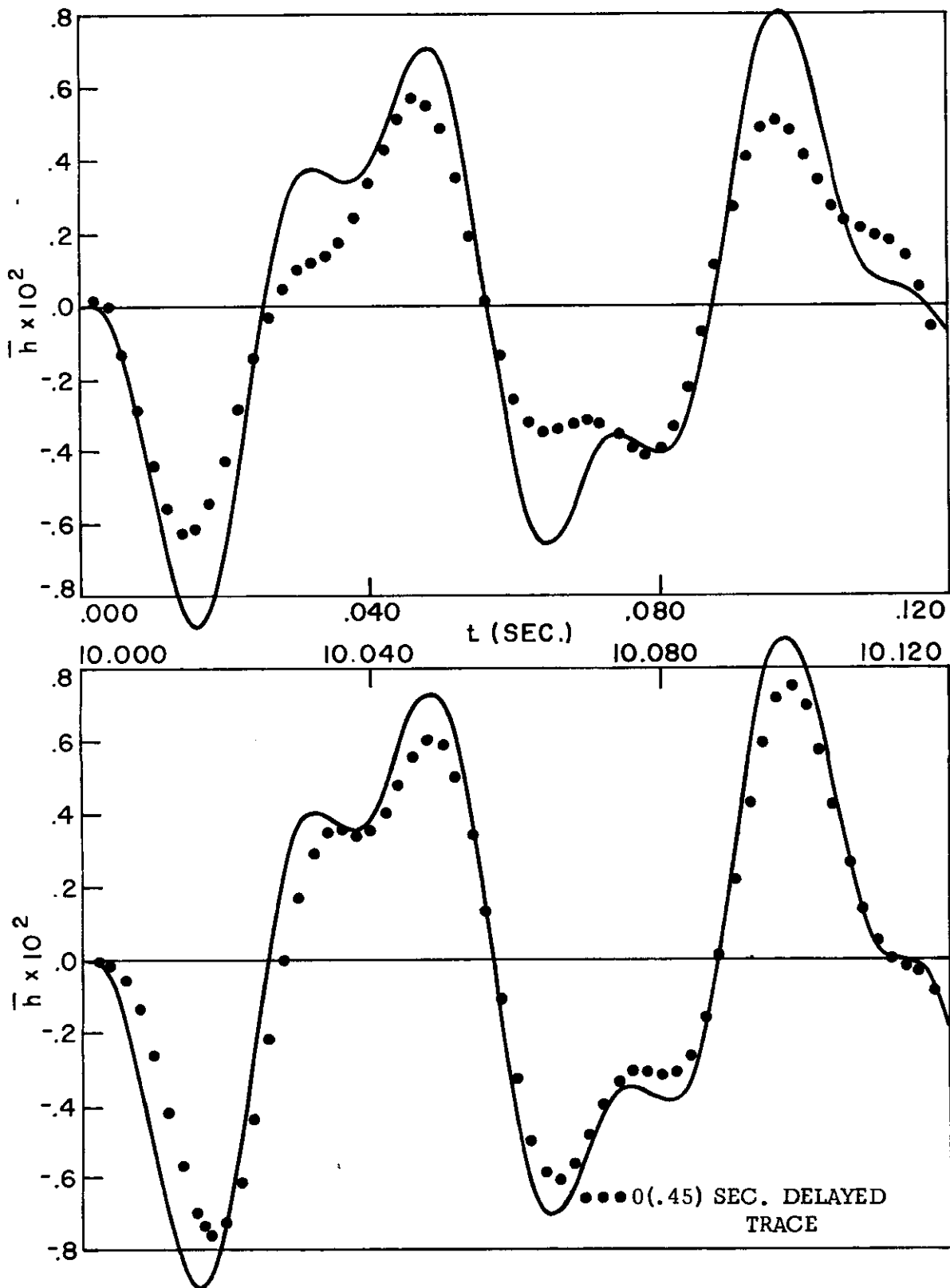


Fig. 38 \bar{h} Time History Due to Case 2 Initial Conditions Applied at $t_0 = 0$ and 10 Seconds Compared with Itself Approximately .45 Seconds Later; $n_g = 270 (1 - \cos .2513t)$

Contrails

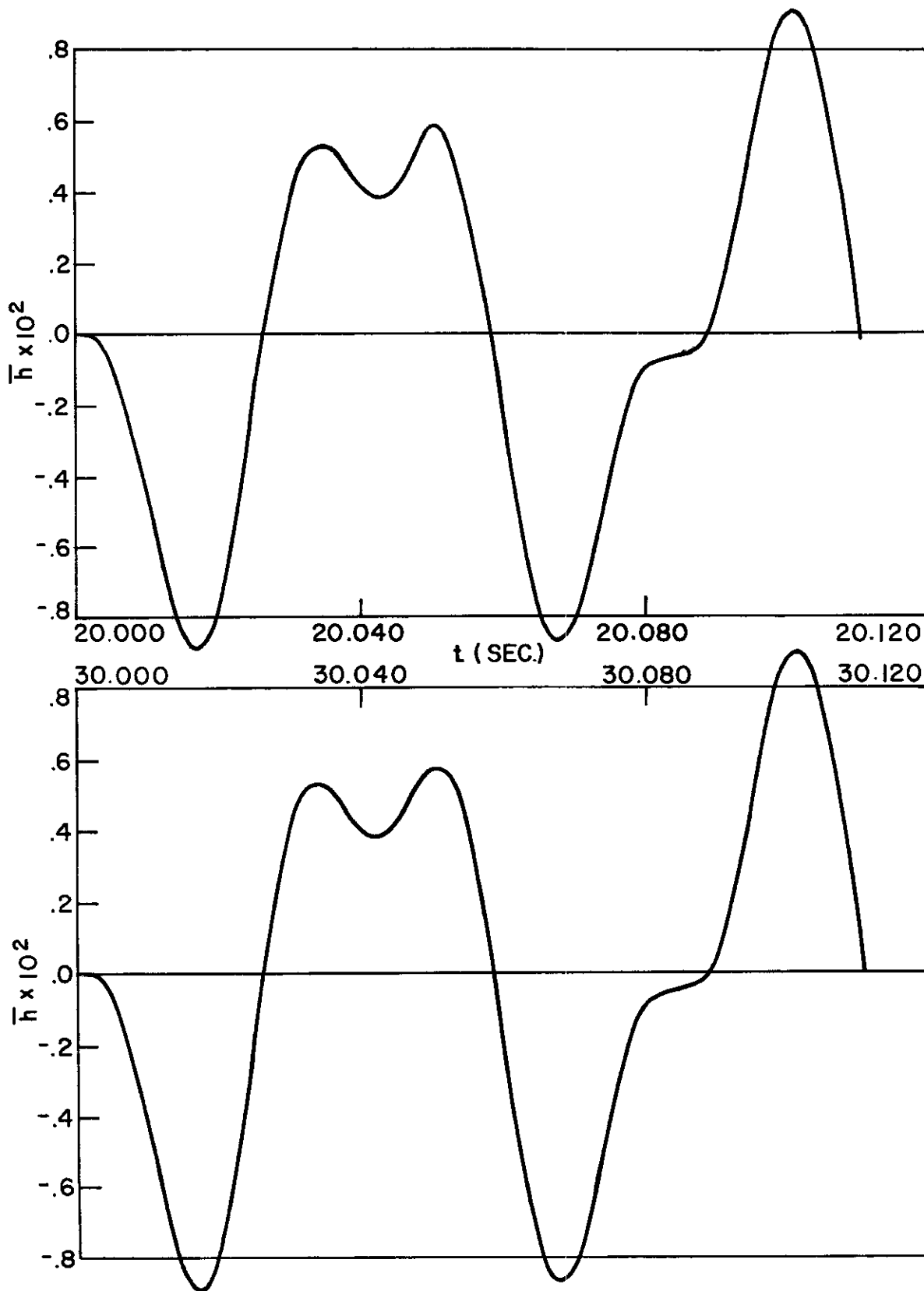


Fig. 39 \bar{h} Time History Due to Case 2 Initial Conditions Applied at $t_0 = 20$ and 30 Seconds; $n_g = 270 (1 - \cos .2513t)$

Contrails

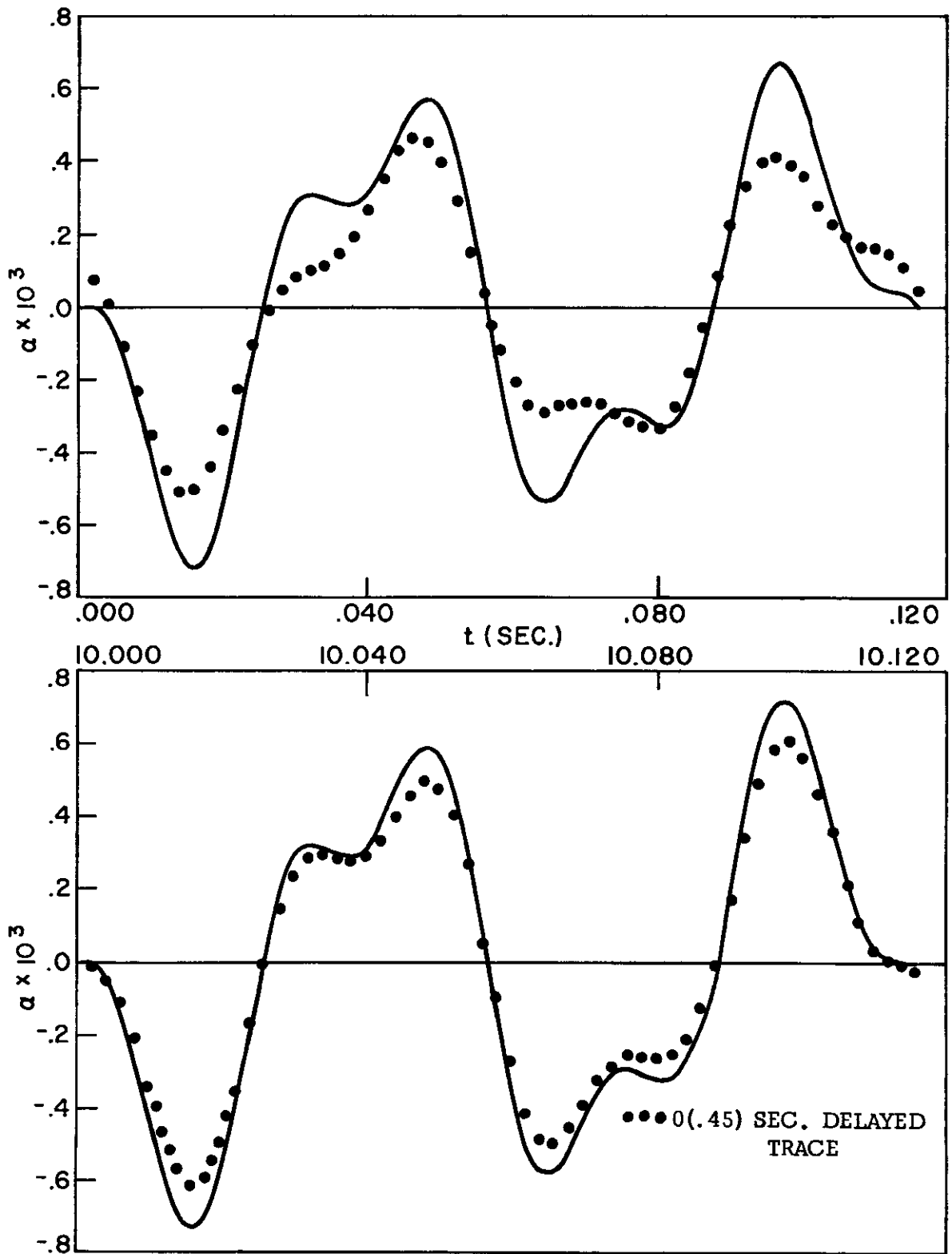


Fig. 40 α Time History Due to Case 1 Initial Conditions Applied at $t_0 = 0$ and 10 Seconds Compared with Itself Approximately .45 Seconds Later; $n_g = 270 (1 - \cos .2513t)$

Contrails

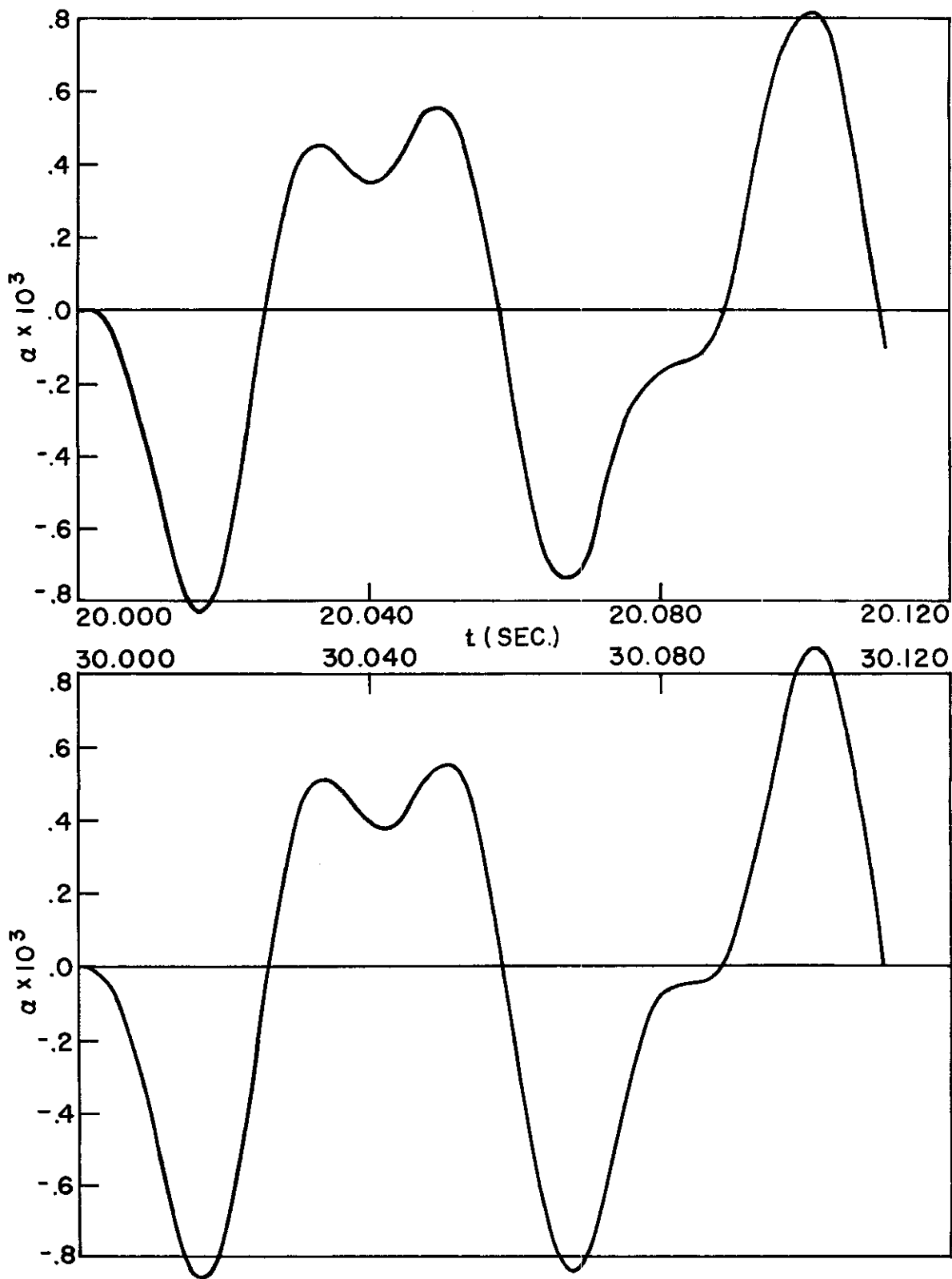


Fig. 41 α Time History Due to Case 1 Initial Conditions Applied at $t_0 = 20$ and 30 Seconds; $n_g = 270 (1 - \cos .2513t)$

Contrails

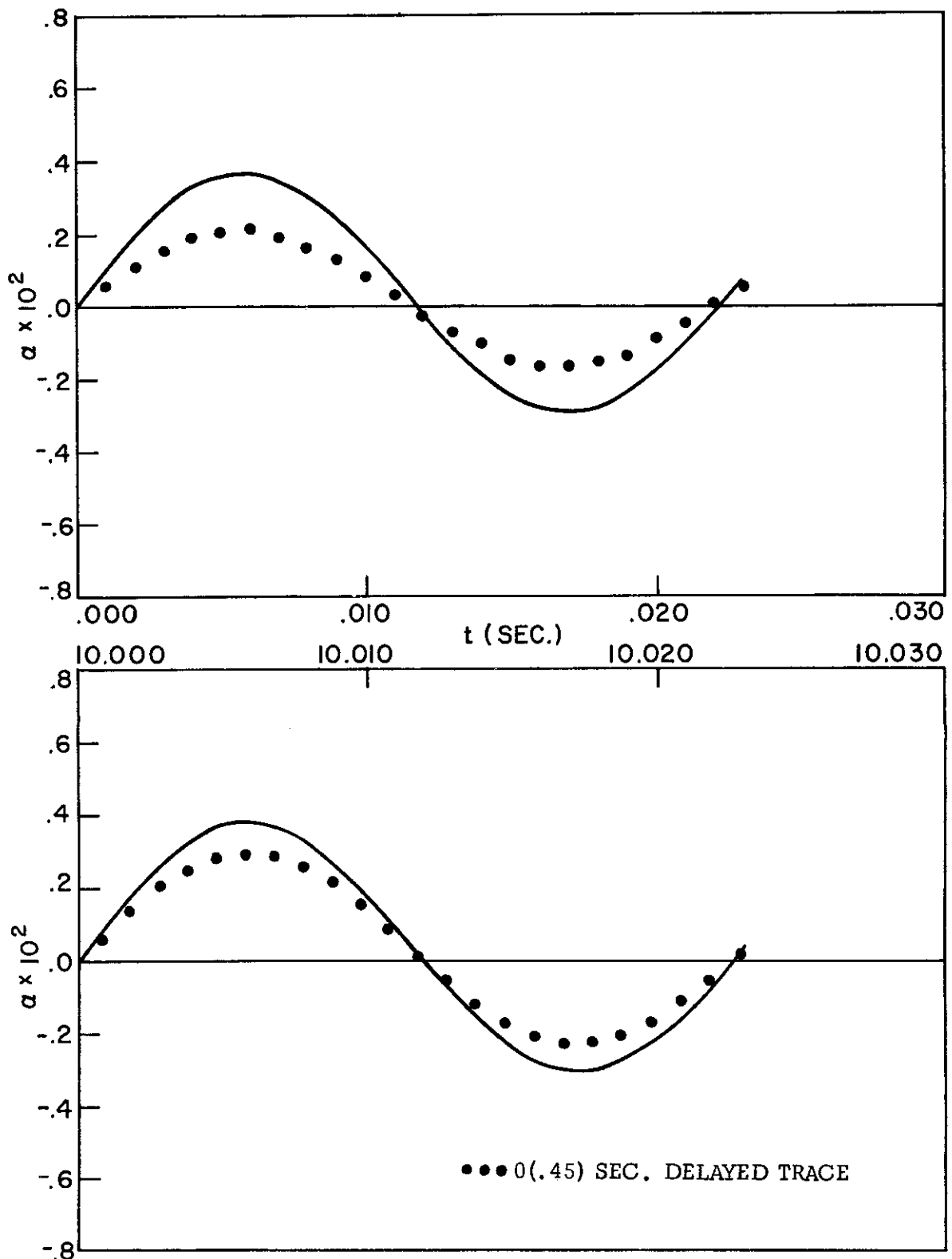


Fig. 42 α Time History Due to Case 2 Initial Conditions Applied at $t_0 = 0$ and 10 Seconds Compared with Itself Approximately .45 Seconds Later; $n_g = 270 (1 - \cos .2513t)$

Contrails

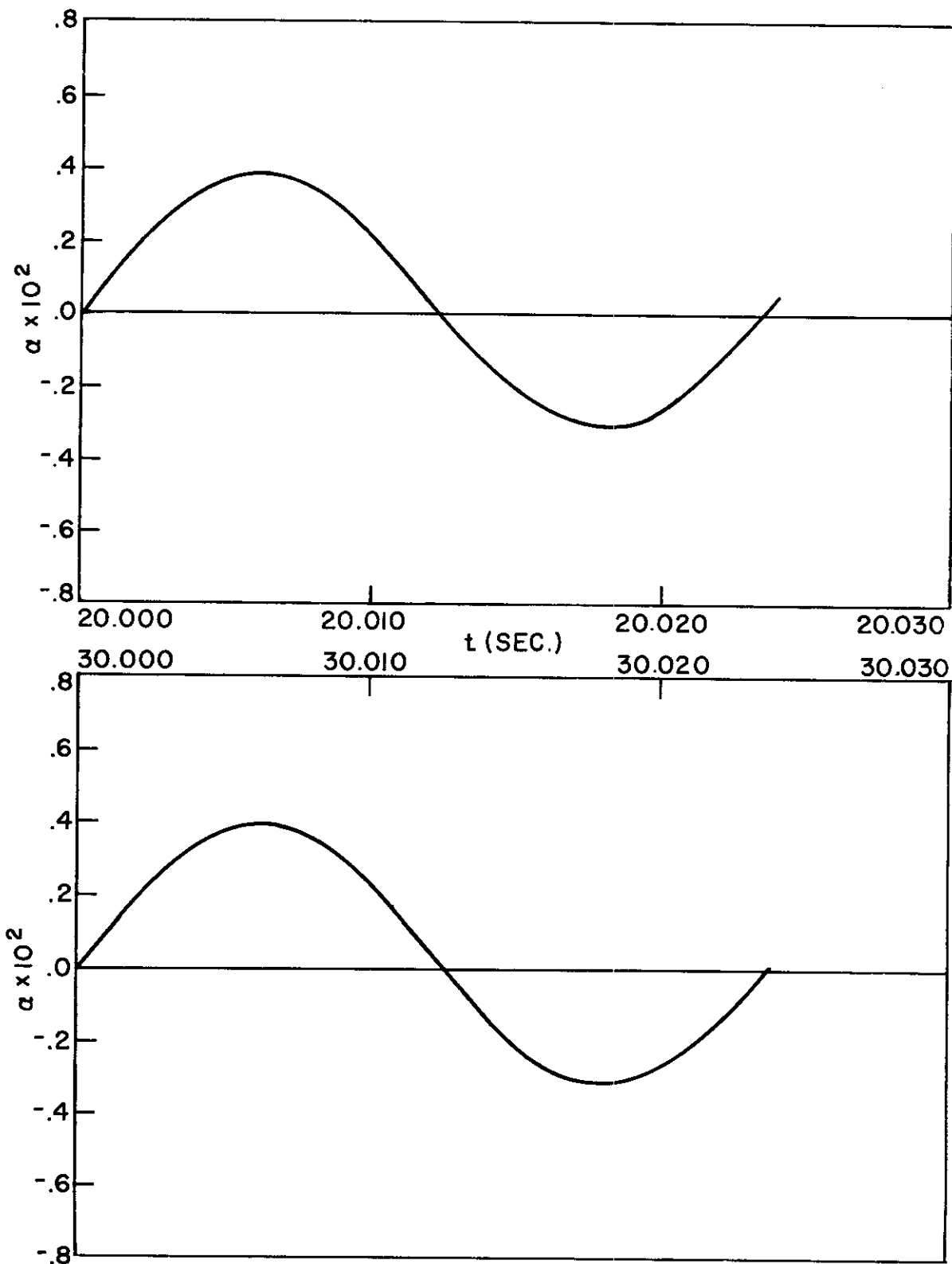


Fig. 43 α Time History Due to Case 2 Initial Conditions Applied at $t_0 = 20$ and 30 Seconds; $n_g = 270 (1 - \cos .2513t)$

Contrails

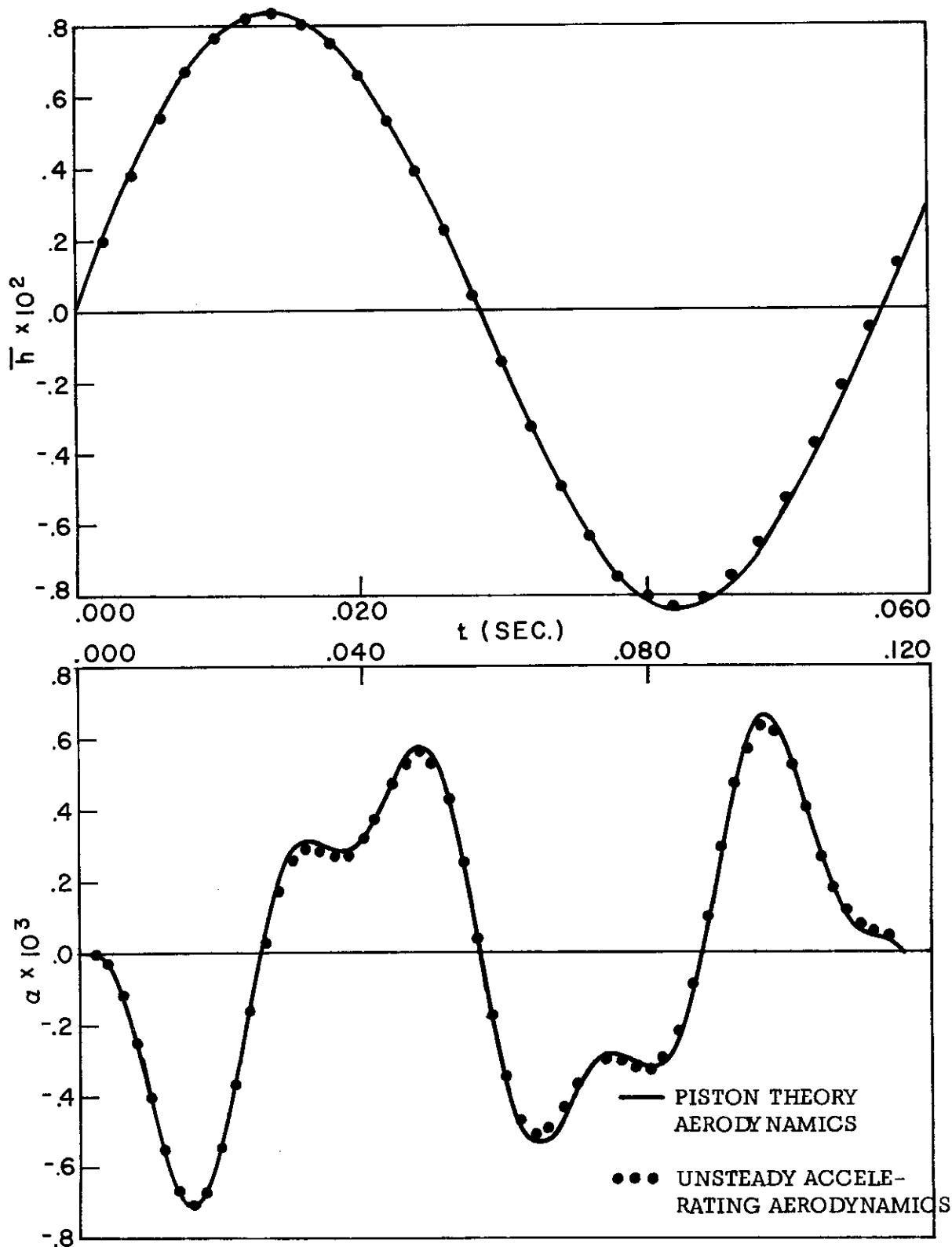


Fig. 44 \bar{h} and α Time Histories Observed First at $t = 0$ Seconds Due to Case 1 Initial Conditions Applied at $t_0 = 0$ Seconds; $n\omega = 270 (1 - \cos .2513t)$

Contrails

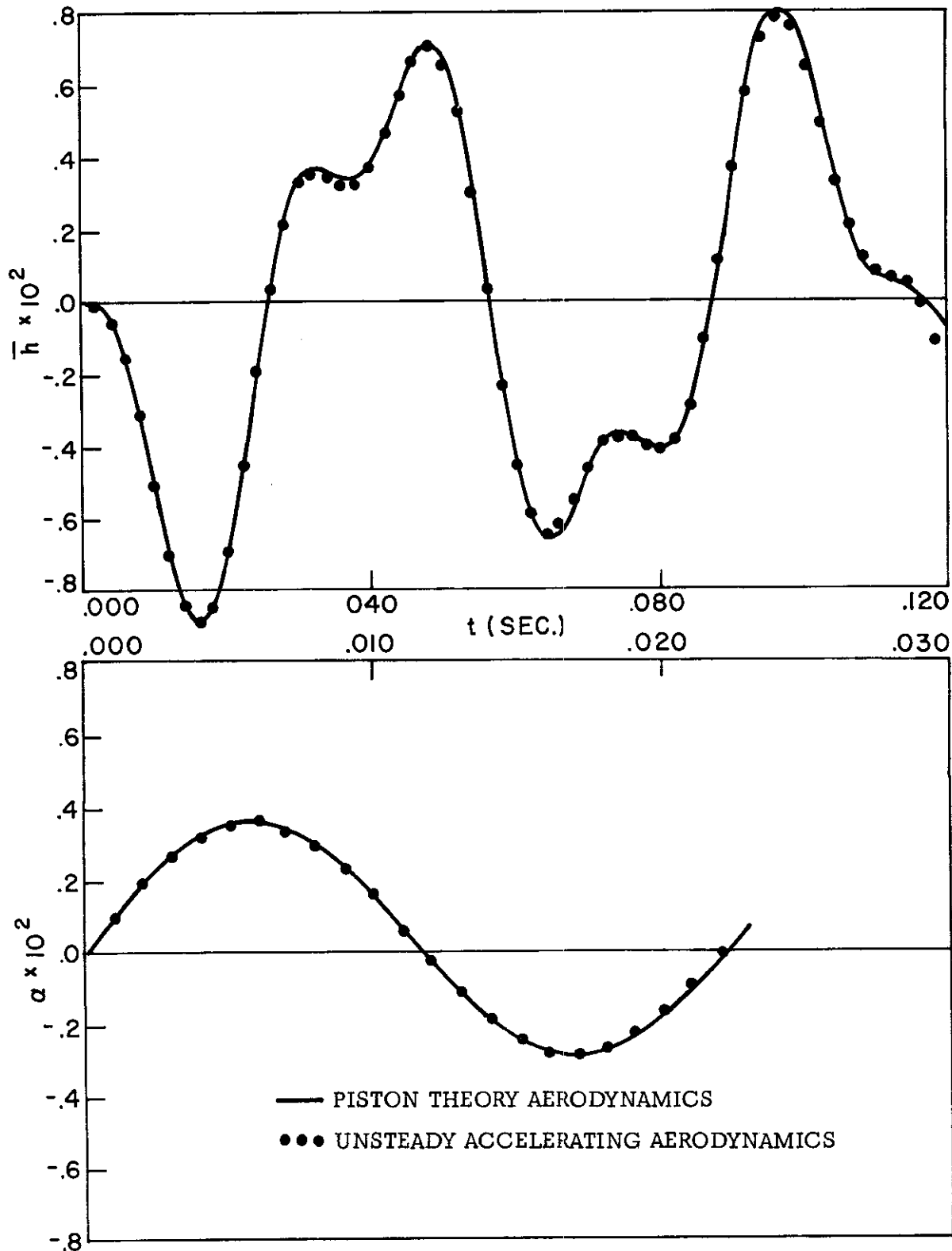


Fig. 45 \bar{h} and α Time Histories Observed First at $t = 0$ Seconds Due to Case 2 Initial Conditions Applied at $t_0 = 0$ Seconds; $n_g = 270 (1 - \cos .2513t)$

Contrails

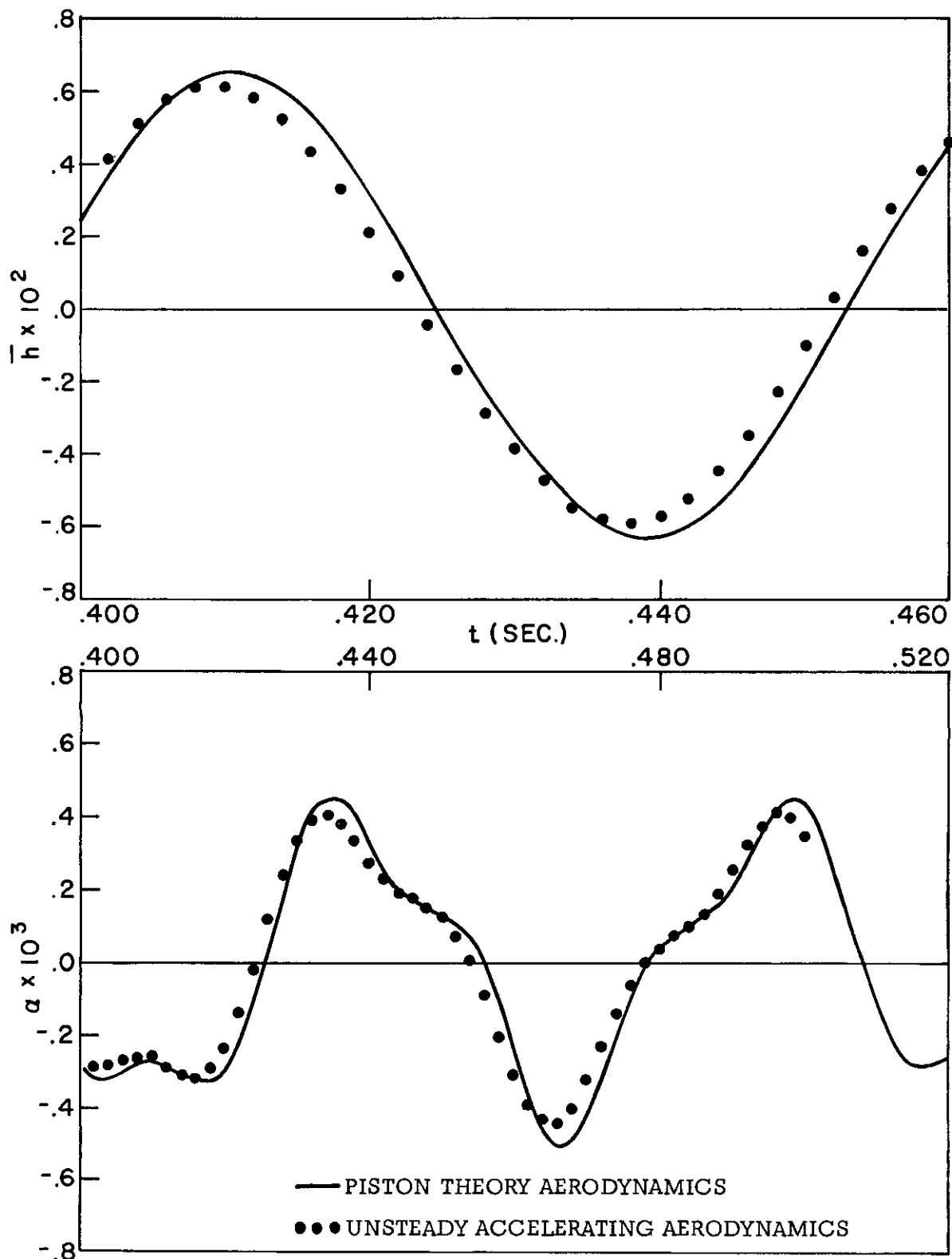


Fig. 46 \bar{h} and α Time Histories Observed First at $t = .4$ Seconds Due to Case 1 Initial Conditions Applied at $t_0 = 0$ Seconds; $n\omega = 270 (1 - \cos .2513t)$

Contrails

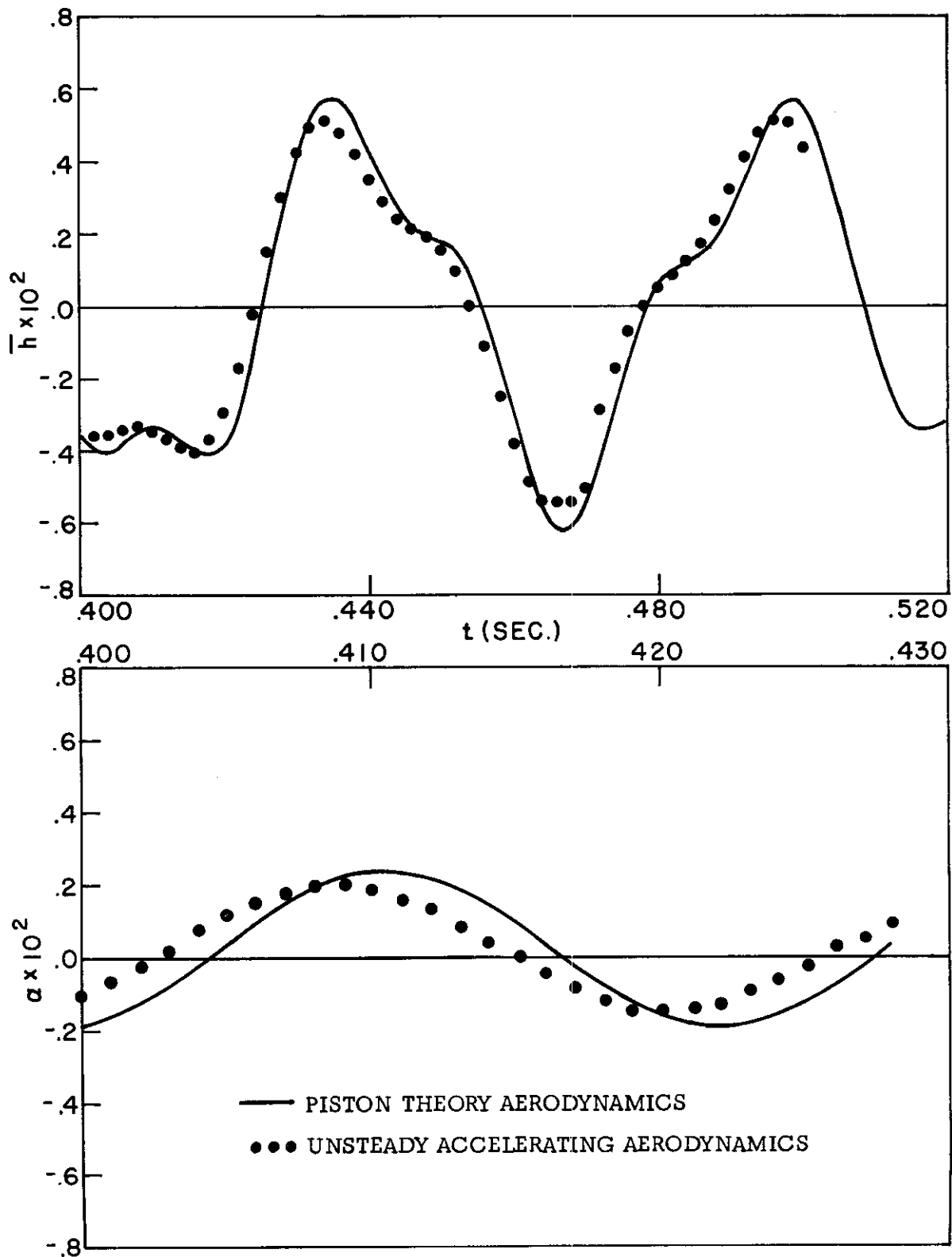


Fig. 47 \bar{h} and α Time Histories Observed First at $t = .4$ Seconds Due to Case 2 Initial Conditions Applied at $t_0 = 0$ Seconds; $n\gamma = 270 (1 - \cos .2513t)$

Contrails

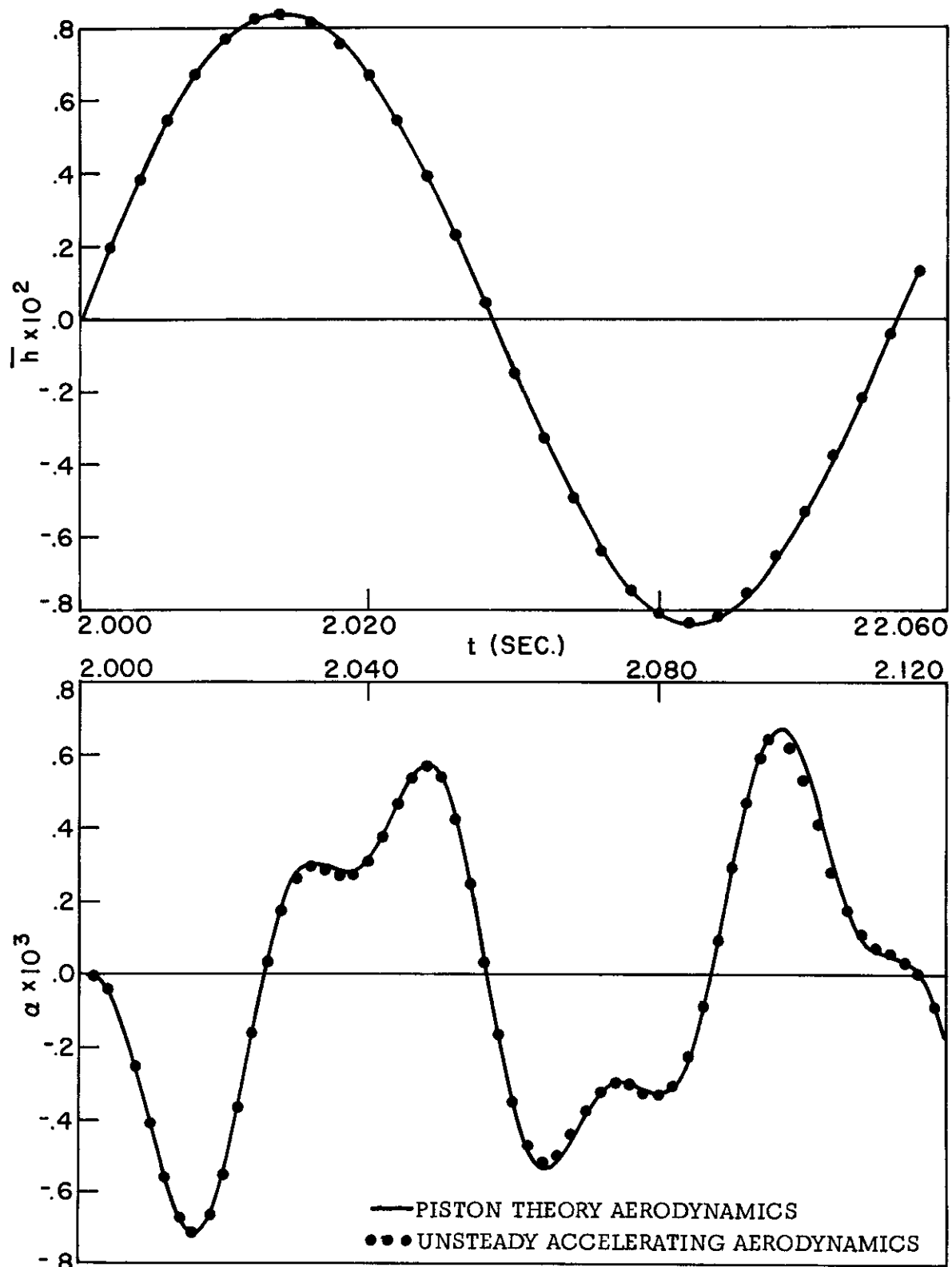


Fig. 48 \bar{h} and α Time Histories Observed First at $t = 2.0$ Seconds Due to Case 1 Initial Conditions Applied at $t_0 = 2.0$ Seconds; $n_g = 270 (1 - \cos .2513t)$

Contrails

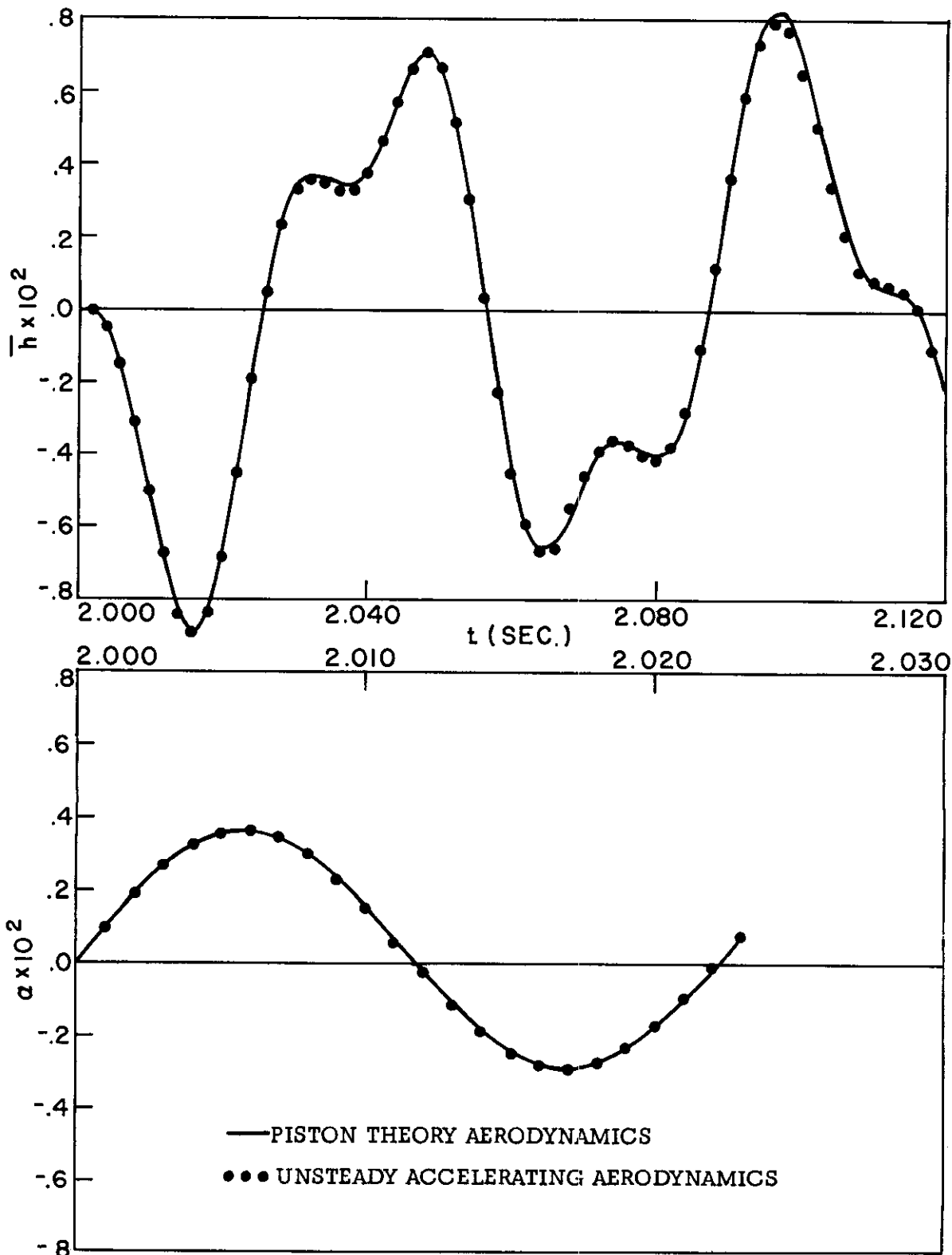


Fig. 49 \bar{h} and α Time Histories Observed First at $t = 2.0$ Seconds Due to Case 2 Initial Conditions Applied at $t_0 = 2.0$ Seconds; $n_g = 270 (1 - \cos .2513t)$

Contrails

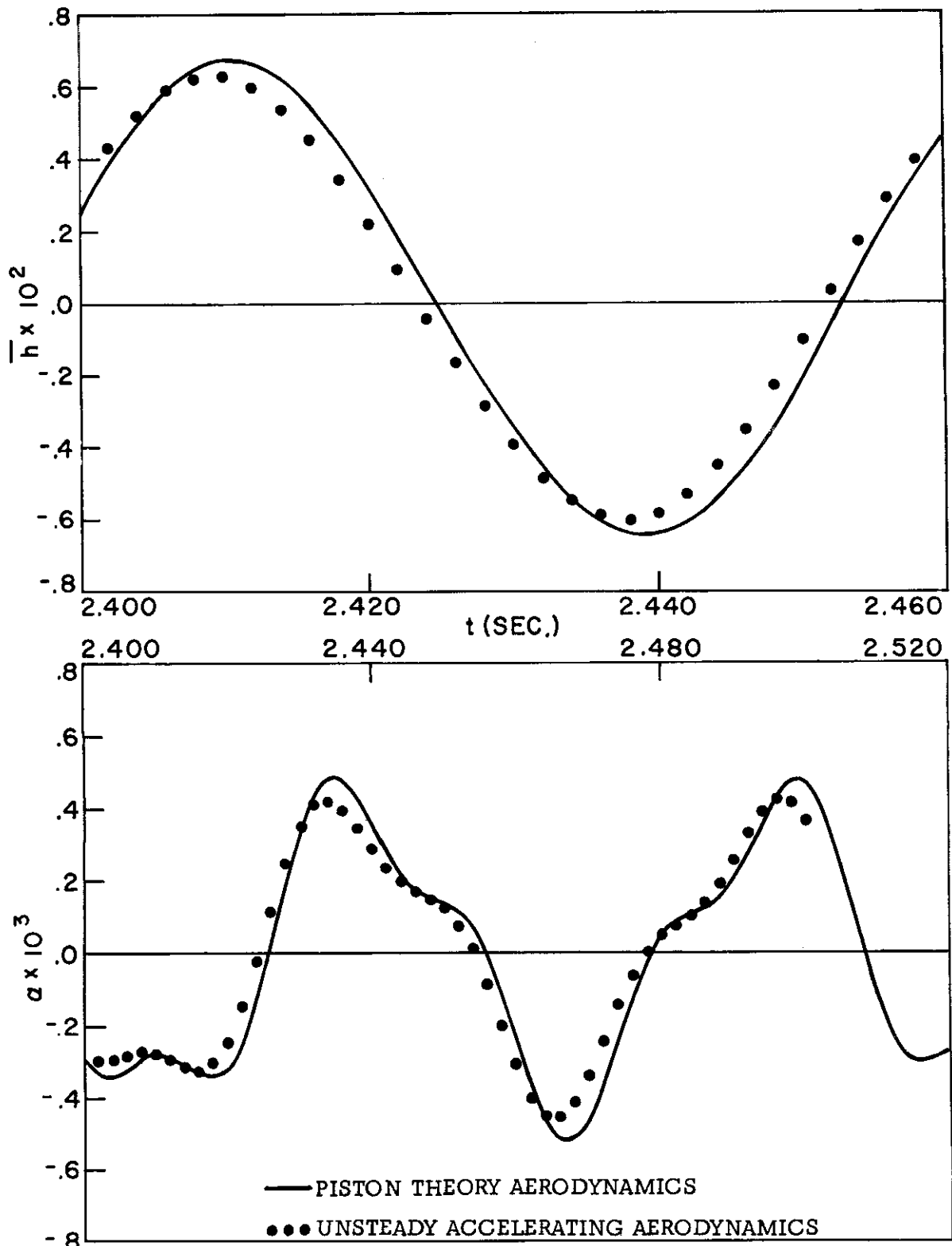


Fig. 50 \bar{h} and α Time Histories Observed First at $t = 2.4$ Seconds Due to Case 1 Initial Conditions Applied at $t_0 = 2.0$ Seconds; $n_g = 270 (1 - \cos .2513t)$

Contrails

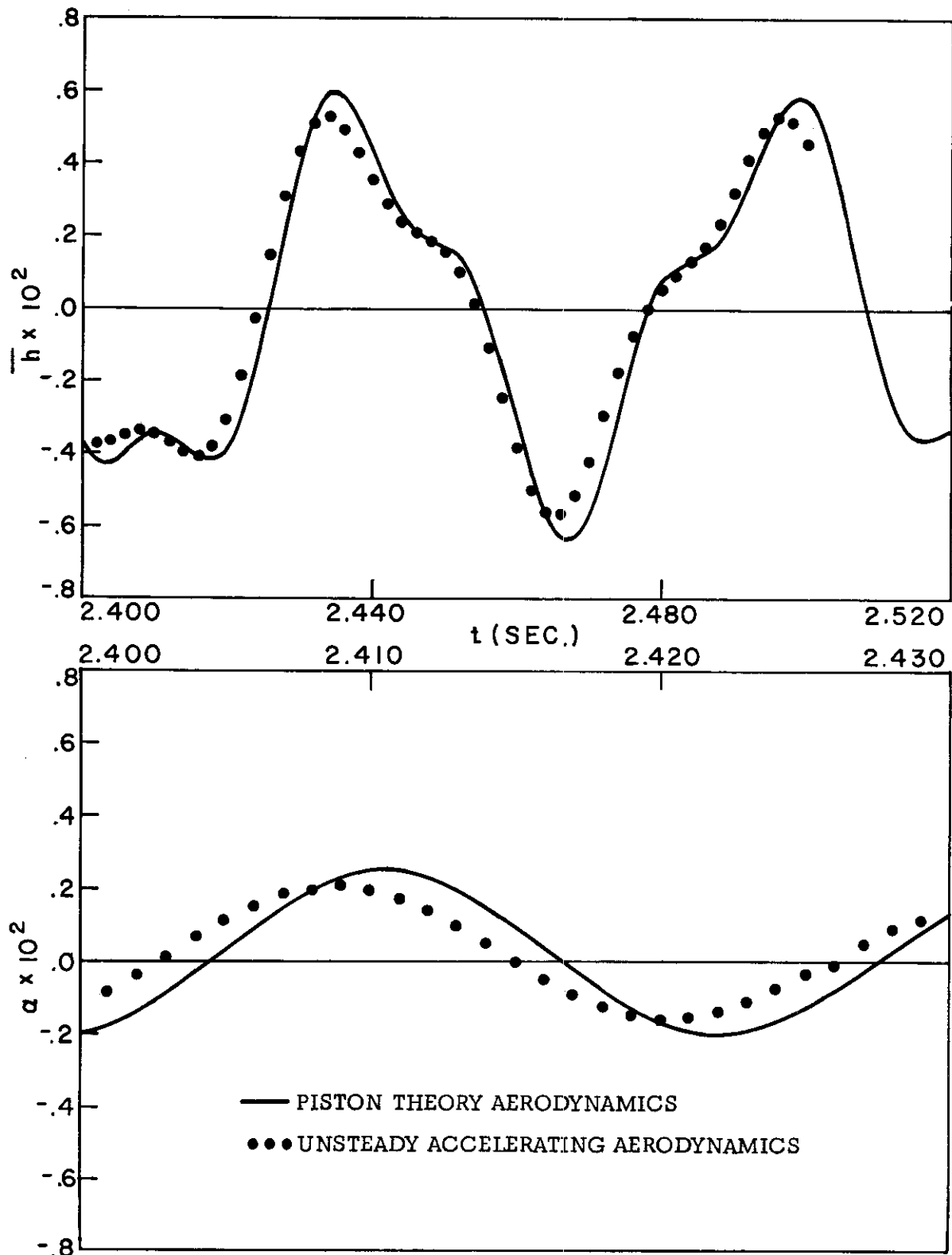


Fig. 51 \bar{h} and α Time Histories Observed First at $t = 2.4$ Seconds Due to Case 2 Initial Conditions Applied at $t_0 = 2.0$ Seconds; $n_g = 270 (1 - \cos .2513t)$

Contrails

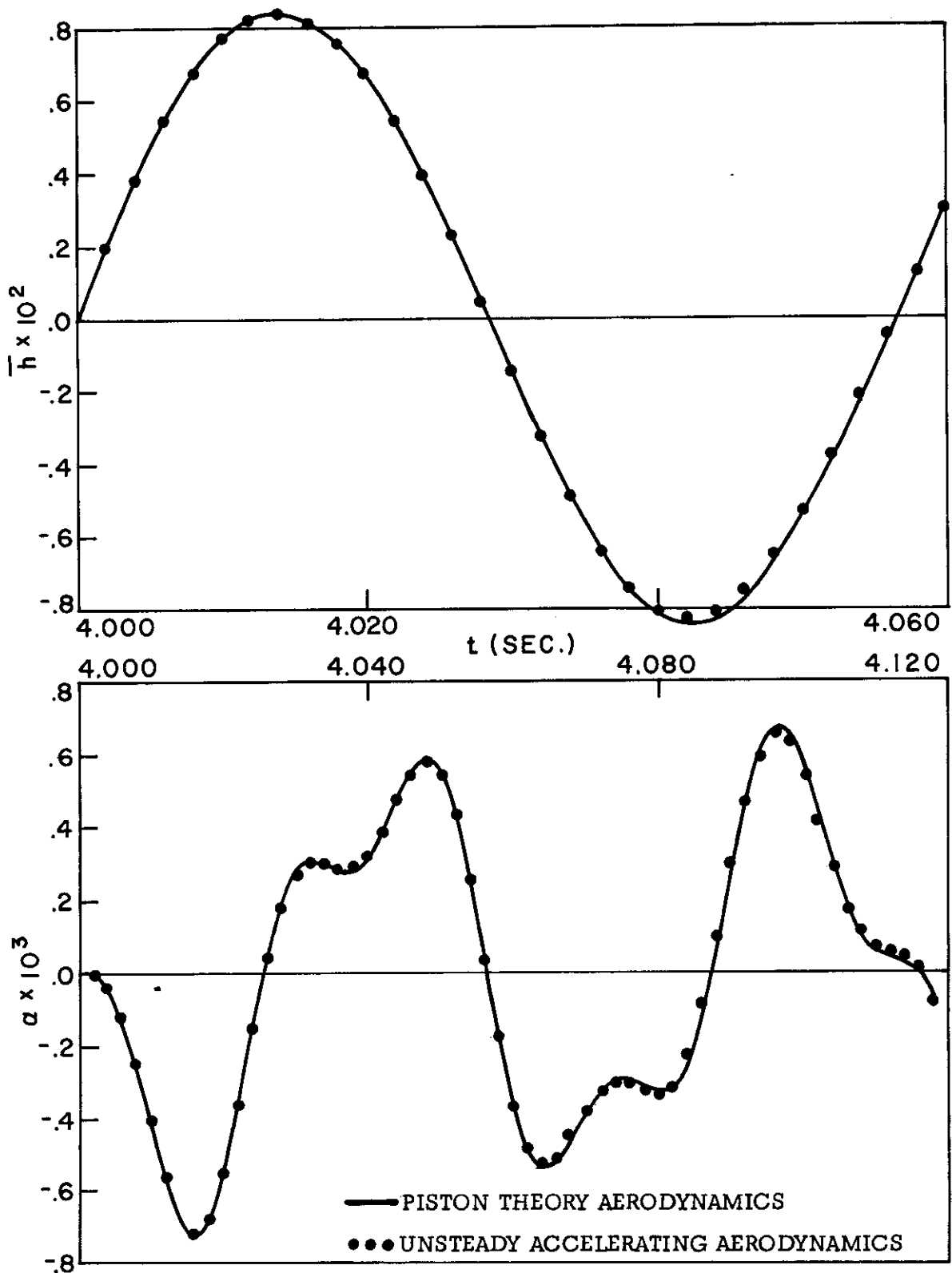


Fig. 52 \bar{h} and α Time Histories Observed First at $t = 4.0$ Seconds Due to Case 1 Initial Conditions Applied at $t_0 = 4.0$ Seconds; $n_g = 270 (1 - \cos .2513t)$

Contrails

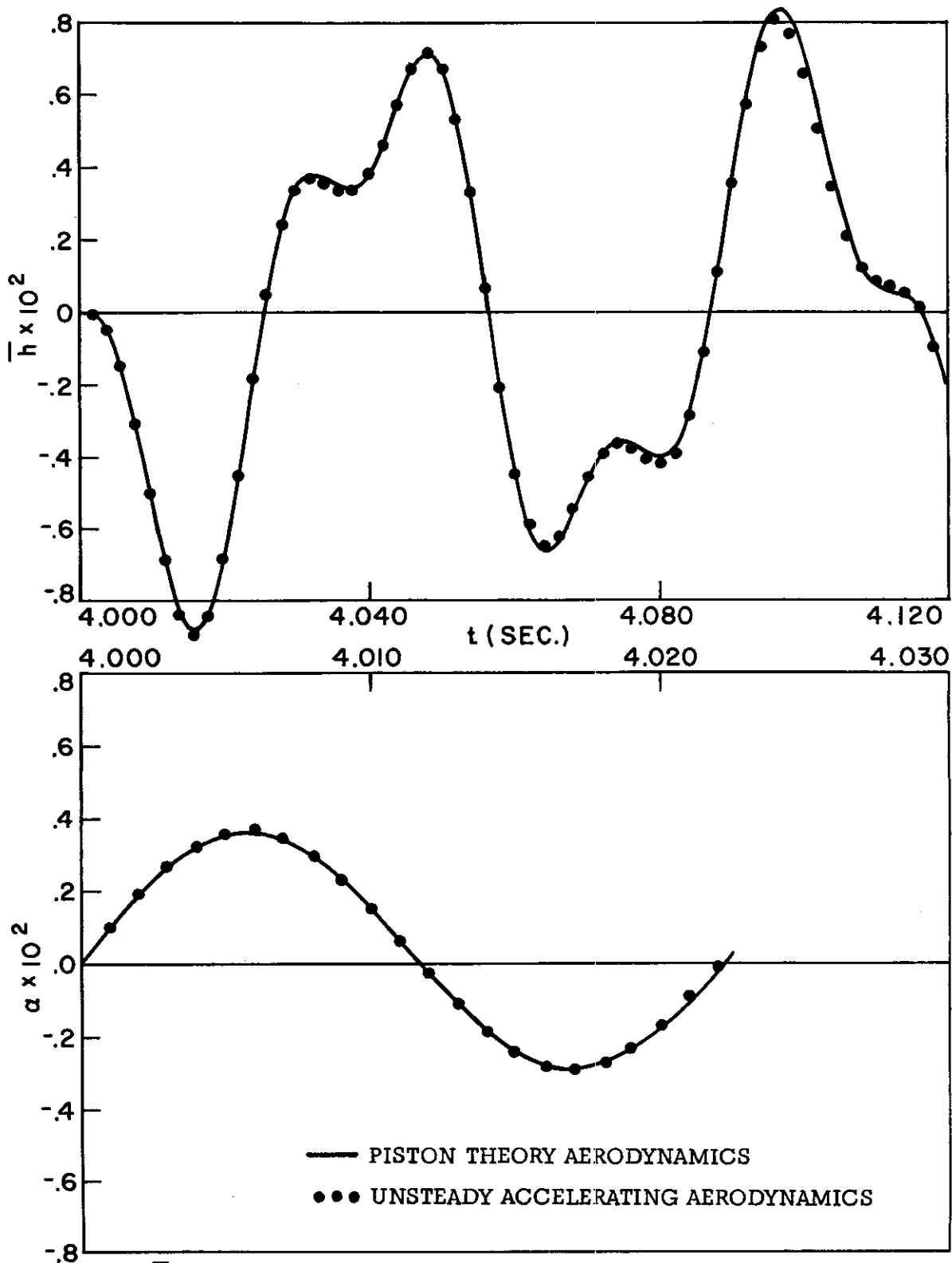


Fig. 53 \bar{h} and α Time Histories Observed First at $t \approx 4.0$ Seconds Due to Case 2 Initial Conditions Applied at $t_0 = 4.0$ Seconds; $n\bar{g} = 270 (1 - \cos .2513t)$

Contrails

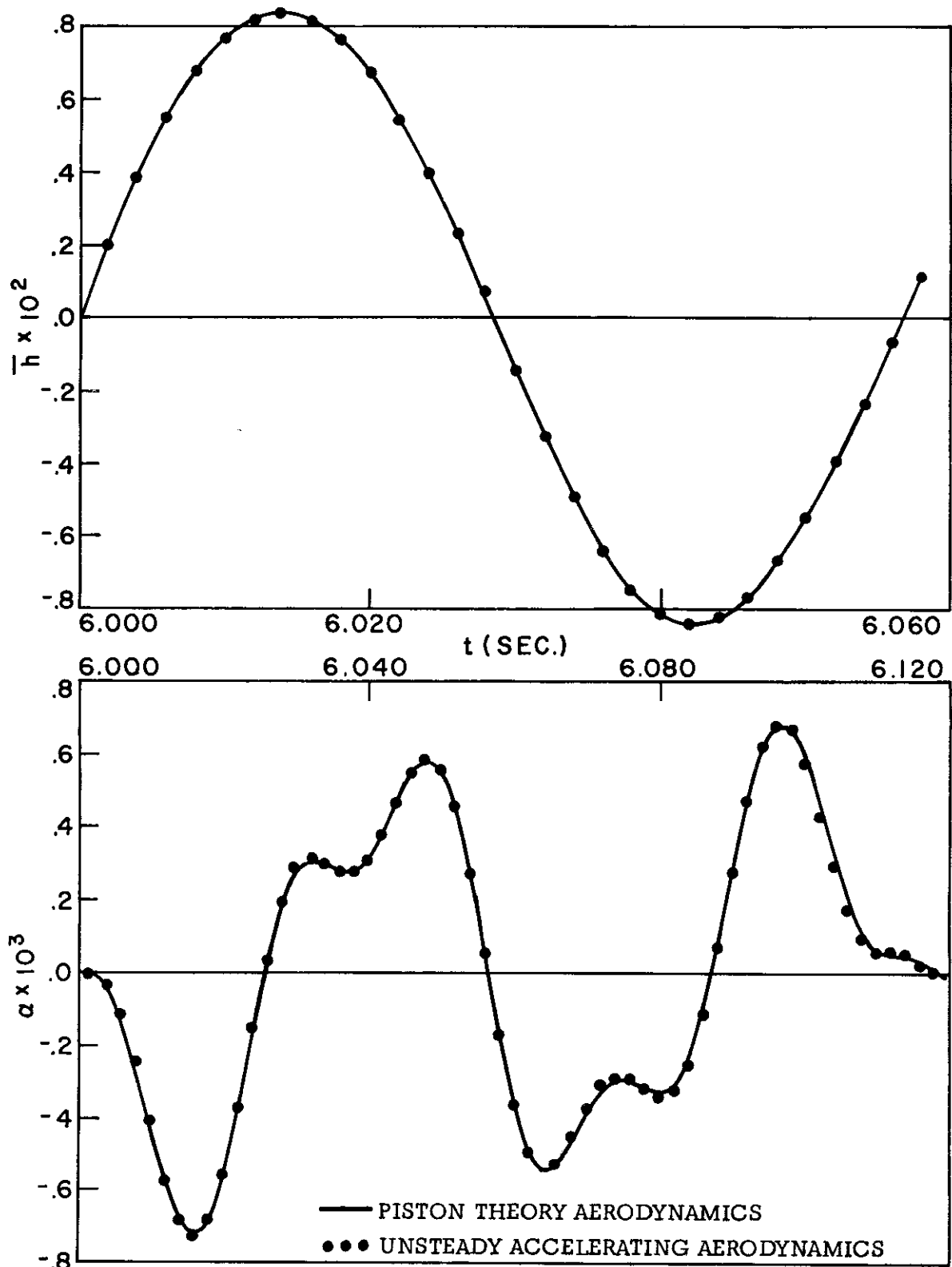


Fig. 54 \bar{h} and α Time Histories Observed First at $t = 6.0$ Seconds Due to Case 1 Initial Conditions Applied at $t_0 = 6.0$ Seconds; $ng = 270 (1 - \cos .2513t)$

Contrails

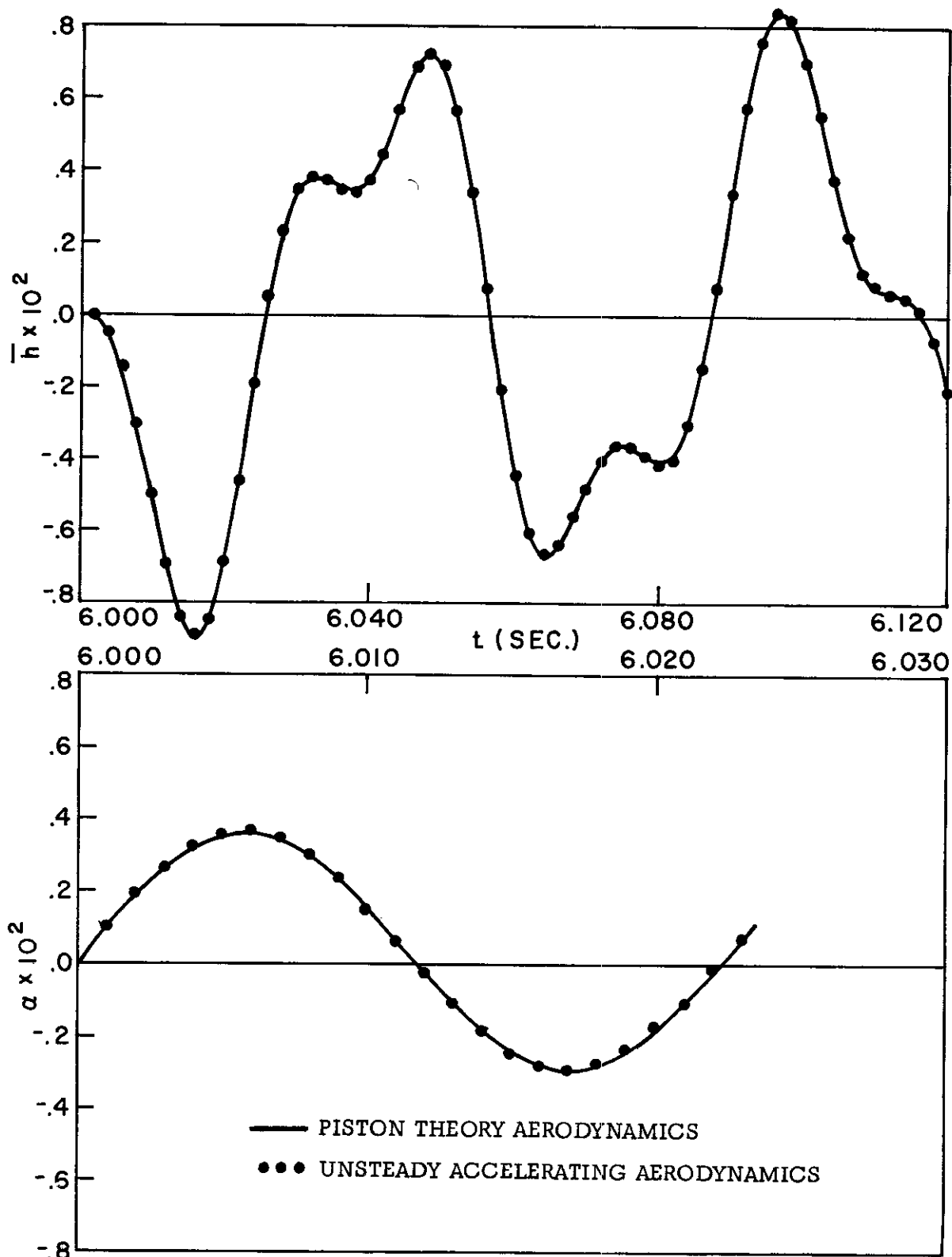


Fig. 55 \bar{h} and α Time Histories Observed First at $t = 6.0$ Seconds Due to Case 2 Initial Conditions Applied at $t_0 = 6.0$ Seconds; $n\omega = 270 (1 - \cos .2513t)$

Contrails

Table 1 Comparison of System Frequencies (cycles/sec.) Obtained by Various Methods of Analysis due to Case 1 Inputs for the Time Interval $0 \leq t_0 \leq 8$ Seconds; $n_g = 270 (1 - \cos.2513t)$

t_0 (sec)	t_{ref} (sec)	\bar{h}			α		
		$\omega_{Q.S.}$	$\omega_{P.T.}$	$\omega_{U.A.A.}$	$\omega_{Q.S.}$	$\omega_{P.T.}$	$\omega_{U.A.A.}$
0	0	17.65	17.7	17.72	17.65	17.2	17.26
0	0.5			17.71			17.61
0	1.0		17.7			17.7	
2	2.0	17.67	17.7	17.72	17.67	17.2	17.27
2	2.5			17.71			17.63
2	3.0		17.7			17.7	
4	4.0	17.65	17.7	17.70	17.65	17.2	17.26
4	4.5			17.70			17.59
4	5.0		17.7			17.7	
6	6.0	17.65	17.7	17.66	17.65	17.2	17.16
6	6.5			17.65			17.62
6	7.0		17.6			17.7	
8	8.0	17.63	17.6	17.64	17.63	17.2	17.14
8	8.5			17.64			17.61
8	9.0		17.6			17.7	

Q.S. = Quasi-Steady
P. T. = Piston Theory with time-varying coefficients
U.A.A. = Unsteady Accelerating Aerodynamics with time-varying coefficients

Contrails

Table 2 Comparison of System Frequencies (cycles/second) Obtained by Various Methods of Analysis due to Case 1 Inputs for the Time Interval $10 \leq t_0 \leq 30$ Seconds; $n_g = 270 (1 - \cos .2513t)$

t_0 (sec)	t_{ref} (sec)	\bar{h}		α	
		$\omega_{Q.S.}$	$\omega_{P.T.}$	$\omega_{Q.S.}$	$\omega_{P.T.}$
10	10.0	17.62	17.6	17.62	17.5
10	11.0		17.6		17.6
12	12.0	17.60	17.6	17.60	18.2
12	13.0		17.6		17.5
14	14.0	17.62	17.6	17.62	18.2
14	15.0		17.6		17.5
16	16.0	17.62	17.6	17.62	18.2
16	17.0		17.6		17.3
18	18.0	17.63	17.6	17.63	18.1
18	19.0		17.7		17.2
20	20.0	17.65	17.6	17.65	18.1
20	21.0		17.6		18.4
22	22.0	17.65	17.6	17.65	18.1
22	23.0		17.6		18.9
24	24.0	17.65	17.6	17.65	18.1
24	25.0		17.6		18.8
26	26.0	17.65	17.6	17.65	18.05
26	27.0		17.6		18.6
28	28.0	17.65	17.6	17.65	18.0
28	29.0		17.6		17.7
30	30.0	17.65	17.6	17.65	18.0
30	31.0		17.6		17.4

Contrails

Table 3 Comparison of System Frequencies (cycles/second) Obtained by Various Methods of Analysis due to Case 2 Inputs for the Time Interval $0 \leq t_0 \leq 8$ Seconds; $n_g = 270 (1 - \cos .2513t)$

t_0 (sec)	t_{ref} (sec)	\bar{h}			α		
		$\omega_{Q.S.}$	$\omega_{R.T.}$	$\omega_{U.A.A.}$	$\omega_{Q.S.}$	$\omega_{P.T.}$	$\omega_{U.A.A.}$
0	0	17.65	17.2	17.26	44.47	44.1	44.22
0	0.5			17.62			44.23
0	1.5		17.7			45.2	
2	2.0	17.67	17.2	17.25	44.45	44.1	44.20
2	2.5			17.63			44.24
2	3.0		17.7			45.1	
4	4.0	17.65	17.2	17.22	44.45	44.1	44.17
4	4.5			17.58			44.20
4	5.0		17.7			45.1	
6	6.0	17.65	17.2	17.15	44.43	44.1	44.11
6	6.5			17.61			44.24
6	7.0		17.7			45.0	
8	8.0	17.63	17.2	17.13	44.34	44.0	44.05
8	8.5			17.61			44.16
8	9.0		17.7			44.8	

Contrails

Table 4 Comparison of System Frequencies (cycles/second) Obtained by Various Methods of Analysis due to Case 2 Inputs for the Time Interval $10 \leq t_0 \leq 30$ Seconds; $n_g = 270 (1 - \cos .2513t)$

t_0 (sec)	t_{ref} (sec)	\bar{h}		α	
		$\omega_{Q.S.}$	$\omega_{P.T.}$	$\omega_{Q.S.}$	$\omega_{P.T.}$
10	10.0	17.62	17.5	44.07	43.7
10	11.0		17.6		43.3
12	12.0	17.60	18.0	43.61	43.2
12	13.0		17.5		44.0
14	14.0	17.62	18.2	43.05	42.6
14	15.0		17.5		42.3
16	16.0	17.62	18.2	42.52	42.1
16	17.0		17.3		43.7
18	18.0	17.63	18.1	42.14	41.8
18	19.0		17.2		42.2
20	20.0	17.65	18.1	41.89	41.5
20	21.0		18.5		41.4
22	22.0	17.65	18.1	41.73	41.4
22	23.0		18.9		41.4
24	24.0	17.65	18.1	41.65	41.3
24	25.0		18.8		41.4
26	26.0	17.65	18.05	41.60	41.2
26	27.0		18.6		41.4
28	28.0	17.65	18.0	41.57	41.2
28	29.0		17.7		41.4
30	30.0	17.65	18.0	41.54	41.2
30	31.0		17.4		41.4

Contrails

Table 5 Comparison of System Frequencies (cycles/second) Obtained by Various Methods of Analysis due to both Case 1 and Case 2 Inputs for the Time Interval $0 \leq t_0 \leq 30$ Seconds; $ng = 9g$

t_0 (sec)	t_{ref} (sec)	Case 1				Case 2			
		\bar{h}		α		\bar{h}		α	
		$\omega_{Q.S.}$	$\omega_{P.T.}$	$\omega_{Q.S.}$	$\omega_{P.T.}$	$\omega_{Q.S.}$	$\omega_{P.T.}$	$\omega_{Q.S.}$	$\omega_{P.T.}$
0	0	17.65	17.7	17.65	17.2	17.65	17.2	44.47	44.1
0	1		17.7		17.7		17.7		45.2
2	2	17.63	17.6	17.63	17.2	17.63	17.2	44.47	44.1
2	3		17.6		17.7		17.7		45.2
4	4	17.62	17.6	17.62	17.2	17.62	17.2	44.37	44.0
4	5		17.6		17.6		17.7		44.9
6	6	17.60	17.6	17.60	17.3	17.60	17.3	44.12	43.7
6	7		17.6		17.6		17.6		44.2
8	8	17.60	17.6	17.60	18.1	17.60	18.1	43.73	43.3
8	9		17.6		17.6		17.6		43.1
10	10	17.62	17.6	17.62	18.2	17.62	18.2	43.30	42.9
10	11		17.6		17.5		17.5		43.5
12	12	17.62	17.6	17.62	18.2	17.62	18.2	42.88	42.5
12	13		17.6		18.4		18.5		42.3
14	14	17.63	17.6	17.63	18.2	17.63	18.2	42.51	42.1
14	15		17.6		17.3		17.3		42.8
16	16	17.63	17.6	17.63	18.1	17.63	18.1	42.21	41.8
16	17		17.7		17.3		17.3		42.4
18	18	17.65	17.6	17.65	18.1	17.65	18.1	42.00	41.7
18	19		17.6		17.3		17.3		41.5
20	20	17.65	17.6	17.65	18.1	17.65	18.1	41.84	41.5
20	21		17.6		18.7		18.7		41.4
22	22	17.65	17.6	17.65	18.1	17.65	18.1	41.75	41.4
22	23		17.6		18.9		18.9		41.4

Table 5 (continued)

to (sec)	t _{ref} (sec)	Case 1				Case 2			
		\bar{h}		α		\bar{h}		α	
		$\omega_{Q.S.}$	$\omega_{P.T.}$	$\omega_{Q.S.}$	$\omega_{P.T.}$	$\omega_{Q.S.}$	$\omega_{P.T.}$	$\omega_{Q.S.}$	$\omega_{P.T.}$
24	24	17.65	17.6	17.65	18.1	17.65	18.1	41.3	41.68
24	25		17.6		18.9		18.9	41.4	
26	26	17.65	17.6	17.65	18.1	17.65	18.1	41.3	41.63
26	27		17.6		18.7		18.7	41.4	
28	28	17.65	17.6	17.65	18.1	17.65	18.1	41.2	41.59
28	29		17.6		18.4		18.4	41.4	
30	30	17.65	17.6	17.65	18.0	17.65	18.0	41.2	41.54
30	31		17.6		17.4		17.4	41.4	